Study of Spurious Oscillations Due to Backstreaming Electrons from Collector in Klystron

Zhigao Fang

Doctor of Philosophy

Department of Accelerator Science
School of Mathematical and Physical Science
The Graduate University for Advanced Studies

March 2001

Contents

List of Symbols Used

$\mathbf{A}$	Complex voltage gain of klystron
$\mathbf{B}$	Magnetic vector flux density
B_c	Magnetic flux density on cathode
B_z	Magnetic flux density on the axis of electron beam
B_θ	Angular component of magnetic flux density in cylindrical coordinates
c	Velocity of light in vacuum
$\mathbf{D}$	Electric vector flux density
D_c	Diameter of collector
D_t	Diameter of drift tube
e	Charge on electron
E_0	Beam energy
E_k	Kinetic energy
E_z	Z-component of kinetic energy
$\mathbf{F}$	Force vector
$\mathbf{H}$	Magnetic field vector
I_0	Beam current
I_1	Fundamental component of rf current
I_b	Current of backstreaming electrons
$\mathbf{J}$	Current-density vector
L_c	Length of collector
m	Mass of electron
M	Beam coupling coefficient
P_{er}	Perveance
Q_e	External Q of a cavity
Q_L	Loaded Q of a cavity
r_0	Initial radial position of electron
R_b	Radius of beam
R_c	Radius of cathode
$\mathbf{S}$	Position vector
u_0	Velocity of electron at beam voltage
V_0	Beam voltage

V_d	rf-voltage vector in input cavity gap
V_f	Feedback rf-voltage vector in input cavity gap
V_i	Driving rf-voltage vector in input cavity gap
V_o	rf-voltage vector in output cavity gap
v	Velocity vector
X	Bunching parameter
Z	Atomic number
α	Modulation index
β	Complex feedback coefficient caused by backstreaming electrons
γ	Relativistic factor
$\delta\eta$	Relative error of backscattering coefficient
ε_0	Permittivity of free space
η	Backscattering coefficient
	Ratio of charge to mass of an electron
η_b	Backstreaming electron coefficient
$\eta(x)$	Energy distribution function of backstreaming electrons, $x = E_z / E_0$
μ_0	Permeability of free space
ρ	Charge density
ψ	Magnetic flux
ψ_c	Magnetic flux on the cathode
ω	Angular frequency

List of Figures

List of Tables

Abstract

Recently we observed strong spurious oscillations caused by the backstreaming electrons from the collector in the 324MHz 3MW 650μs klystrons developed at KEK. During the high-voltage processing of 324MHz klystron tube #1, unexpected oscillations were observed from both the output and input cavities when there was no driving input power. These oscillations occurred when the beam voltage was 63~71kV or higher than 90kV, and had frequencies close to 324MHz. After some investigations, the oscillations were identified to be the results of the backstreaming electrons from the collector. The collector size was accordingly changed to evaluate its effect on the backstreaming electrons. The experiment results of klystron tube #1A and #2 with modified collectors of increased radiuses and lengths, indicated that the oscillations disappeared in the low beam-voltage region, and started from 95kV and higher than 104kV respectively.

In order to understand the oscillations and to improve the klystron tubes, this thesis has studied on these spurious oscillations due to the backstreaming electrons from the collector. These electrons originally come from the backscattering of the electron beam on the collector surface. According to the course of the oscillations, the study covers three parts: the production of the backscattered electrons on the collector surface, the formation of the backstreaming electrons into the drift tube, and the oscillation mechanism due to the interaction between the electrons and rf fields.

At first, the electron backscattering process has been investigated and simulated using the EGS4 Monte Carlo method. Electrons emitted from a bombarded material-surface are generally divided into two classes: the true secondary electrons whose energies are less than approximately 50eV, and the backscattered primary electrons whose energies vary continuously from the primary electron energy to lower energies. In this thesis, we concern those backscattered electrons that have high energies corresponding to the klystron applied-voltage from a few keV to several hundred keV. These backscattered electrons have been calculated by an EGS4 user code. The electron backscattering coefficients and energy distributions have been obtained under

different conditions of incident energy and angle. For example, for the normal incidence on copper, the backscattering coefficient is equal to 0.3, and it increases with the incident angle. The trajectories of the backscattered electrons are also plotted out by a FORTRAN90 program. The EGS4 simulation results agree well with the experimental data of the reflected electrons.

After the above confirmation of the EGS4 code validity for the fundamental process, the simulations of the backstreaming electrons from the klystron collector have been performed by the EGS4 code. The simulation method includes three steps. (1) The trajectory calculation for the incident beam in the collector up to the collector wall. This step is performed by a FORTRAN90 program. Besides space-charge forces, relativistic effects, self-magnetic fields and external magnetic field effects are included in this calculation. The calculation results have shown a good agreement with the EGUN95 simulation results. (2) The simulation of the electron backscattering in the collector using the EGS4 Monte Carlo method. This step is performed by an EGS4 user code, which processes the initial conditions, collector geometry, electron motion in the magnetic fields, and output of the backscattered and backstreaming electrons. (3) The post-process for the backscattered and backstreaming electrons. This step includes two FORTRAN90 programs; one is for the electron trajectory plotting, and the other is for the calculation of the z-component energy distribution of the backstreaming electrons. Some simulation results are also given in this thesis. The backstreaming electron coefficients and energy distributions have been obtained under different conditions of the klystron. The simulation results indicate that the backstreaming electrons are essentially independent of the beam voltage. For klystron #1, #1A, and #2, the backstreaming electron coefficients are 0.66%, 0.17%, and 0.13%, respectively. The contributions to the backstreaming coefficients from the cylindrical surface and cone-shaped surface of the collector have also been investigated. The former contribution mainly comes from the backscattering of the beam edge, and the latter contribution increases with the collector length shortening due to the direct reflection. The backstreaming coefficients have been carried out as function of collector diameter and length. Also the backstreaming electrons as function of various materials are obtained. It is clarified that a lower atomic-number

material results in a smaller backstreaming coefficient. Furthermore, the transmission of the backstreaming electrons in the drift tube is investigated. It is indicated that most of the backstreaming electrons can pass through the drift tube to the input cavity region under the focusing fields of the klystron.

Finally, the study of the oscillation mechanism and conditions due to the backstreaming electrons has been performed, and relevant calculations of the oscillation conditions have also been executed using the previous results of the backstreaming electrons. Since the backstreaming electrons modulated by the gap voltage of the output cavity can induce an rf signal in the input cavity, they result in a formation of a feedback loop inside the tube. From the feedback theory, if an input cavity voltage can be regenerated by the backstreaming electrons, the oscillations will occur. Thus the oscillation conditions can be expressed by the complex product of the klystron voltage-gain and the feedback coefficient caused by the backstreaming electrons: (1) the amplitude of the product should be larger than unity, and (2) the phase of the product should be zero or integral times of 2π. The voltage gain of the klystron has been simulated by JPNDISK. Since we are interested in the beginning of the oscillations, which is in a small-signal linear region, the ballistic theory has been applied to calculate the feedback coefficient due to the backstreaming electrons by a FORTRAN90 program. Based on the calculations of the oscillation conditions, the beam-voltage regions of the oscillations for the 324MHz klystrons have been worked out. For klystron #1, the beam-voltage regions are 65~70kV and higher than 79kV. For the collector of #1A and #2, the regions are higher than 100kV and 105kV, respectively. These results show a good agreement with the experiments. With these analyses and calculations, the oscillation mechanism including the oscillation phenomena has been understood physically and numerically. Suitable collector dimensions are proposed for 324MHz klystron in order to suppress the oscillations due to the backstreaming electrons completely. Furthermore, some discussions and directions for future investigations on the oscillations are presented.

Chapter 1

Introduction

This chapter briefly introduces the rf source for the linac of the Japan Hadron Facility (JHF), and the development of the 324MHz klystrons which are used as the rf source for the 200MeV low-β section of the JHF linac. Furthermore this chapter introduces the spurious oscillations occurring in these klystrons caused by the backstreaming electrons* from the collector. In order to understand the oscillations and to improve the klystron tubes, this thesis has a study on these spurious oscillations due to the backstreaming electrons from the collector, which originally come from the backscattering of the electron beam on the collector surface. According to the course of the oscillations, the study covers three parts: the production of the backscattered electrons on the collector surface, the formation of the backstreaming electrons into the drift tube, and the oscillation mechanism due to the interaction between the electrons and rf fields.

1.1 RF source for the Linac of JHF

The Japan Hadron Facility (JHF) project, which is a joint project of High Energy Accelerator Research Organization (KEK) and Japan Atomic Energy Research Institute (JAERI), consists of a 600MeV proton linac, a 3GeV rapid-cycling synchrotron (RCS), and a 50MeV main synchrotron [1-1]. The schematic view of JHF is shown in Figure 1-1. A 400MeV proton beam accelerated by a normal conducting linac is injected into the RCS; Another beam for an accelerator-driven nuclear waste transmutation system (ADS) is

* The term "backstreaming electrons" is used in this thesis instead of "back-going electrons" and "returning electrons" used in [1-7], [1-21], and [1-22].

further accelerated up to 600MeV by a 972MHz superconducting linac. The 400MeV linac comprises a 324MHz low-β section of 200MeV and a 972MHz high-β section from 200Mev to 400Mev. The 324MHz 200MeV section consists of a 3MeV radio-frequency quadrupole linac (RFQ), a 50MeV drift tube linac (DTL) and a 200MeV separated-type drift tube linac (SDTL). In the sections of energy above 200MeV, 972MHz annular-coupled structures (ACS) are used. The klystrons are used as the rf source for all of the accelerating structures.

At KEK, a construction of a 60MeV proton linac has been started as the low-energy front of the linac for JHF [1-2]. The scheme of the 60MeV proton linac is shown in Figure 1-2. The 60MeV linac, whose accelerating frequency is 324MHz, consists of a negative hydrogen ion source, a 3MeV RFQ, a 50MeV DTL, and a 60MeV SDTL.

For the 60MeV linac, five 324MHz modulating-anode klystrons are used as the rf-power source. The specifications of the klystrons are shown in Table 1-1. In order to control well both the amplitude and phase through the driving power, we operate the klystrons with an output power of 2.5MW, instead of the saturating power, 3MW, with an rf pulse width of 650μs and a repetition rate of 50pps. The maximum applied beam-voltage of the klystrons is 110kV with a pulse width of 700μs.

Table 1-1: Specifications of the klystrons

		Maximum rating	Working point
Operating frequency	MHz	324	
Peak output power	MW	3.0	2.5
Beam pulse width	μs	700	
RF pulse width	μs	650	
Repetition rate	pps	50	
RF duty	%	3.25	
Beam voltage	kV	110	102
Beam current	A	50	45
Mod. Anode voltage	kV	93	86
Beam perveance	μPer	1.37	
Efficiency	%	55	
Gain	dB	46	
Number of cavities		5	
Input type		N-type	
Output type		WR-2300	
RF window		Coaxial ceramic window	
Mounting configuration		Horizontal	
Focusing		Electromagnet focusing	

1.2 Development of the 324MHz klystrons and the purposes of the thesis

Concerning the frequency of the klytrons, 324MHz, is the lowest one in practical use at KEK, prior to these tubes, a high-power test model of a coaxial window for klystron output had been manufactured in 1998 [1-3]. Then, a beam-test-tube constituted of an electron gun and a collector had been made and tested in 1999 [1-4]. The results of the above tests had met the designed performance, and after the technical feasibility being confirmed, the developments of the first prototype klystron and the WR-2300 waveguide components [1-5] started in 1999. The main parameters of klystron tube #1 are shown in Table 1-2, and the picture of the klystron tube is shown in Figure 1-3.

Table 1-2: Main parameters of klystron #1

Beam voltage	110	kV
Beam current	44.2	A
Operating frequency	324	MHz
Drift tube radius	0.050	m
Beam radius	0.035	m
Driving power	12	W

Cavity No.	1	2	3	4	5
Cavity type*	1	1	2	1	-1
Q_e	1000	3000	2000	3000	20.0
R/Q (Ohm)	85	90	74	90	90
Gap distance (m)	0.016	0.042	0.025	0.042	0.040
Gap position (m)	0	0.85	1.20	1.95	2.50
De-tuned frequency (MHz)	0.2	0.9	317	20	0.25

*Cavity type: 1, 1st mode cavity; 2, 2nd harmonic mode cavity; -1, output cavity.

In June 1999, we started to have a high-power test of the klystron [1-6] using a test system shown in Figure 1-4. The structure configuration of the klystron output port consists of a loop coupler, a coaxial window, and a coaxial (WX-203)-to-waveguide(WR-2300) transition. The WR-2300 rectangular waveguide system consists of a directional coupler, a triple-stub tuner, a T-divider, and two T-bar type coaxial-to-waveguide transitions. Two water-cooling type coaxial dummy loads are used to absorb the rf power. The output power is measured by the directional coupler mounted in the rectangular waveguide system.

During the high-voltage processing of 324MHz klystron tube #1, unexpected oscillations were observed from both the output and input cavities when there was no driving input power [1-7]. These oscillations occurred when the beam voltage was 63~71kV or higher than 90kV, and had a frequency close to 324MHz. When a magnetic field was applied at the collector region to deflect the electron beam, the oscillations were partially suppressed. This indicated that the source of these oscillations was at the collector region. However, corresponding to the dimensions of the collector, there was no resonance of frequency close to 324MHz, so the oscillations were identified to be the result of the backstreaming electrons from the collectors.

The collector size was accordingly changed to evaluate its effect on the backstreaming electrons. The experiment results of modified klystron #1A with a reformed collector of an increased radius and length indicated that the oscillations disappeared in the low beam-voltage region and started from 95kV.

In order to suppress the oscillations, a new klystron named tube #2 was manufactured with a further increased collector length and a decreased Q_e of the input cavity from 1000 to 500. Both of these two factor-changes were expected effective to reduce the effects of the backstreaming electrons. In the high-voltage processing, again there were no oscillations in the low beam-voltage region, and the oscillations did not occur until the beam voltage was higher than 104kV. After the proper conditioning and selecting the focusing condition, we succeeded in suppressing the oscillation up to 110kV, namely our specification rating of the beam voltage, and successfully obtained an output power near 2.6MW with an efficiency of 52%. This klystron tube had been

operated successfully in the stable low-voltage region for the testing of the linear accelerator components, such as DTL and RFQ, of the KEK/JAERI Project.

In the process of the 324MHz klystron developments, it was found that the spurious oscillations and the instabilities due to the backstreaming electrons from the collector were the most serious problems encountered in the tubes. After our modifying the klystrons with larger collectors, the performances of the klystrons were improved, with the oscillations being suppressed gradually. But, sometimes an irregularity in the input-to-output power relations and an instability in the waveform of the output power envelop were still observed even in klystron tube #2. This meant that it was necessary to reduce the backstreaming electrons from the collector furthermore.

In order to improve the klystron tubes to get the desired performances, it is important to have a study on the spurious oscillations due to the backstreaming electrons from the collector. At first, it is necessary to understand the process of the backstreaming electrons coming out, and the numerical relations between the information of the backstreaming electrons and the collector conditions should be clarified. The backstreaming electron current and the energy distribution are expectedly carried out as function of the beam voltage, collector shape, and materials. On the other hand, it is essential to understand the oscillation mechanism and conditions due to the backstreaming electrons. Based on the relevant calculations of the oscillation conditions, the oscillation phenomena are expected to understand physically and numerically, such as the voltage region of the oscillations, which have been mentioned in the previous paragraphs. Furthermore, these analyses are very helpful for the development of the klystron, in which the spurious oscillations due to the backstreaming electrons are expectedly suppressed completely. This thesis focuses on the study of the spurious oscillations due to the backstreaming electrons from the collector, covering these fields described above in this paragraph.

1.3 Klystron oscillations due to the backstreaming electrons from the collector

As described in the previous section, recently we observed the strong oscillations in the 324MHz UHF klystrons developed at KEK, which occurred without any input drive power in the input cavity, and whose frequencies were close to the operation frequency [1-2]. After some investigations, these oscillations were finally concluded being caused by the backstreaming electrons from the collector. Generally, instability is one of the most serious problems encountered in linear microwave tubes, and many studies had been performed on the oscillations and instabilities in the microwave tubes including klystrons. For example, gun oscillations, drift-tube oscillations, cavity higher-order oscillations, oscillations associating with multipactoring, and collector oscillations had been reported. In many cases, the frequencies of the oscillations are different from the operation frequency. Concerning about the collector, sometimes spurious resonance induced by the spent beam in the collector can cause the serious oscillations or instabilities in the tube, and sometimes the backstreaming electrons from the collector can also involve the instabilities. In our 324MHz klystrons, it is the latter case, the oscillations being caused by the backstreaming electrons. This kind of oscillations had also occurred in other tubes, which were reported in reference [1-8]. Same as other kinds of the spurious oscillations, these oscillations are also undesirable since they cause the instabilities of both the amplitude and phase of the rf output to limit the klystron from reaching its designed performance. In order to develop a stable klystron avoiding these serious problems, it is important to understand the conditions for the oscillations occurring and to apply the stability criteria to the klystron to be designed and developed in the future. However, up to now there was no paper describing the mechanism of this kind of oscillations in detail. In order to make clear the oscillations and to improve the tubes, the mechanism of the oscillations are investigated in this thesis, including the backstreaming-electron generation from the collector and the oscillation conditions due to these backstreaming electrons.

For a collector of the linear microwave tube, various efforts had been

made to consider power dissipation, cooling method, collector potential depression, and so on [1-9] [1-10] [1-11]. Also, many textbooks and review papers [1-12] had described the backstreaming electrons from the collector, since they generally involved the instabilities and noise problems. Of course, similarly, the backstreaming electrons that are generated at the gap of the output gap through the large signal interaction between the beam and the cavity fields can also cause the spurious oscillations and instabilities. In the collector, many electrons are emitted when the spent beam impinges the collector wall, and some of them can return into the rf interaction region of the drift tube to cause the instabilities. It is also interesting that these backstreaming electrons are related with the abnormal local heating in the collector, since it is difficult to simulate the actual collector heating by using the usual beam trajectory codes. The problems involved with the backstreaming electrons had been studied intensively in the microwave tubes using the technology of the collector potential depression, especially the multistage depressed collector (MDC) [1-13]. Obviously, the backstreaming electrons should be eliminated as much as possible, since they can not only cause the instabilities, but also decrease the efficiency of MDC. There were many proposals to suppress them, such as using a different collector structure [1-14] and choosing a different material to minimize the secondary electrons. As for the collector material, typically the carbon material was applied to MDC for decreasing the true secondary electrons [1-15]. A study of MDC for a high power gyrotron [1-16] was reported, and we were interested in this report, since the operation voltage of this high power gyrotron was close to that of our klystrons, while in other MDC applications for the TWT and the klystron [1-17] [1-18], the operation voltages were quite low. That paper investigated not only the true secondary electrons but also the reflected electrons due to the atomic scattering in the materials by using a modified version of EGUN. In this thesis, we are much more interested in the backscattered electrons than in the true secondary electrons which many other authors were interested in, since the backscattered electrons are considered to contribute to our observed oscillations mainly. In order to simulate the backscattered electrons, the EGS4 (Electron-Gamma Shower) code [1-19] [1-20] well known in high-energy physics, which was developed at SLAC and KEK, is used. This code enables us to simulate the general interaction between the gamma rays, electrons and

materials, including the high energy particle generation, pair creation, positron generation, and so on. The true secondary electron process is not possible to be calculated in this code due to the limitation of the energy range of the code simulation, while the reflected electrons can be simulated. In this thesis, the numerical calculation results are carried out for backstreaming-electron current and the energy distribution as function of the collector conditions of the 324MHz klystrons.

On the other hand, there was no paper that had described the oscillation conditions due to the backstreaming electrons after they return into the interaction region with the microwave fields. It can be regarded that the backstreaming electrons generated in the collector and output cavity gap might cause the instability, since they can feedback the output signal to the input port in the amplification process. And many observed phenomena in the actual experiments, which have been mentioned in the previous section, such as the irregularity in the input-to-output power characteristics and the rapid amplitude-change of the output waveform, are considered to relate to the backstreaming electrons also. But it was too complicated to investigate the oscillations in the large signal dynamic process quantitatively by simulation. In this thesis, we analyze and calculate the contribution of the backstreaming electrons to the oscillations in the case of no driving power in the input cavity. The oscillation criteria are expressed mathematically, and the calculations are performed by using some programs. From these study, the oscillation conditions are expectedly understood.

In order to make clear the mechanism of the spurious oscillations caused by the backstreaming electrons from the collector, much effort should be put into the study of this kind of oscillations. This thesis focuses on the analyses and calculations for the oscillations, which occurred in the 324MHz klystrons. By these analyses and calculations, it is expected that the experiment phenomena can be explained, and some proper suggestions can be derived for the klystron to be developed in the future. According to the course of the oscillations, the study covers three parts, as shown in Figure 1-5. (1) The production of the backscattered electrons on the collector surface. The relation between the backscattered electrons and the primary electrons is investigated for different incident energy and angle. The energy distribution of the backscattered electrons is also obtained. (2) The formation of the

backstreaming electrons from the collector into the drift tube of the klystron. The effects to the backstreaming electrons from the beam voltages, collector shapes, and collector materials, are studied. (3) The oscillation mechanism due to the interaction between the backstreaming electrons and rf fields. The oscillation conditions are studied physically and numerically.

These three parts are solved in the following chapters respectively. At first, Chapter 2 describes the oscillation phenomena observed in the 324 MHz klystrons in details, including the experimental results of our investigations and countermeasures.

For the first and second parts of the oscillation study, some programs have been developed to simulate these electrons using the EGS4 Monte Carlo method. In Chapter 3, a comparison between the EGS4 simulation and the experimental data of the reflected electrons is presented. The validity of the EGS4 code is confirmed for the simulation of the electron backscattering process in the energy range corresponding to the applied voltage in the klystrons.

After confirmation of the code validity, Chapter 4 describes the backstreaming electron simulation from the klystron collector by using EGS4 code. At first the simulation method, in which three steps are included, is introduced for the backstreaming electrons from the collector. Then the results are also given. The backstreaming electron current and energy distribution have been obtained for different collector shapes [1-21]. The backstreaming electrons as function of various materials are also obtained.

In Chapter 5, the last part of the oscillation study is performed, including the analyses of the oscillation mechanism and conditions due to the backstreaming electrons with no drive input power, and calculations of the oscillation conditions using the backstreaming current derived before [1-22]. Obviously, the backstreaming electrons can carry an rf signal from the output cavity to the input cavity; it results in a formation of a feedback loop inside the tube. From the feedback theory, if an input cavity voltage could be regenerated by the backstreaming electrons, oscillations will occur. Thus the oscillation conditions can be expressed by the complex product of the klystron voltage-gain and the feedback coefficient caused by the backstreaming electrons: (1) the amplitude of the product should be larger than unity, and (2) the phase of the product should be zero or integral times of 2π. Based on the calculations

of the oscillation conditions, the oscillation regions of beam voltage for the 324MHz klystrons have been worked out. A good agreement between experiments and calculations is shown. With these analyses and calculations, the oscillation mechanism including the oscillation phenomena has been understood physically and numerically. Suitable collector dimensions are proposed for 324MHz klystron in order to suppress the oscillations due to the backstreaming electrons completely.

Finally, Chapter 6 concludes the thesis with the successful analyses and calculations on the oscillations due to the backstreaming electrons.

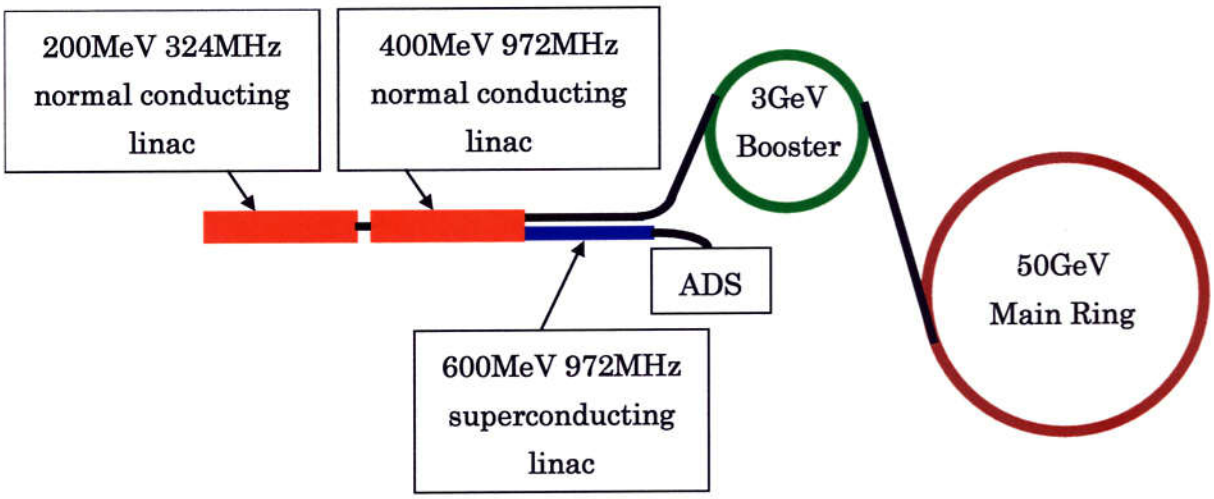

Figure 1-1: Schematic view of JHF.

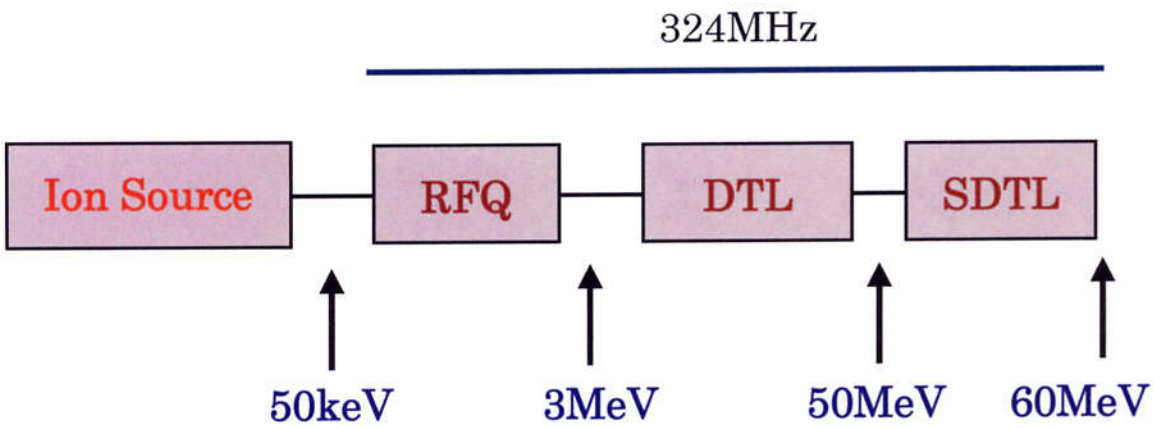

Figure 1-2: Scheme of the 60MeV proton linac.

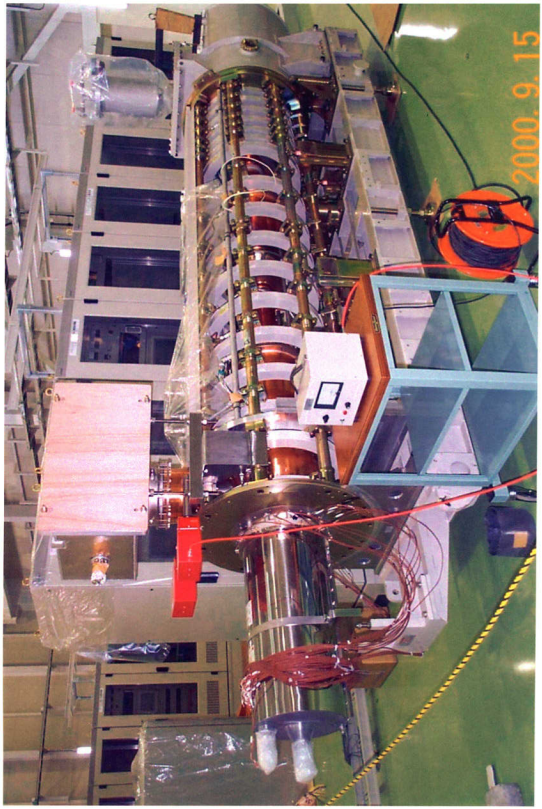

Figure 1-3: Picture of the 324MHz klystron tube.

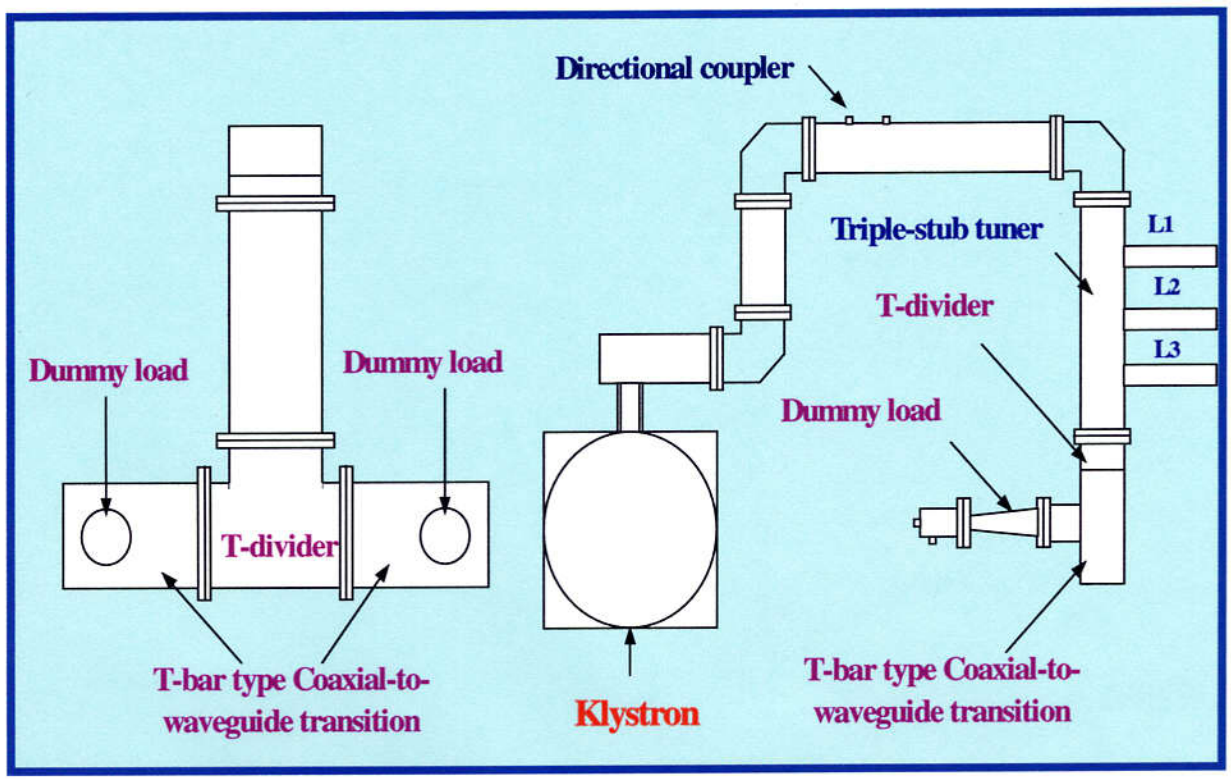

Figure 1-4: Setup of the klystron test system.

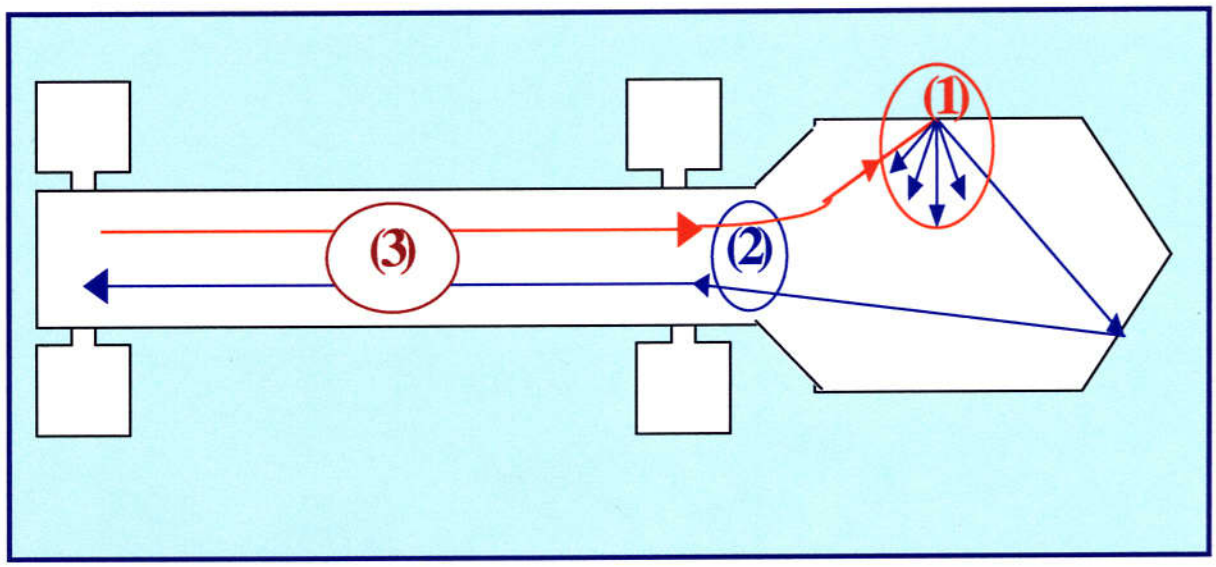

Figure 1-5: Oscillation study including three parts:
(1) Production of the backscattered electrons on the collector surface,
(2) Formation of the backstreaming electrons into the drift tube,
(3) Oscillation mechanism due to the backstreaming electrons.

Chapter 2

Oscillation Phenomena in the 324MHz Klystrons

The KEK/JAERI Joint Project, currently proposed accelerator complex, provides a high-intensity proton accelerator facility with various beams for serving the up-to-date research and application. The 324MHz UHF klystrons have been developed at KEK as the rf source for the proton linear accelerator, the injector of this accelerator complex [2-1]. This chapter describes the phenomena of the oscillations occurring in the 324MHz klystrons.

In June 1999, the first prototype of 324MHz klystron tube was manufactured, and the tube test was started. At first a high-voltage processing was performed for tube #1. However, by observing the signal from the directional coupler for the klystron output, it was found that unexpected oscillations occurred independently of the rf driving power when the beam voltage was applied to 63kV. The later experiments showed that the oscillations were observed from both the output and input cavities when the beam voltage was 63~71kV or larger than 90kV. The waveforms of the oscillations under the different beam voltages are shown in Figure 2-1. It can be seen that the oscillations started at 63kV, and with the voltage rising to 68.5kV the oscillation power gradually intensified and the time delay of the oscillation gradually decreased from 120 to 40μs. However, with the voltage increasing further, the time delay abruptly increased again, namely the oscillation pulse declined, and finally the oscillations disappeared at 72kV. In the voltage region of 72~89kV, there were no oscillations. Above 90kV, the oscillations occurred again, and the oscillation power increased with the beam voltage; also the time delay decreased to shorter than 20μs. The oscillations had a frequency region of 323~325MHz, which is around the operating frequency of the tube, 324MHz. Figure 2-2 shows the frequency spectra of the oscillations under the different beam voltages. The oscillation power was

dependent on the beam voltage, and sometimes it could be around 400kW observed from the output cavity. The experiment result of the oscillation power versus the beam voltage is shown in Figure 2-3. The delayed time of the oscillation waveform also depended on the beam voltages, varying among 5μs ~650μs. The time delay as function of the beam voltage is shown in Figure 2-4.

The investigation for identifying the oscillation source had been conducted by varying the possible parameters of the klystron. Low voltage-band of the oscillations was completely suppressed when an axially asymmetric weak magnetic field was applied at the collector entrance region. High voltage-band of the oscillations could not suppressed by that magnetic fields, however the voltage threshold of the oscillations got a little higher than before. The applied magnetic field was generated by utilizing the several permanent magnets, which were used for an ion pump. The sketch of the side-view of the magnets attached at the collector region is shown in Figure 2-5. These experiments indicated that the collector region might be the source of the oscillations. Therefore, there are two possible reasons of the oscillations. One is the collector resonance. From the diameter of the collector, $D_c = 0.13$m, the resonant frequency of TM_{010} mode is:

$$f_r = 2.998\times10^8 / (1.306\ D_c)$$
$$= 1.77\text{GHz} \qquad (2.1)$$

By the simulation using SUPERFISH, the lowest resonant frequency of the collector is also around 1.8GHz. Since the resonant frequency is much higher than 324MHz, the oscillations were not caused by the collector resonance. The other possibility is the backstreaming electrons from the collector. If the backstreaming electrons exit, there is a coupling between the output and input cavities to form a feedback loop. Since this klystron was the UHF band klystron, the diameter of the drift tube derived from the cut-off frequency was much larger than the required cathode diameter. In order to match with the converged beam from the cathode with the realistic focusing fields, the diameter of the drift tube beam was slightly small at the anode region where the beam was converged, and it was relatively large at the downstream of the input cavity where the beam is also expanded to a larger diameter. Also, the diameter of the collector was slightly larger than that of the drift tube since the required thermal rating was not so large. Thus, some of backscattered electrons in the collector can easily return into the drift tube and cause the

spurious oscillations in the klystron. Therefore, after the above investigations, the oscillations were identified to be the results from the backstreaming electrons generated at the klystron collector.

After the other various surveys, it was found that adjustments such as the variation of the focusing field and the impedance of the stub tuner connected at the input cavity port were a little effective to suppress or change the oscillation status, if they led to lowering the amplification gain of the klystron. By attaching some solenoid coils at the collector region to change the beam focusing status or deflect the electron motions, the oscillations can be apparently suppressed at some beam-voltage region. When an input power was fed into the input cavity, the oscillations still occurred, and the low-voltage band of the oscillations was generally wider than before. For example, a typical voltage region of the oscillations in klystron tube #1 was about 63~82kV and higher than 90kV. Besides, the input-to-output power characteristic curve showed an irregularity with many rapid steps, and the output waveforms showed unstable in the amplitude. They are all considered to be the effects of the backstreaming electrons.

If the backstreaming electrons were generated in the collector and caused the oscillations, simple qualitative consideration gave that the small collector or the small ratio of the diameter of the collector to that of the drift tube increased the returning electrons. Therefore, a collector with an increased diameter and length had been replaced with the old one. The test result of this modified tube #1A showed that the low voltage-band of the oscillations disappeared and the voltage threshold of the high band of the oscillations got higher up to 95kV. It was not possible to suppress the oscillations completely in klystron #1A. Then klystron #2 with a further increased collector length and a decreased Q_e of the input cavity was manufactured. Here the enlarged collector dimension was expected to reduce the backstreaming electron current from the collector, and the decreased Q_e was aimed at a low gain of the klystron amplification process. The test of klystron #2 gave the result that the voltage threshold increased up to 104kV, and after the proper conditioning and selecting the focusing condition, we succeeded in suppressing the oscillation up to 110kV, namely our specification rating of the beam voltage. The shapes of the three klystron-collectors are shown in Figure 2-6 and the oscillation regions for the three tubes are summarized in Table 2-1.

Table 2-1: Collector shapes and experiment results of the beam voltage regions of the oscillations

Tube	Collector radius (cm)	Collector length (cm)	Beam voltage regions of the oscillations (kV)
#1	6.5	62.4	63<V<71,V>90
#1A	11.5	92.4	V>95
#2	11.5	122.4	V>104 or higher

However, in the amplification process when a drive power was fed into the input cavity, we could not obtain the complete stable operation at the rating beam voltage even in klystron #2. Still the irregularity in the input-to-output power relations and the unstable waveform in the output power envelope were observed. This meant that much more effort should be put into the study to eliminate the backstreaming electrons. These studies are described in the following chapters.

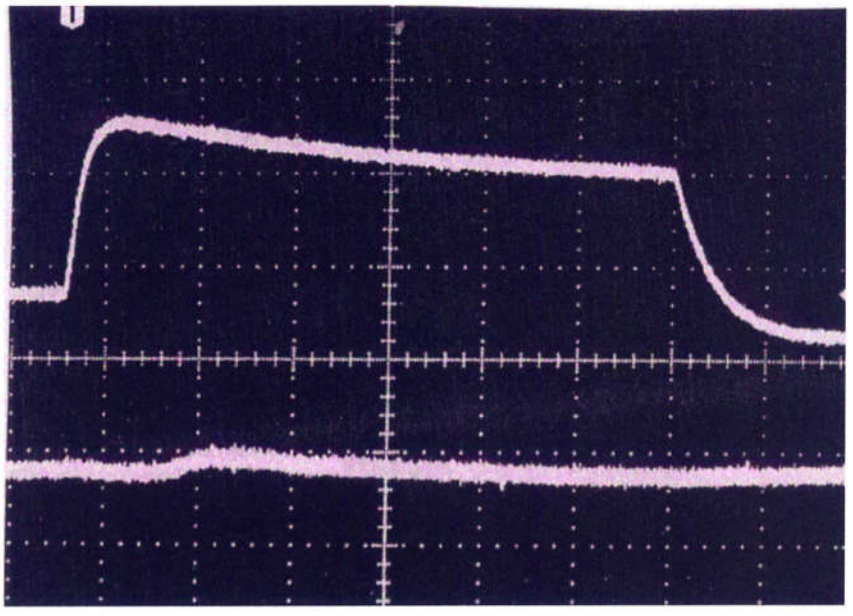

(a) 63kV

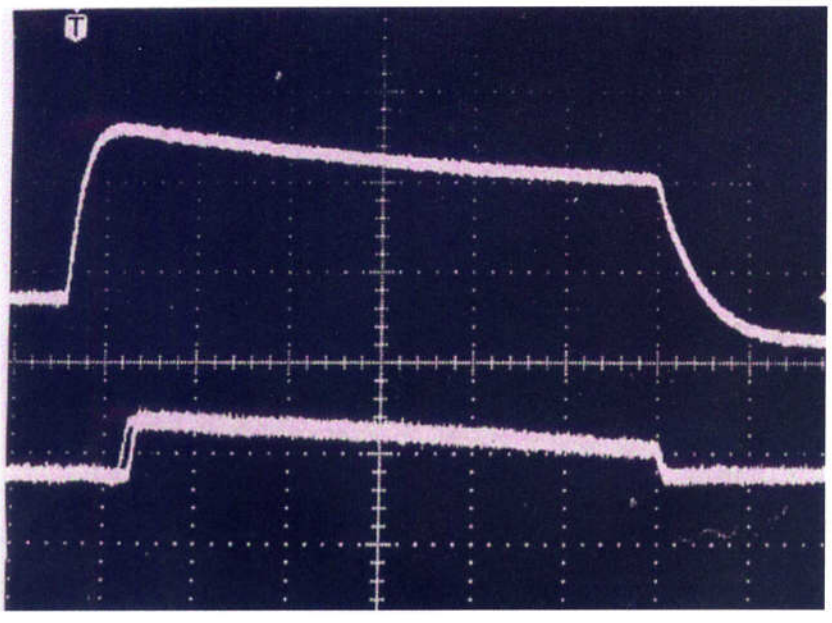

(b) 64kV

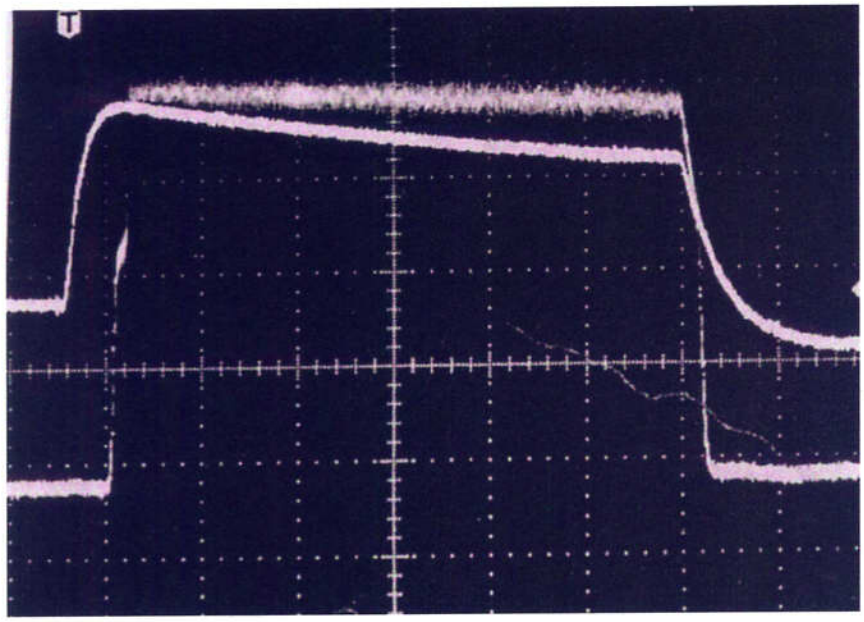

(c) 68.5kV

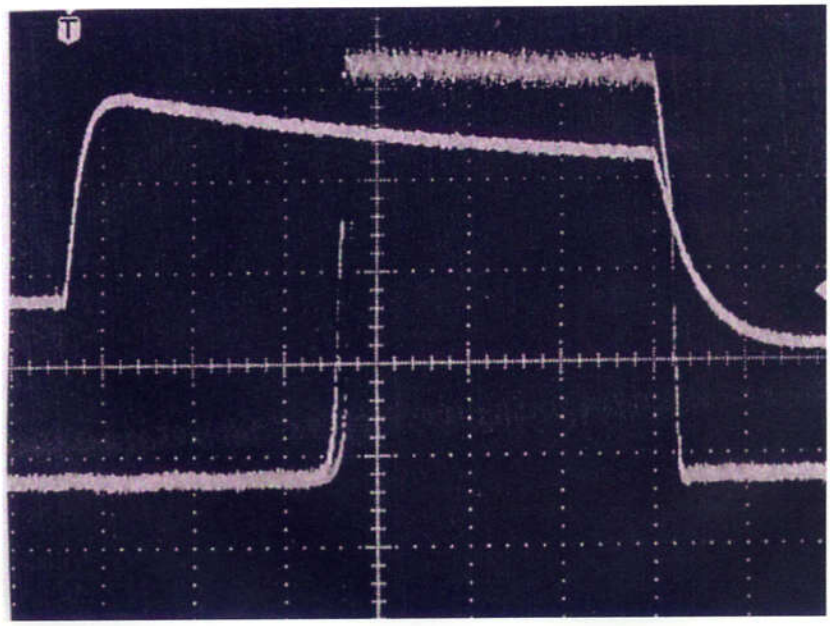

(d) 70kV

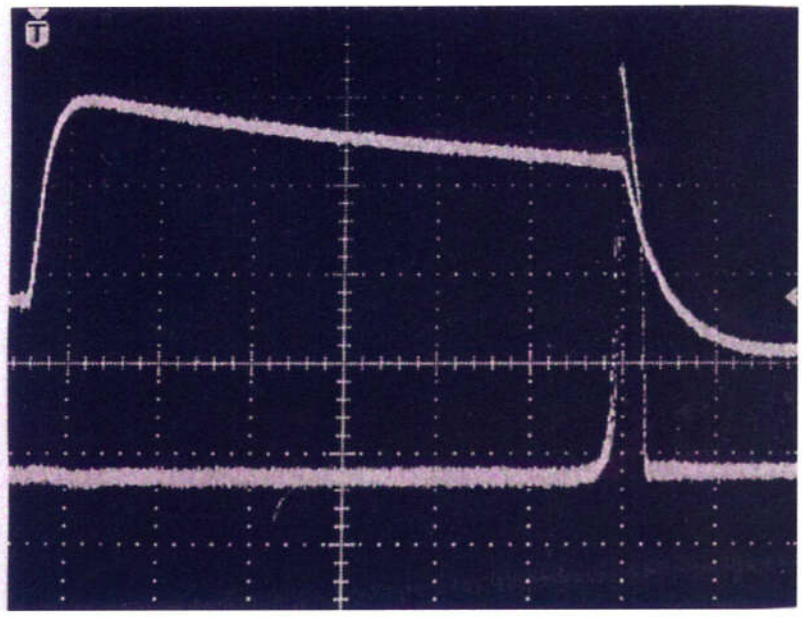

(e) 71kV

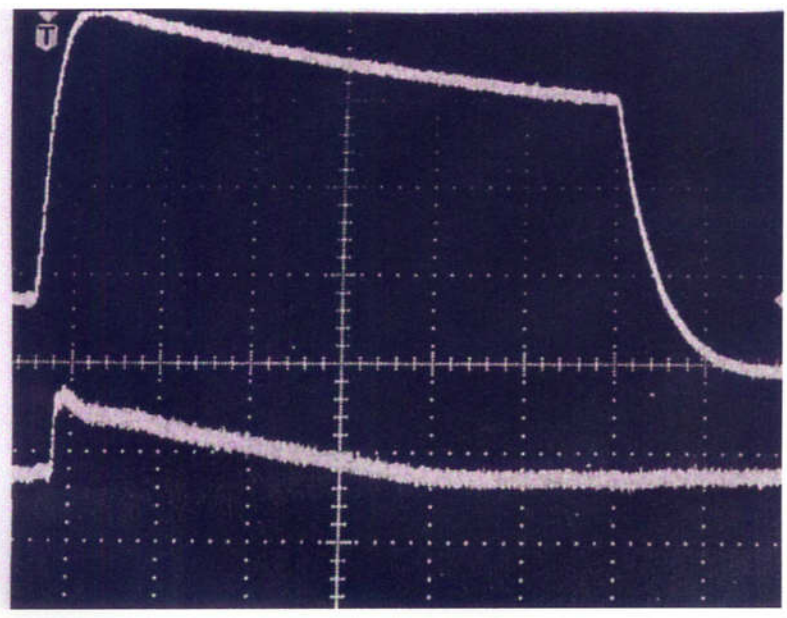

(f) 91kV

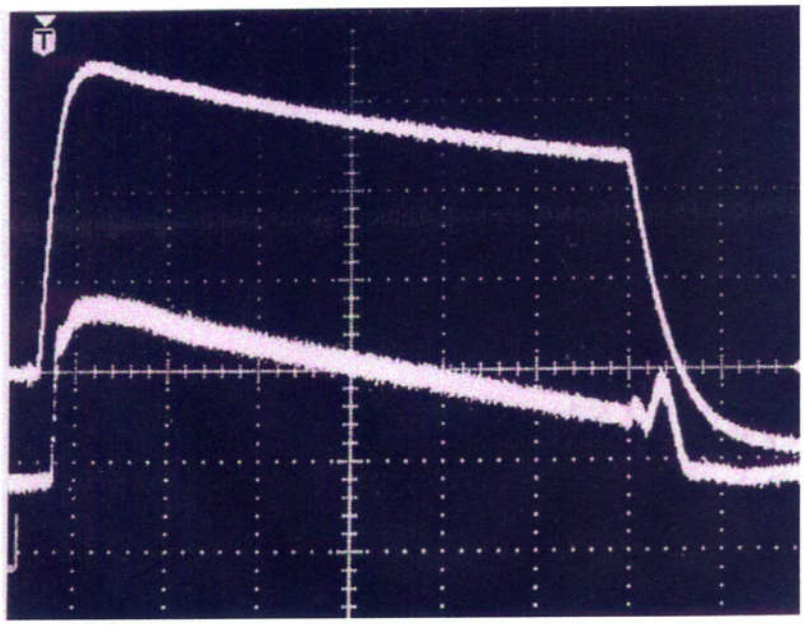

(g) 93kV

Figure 2-1: Waveforms of the oscillations under the different beam voltages in 324MHz klystron #1. (Upper, beam voltage; Lower, oscillations; Time, 100μs /div)

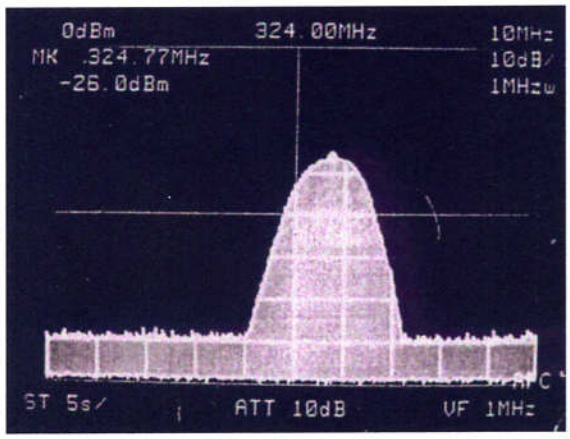

(a) 68kV

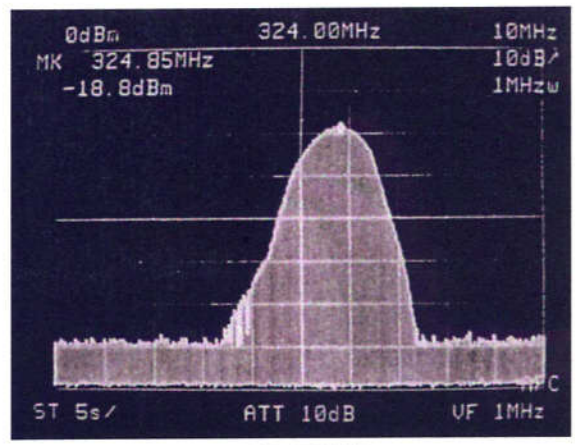

(b) 70kV

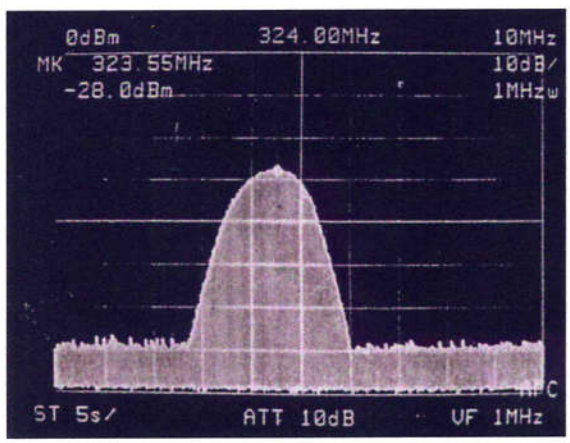

(c) 91kV

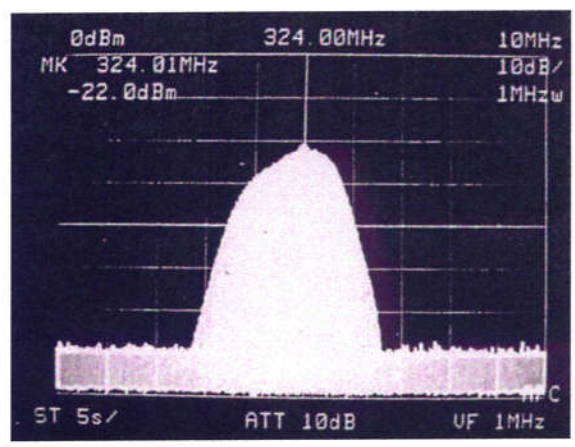

(d) 92kV

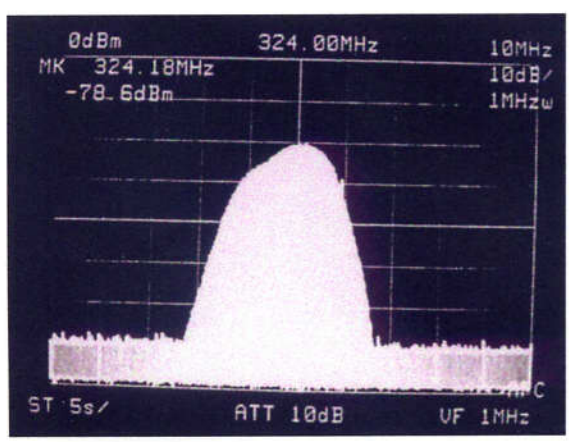

(e) 93kV

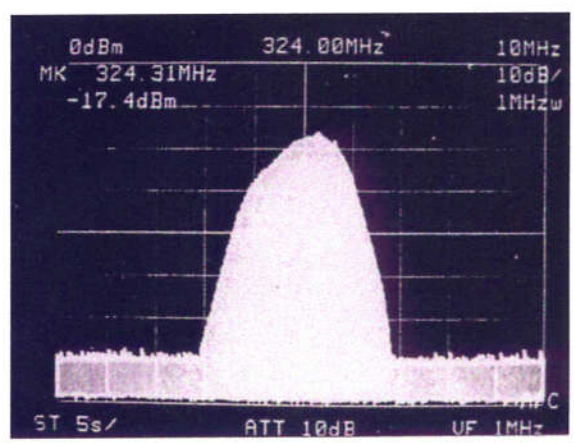

(f) 96kV

Figure 2-2: Frequency spectra of the oscillations under the different beam voltages in 324MHz klystron #1. (Center, 324MHz; Span, 10MHz)

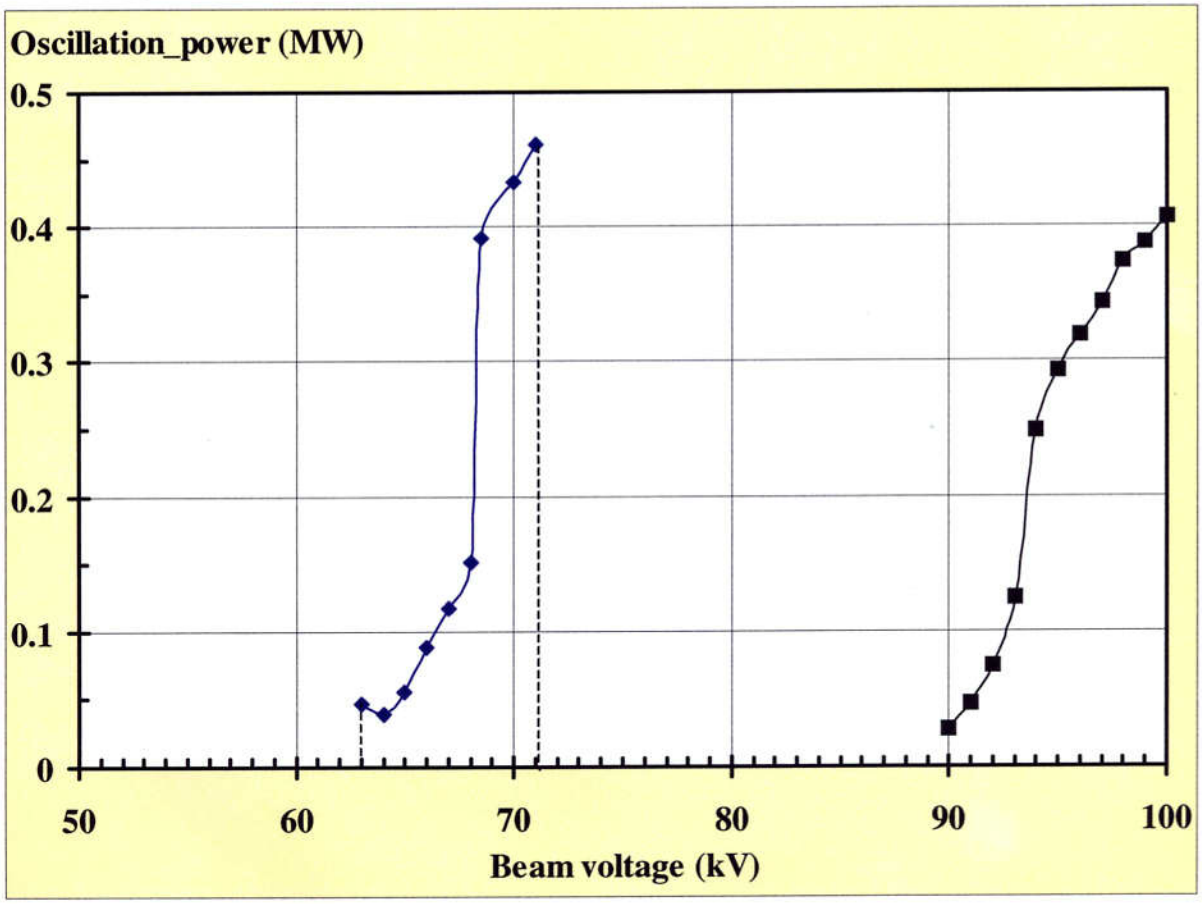

Figure 2-3: Oscillation power versus the beam voltage for 324MHz klystron #1.

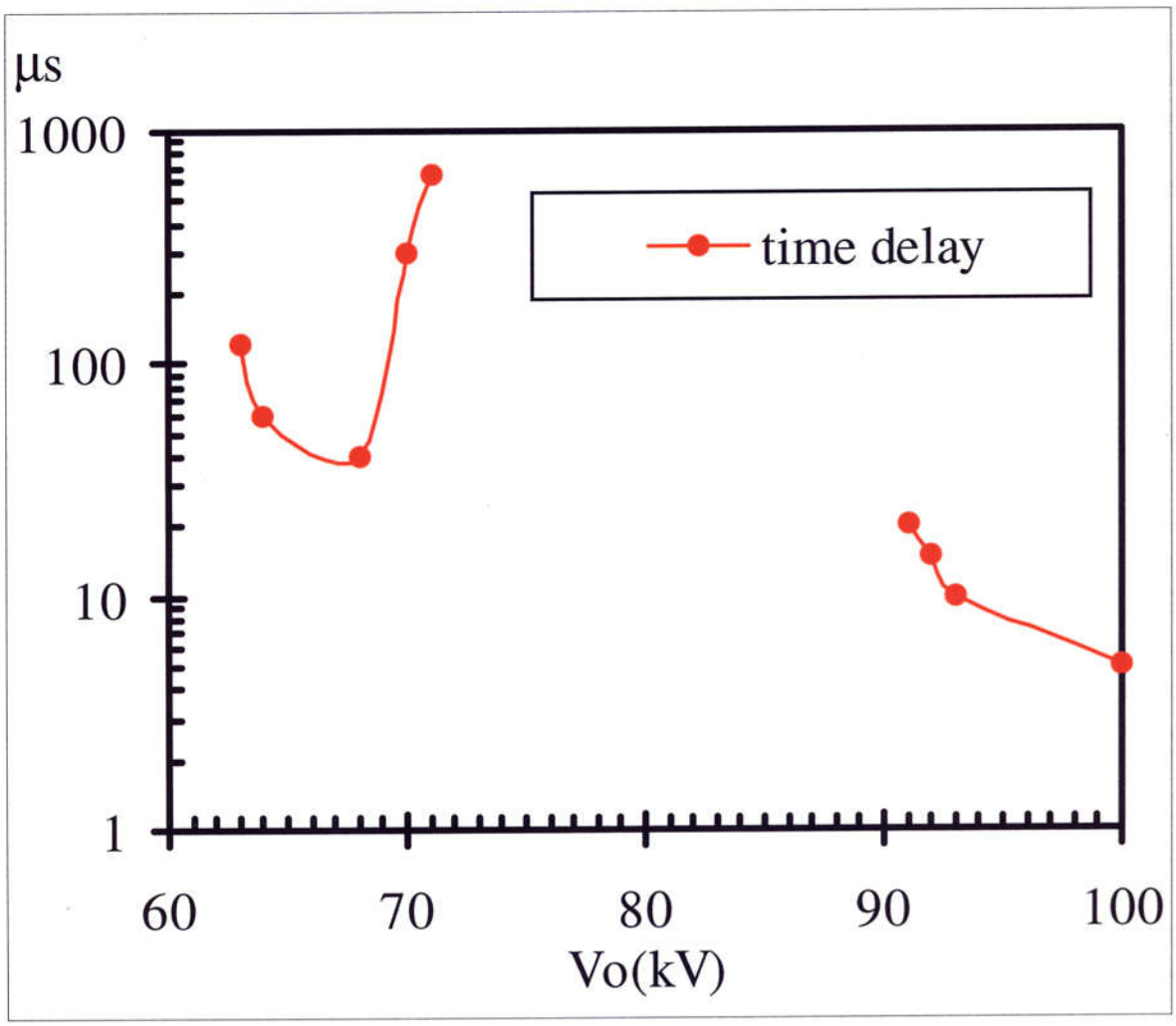

Figure 2-4: Time delay of oscillation waveform as function of the beam voltage for 324MHz klystron #1.

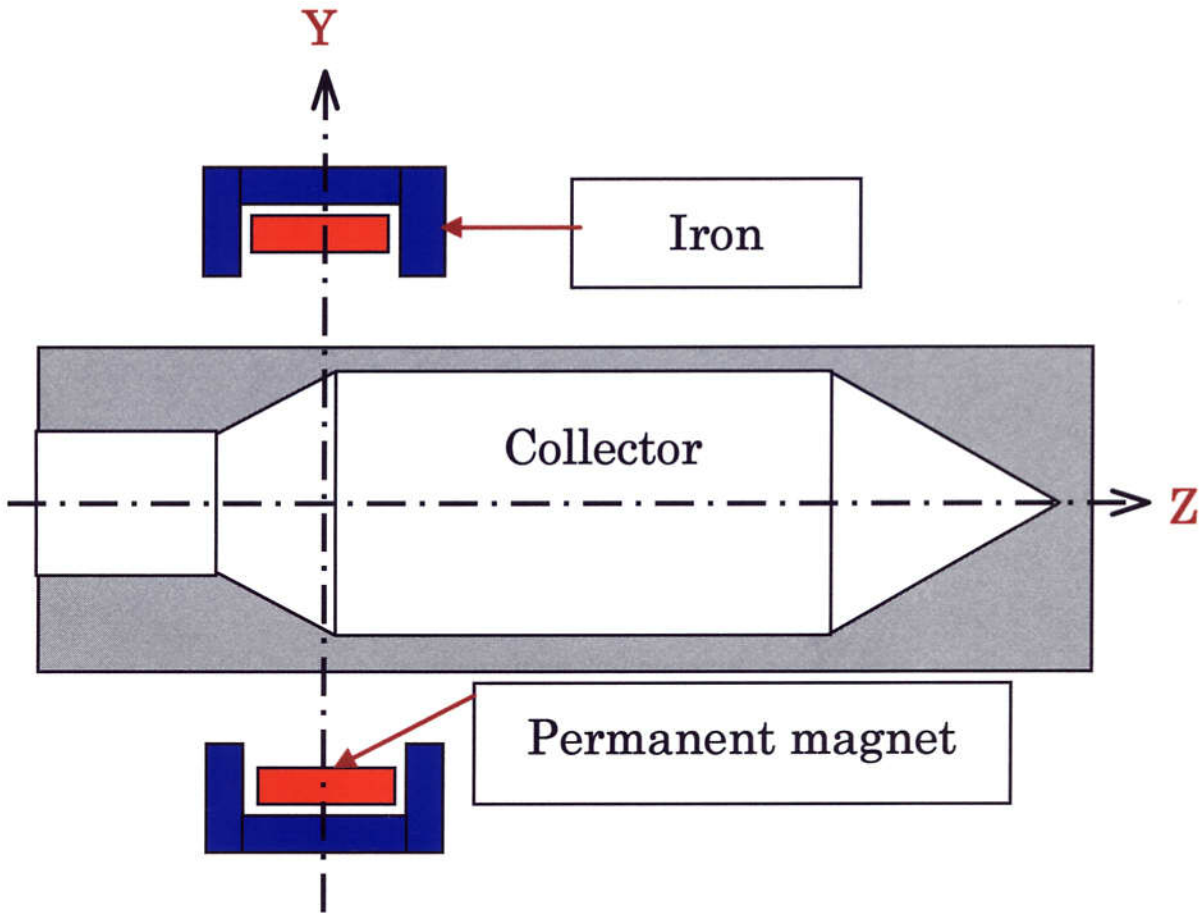

Figure 2-5: Permanent magnets attached at the collector region of klystron.

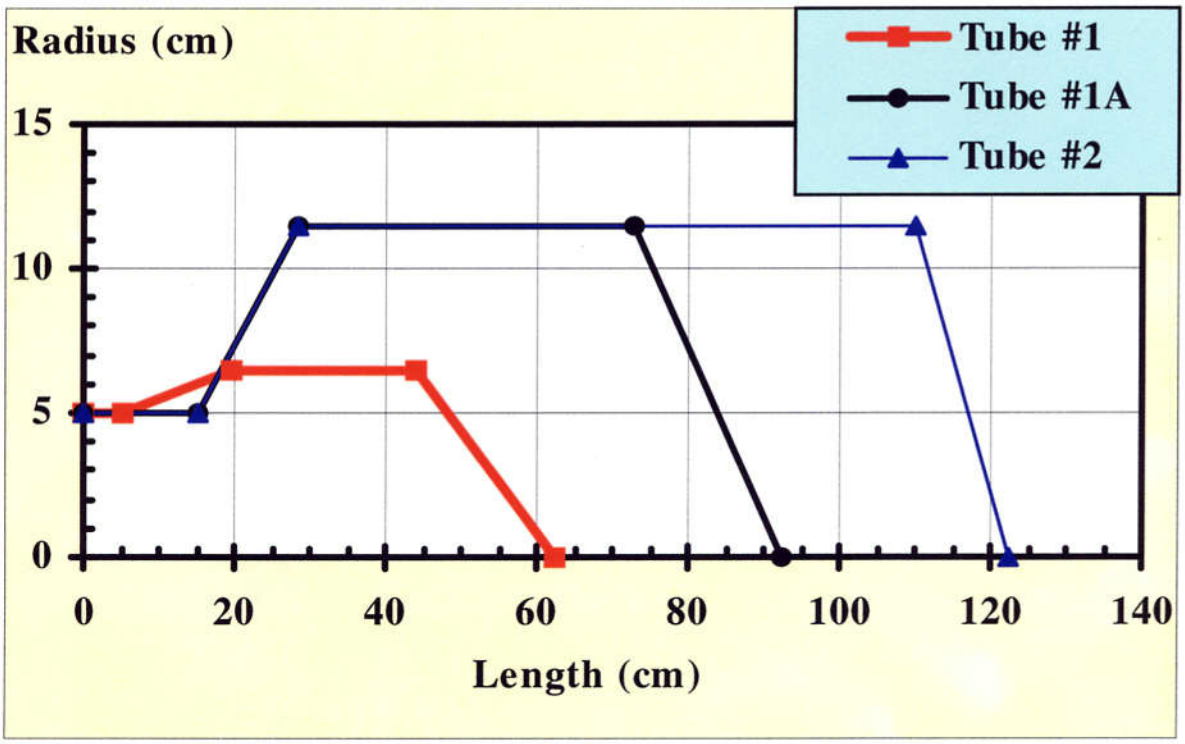

Figure 2-6: Collector shapes of tubes #1, #1A, and #2.

Chapter 3

Comparison between EGS4 Backscattering Simulations and Experiments

3.1 Introduction

As described in the previous chapter, the oscillation source was identified to be the backscattered electrons that return from the collector into the drift tube.

After electrons bombarded a material surface, the total emitted electrons from the surface are generally divided into two classes. The first class is called the true secondary electrons. They initially exist in the material, and escape from the material after getting enough energy from the impacting primary electrons. The energies of these true secondary electrons emitted from the material are very small and less than approximately 50eV. There are many experimental and theoretical works on the secondary electrons. For example, J. R. M. Vaughan [3-1] derived an empirical formula for the secondary electron emission yield, which provides a complete description of the yield as a function of incident energy and angle. The other class consists of the backscattered primaries, which are scattered from the material with energies varying continuously from the primary electron energy to lower energies; they have much higher energies than that of the true secondary electrons. For the elastically scattered electrons at the relatively high energies, the angle of incidence is equal to the angle of reflection [3-2]. For the inelastically scattered electrons, the backscattered coefficient has been estimated analytically [3-3].

In this thesis, we are interested in those electrons that will contribute much to the oscillations. Since the applied beam voltage of the klystron is usually a few of ten or hundred keV. In the 324MHz klystrons, the rating

beam voltage is 110kV. For the true secondary electrons, they are of very low energies and quite different from the forward beam. For example, the velocity is only about 0.01 times of the light velocity for the typical secondary electrons of 30eV energies, and for the klystron beam under 110kV, the electron velocity is 0.57 times of the light velocity. Thus, their transit time between the input cavity and output cavities is also quite different. Considering the bunching process in the klystron, unlike the high-energy forward-beam, those low-energy secondary electrons cannot form a bunch due to the low velocity and long transit time. They will arrive at the input cavity at an arbitrary moment comparing with the rf cycle. So, what we are concerning are those backscattered electrons from the primary electrons, which have the energies corresponding to the klystron applied voltage from a few keV to several hundred keV, and can return into and pass through the drift tube with the externally applied focusing fields.

On the other hand, for the primary electrons of energy higher than 10keV, the number of their produced secondary electrons is much smaller than that of the produced backscattered electrons. The formula of the secondary yield coefficient as function of primary energy [3-4] is

$$\frac{\delta}{\delta_m} = 1.85F\left[\frac{0.92E_{po}}{E_{pm}}\right] \tag{3.1}$$

where E_{po} is the primary energy. For copper, δ_m=1.3 and E_{pm}=600eV. Function F(x) is

$$F(x) = e^{-x^2}\int_0^x e^{y^2}dy \tag{3.2}$$

For $x \ll 1$, $F(x) \approx x$; For $x \gg 1$, $F(x) \approx 0.5/x$.

Thus, δ = 0.08 at E_{po} = 10keV; δ=0.008 at E_{po} =100keV. While the backscattering yield coefficient is about 0.3 in this energy range. Therefore, for higher primary energies, the secondary electrons become insignificant comparing with the backscattered electrons.

For this decade, the EGS4 Monte Carlo method [3-5] [3-6] has enabled us to simulate the electrons interacting with the collector material in the energy range from a few keV to several hundred keV; this energy range corresponds to the applied voltage of the klystron. This code does not calculate the true

secondaries, while we don't need to consider them for our oscillation study as mentioned above. Prior to the simulation of the backstreaming electrons from the klystron collector, which will be described in Chapter 4, it is necessary to confirm the code validity for the backscattered electrons in a bulk material by comparing the calculation with the experimental process. E. J. Sternglass [3-7], E. H. Darlington [3-3], and G. Neubert [3-8] had made a detailed investigation of the backscattering of the primary electrons with the energy range of our interest; EGS4 simulation results are compared with these experiments. Comparison between the calculation results and experiment results indicates that they agree well.

3.2 Experiments

Concerning the klystron collector, we are interested in the electrons in the energy range from a few keV to several hundred keV. Many scientists had measured the backscattered electrons in this energy range. The experimental concept of electron backscattering is shown in Figure 3-1. After the electrons bombarded a material surface, some of the electrons are backscattered, and the secondary electrons are also created. A typical energy distribution of total emitted electrons from the material surface is shown in Figure 3-2. Most of secondary electrons have energies less than 50eV. Those electrons whose energies are greater than 50eV are mainly back-scattered electrons, which have a wide energy distribution. In this thesis, we are interested in those back-scattered electrons with energies above a few keV. Since the energies of the secondary electrons are less than 50eV, we could neglect these effects.

Here, the backscattering coefficient (η) is generally defined as the ratio of the number of backscattered electrons (n) to that of incident electrons (N).

$$\eta = n / N \tag{3.3}$$

The experiment results show that the backscattering coefficient is essentially independent of the incident energies in our concerning range [3-7]. For different materials, η increases with the atomic number Z, as shown in Figure 3-3 for normal incidence [3-3] [3-8]. For some typical materials, Carbon (Z = 6), Aluminum (Z = 13), Iron (Z = 26), Copper (Z = 29), and Tungsten (Z = 74), the

backscattering coefficient is 0.057, 0.15, 0.28, 0.31, and 0.50, respectively. As the incident angle increases towards grazing incidence, the backscattering coefficient increases rapidly. Figure 3-4 shows the incident angle dependence of the backscattering coefficient for copper [3-3] [3-8]. It indicates that the backscattering coefficient increases from 0.31 to 0.74 with the incident angle from 0 to 80 degrees. For incidence with a small angle to normal incident, η is inversely proportional to the cosine of the angle.

$$\eta = \eta_0 / \cos(\theta), \qquad \text{for } \theta < 50\text{degrees} \tag{3.4}$$

where η_0 is the backscattering coefficient at normal incidence, and θ is the incident angle. This can be understood qualitatively, because for large-angle incidence, the primary electrons do not penetrate the material as much, so it is easier for them to escape from the material. The energy distribution of backscattered electrons [3-3] [3-7] for normal incidence is shown in Figure 3-5. In the figure, the energies of backscattering electrons are normalized by the incident energy. The experiments results showed that the backscattered electrons had energies continuously varying from the incident energy to lower energies with an energy peak located around 0.8~0.85.

3.3 EGS4 backscattering simulations

For this decade, an electron backscattering process can be simulated using the EGS4 code. Before applying EGS4 to a klystron, it is necessary to confirm the code validity by comparing the calculation with experiments for the fundamental process. Thus, the EGS4 code is applied to simulate the electron backscattering from a copper plate thicker than 1mm.

The flow control of simulation for electron backscattering using EGS4 is shown in Figure 3-6. At first the material data are created using PEGS4 for a specified material and an energy boundary. Then a so-called user code is written by using MORTRAN [3-9] in order to use the EGS4 code. The incident initial conditions including electron energy, incident angle, and incident electron number will be used as the input of the user code. The geometry of the material is coded in the subroutine called HOWFAR. The output information is specified in the subroutine called AUSGAB. Here the information of

backscattered electrons, including their energies and angles, is outputted.

The trajectories of incident and backscattered electrons have been plotted by using a FORTRAN90 program. Figure 3-7 shows two examples of the trajectories of incident and backscattered electrons.

It is well known experimentally that the backscattering coefficient is essentially independent of the primary energy [3-7]; the simulations reproduced this successfully. Figure 3-3 shows the simulation results of backscattering coefficient as a function of atomic number of material for normal incidence. The curve is very close to that of the experiments. For Iron and Copper, the simulation results are almost the same as the experimental data. For other material, such as Carbon, Aluminum and Tungsten, the backscattering coefficient (η) of the simulation results is slightly lower than the experimental data. Figure 3-4 gives the simulation results of the backscattering coefficient as a function of the incident angle. For normal incidence on copper, a common collector material, the backscattering coefficient is equal to 0.3 for a wide range of primary energy, and the simulation gave the same value. The backscattering coefficient increases with the incident angle. Again, the simulation results indicates the same feature as the experiments. The curves of simulations and experiments agree very well. The calculated energy distributions of backscattered electrons for normal incidence are shown in Figure 3-5. A continuous distribution is also shown with a energy peak of 0.8, which is close to the experimental results. Therefore, from Figure 3-3, Figure 3-4, and Figure 3-5, it is indicated that the simulation results of backscattered electrons agree well with the experiment results. From these studies, it is concluded that the EGS4 code is sufficiently reliable to be applied to backscattered electrons from a klystron collector.

3.4 Discussion of simulation error

Considering the simulation error, the question is described as the following:

For one simulation using N incident electrons, supposing there are n output electrons, which are backscattered electrons in this case, as the

simulation result under some specified conditions, then how to evaluate the accuracy of backscattering coefficient η?

From the Central Limit Theorem in statistics, if x is a random variable with a mean μ and a standard deviation σ, the sample mean $\bar{x}$ for random samples of a size N has the standard deviation

$$\sigma_{\bar{x}} = \frac{\sigma}{\sqrt{N}} \tag{3.5}$$

For one incident electron, if there is an output electron, x = 1. Otherwise x = 0, in case of no output electron. So, for N incident electrons, if there are n output electrons, sample mean is:

$$\begin{aligned} \bar{x} &= \mu \\ &= \Sigma x / N \\ &= n / N \end{aligned} \tag{3.6}$$

The standard deviation of x is:

$$\sigma = \sqrt{\frac{\Sigma(x-\mu)^2}{N}} \tag{3.7}$$

Therefore for the sample mean, namely the backscattering coefficient η here, the standard deviation can be evaluated by

$$\begin{aligned} \sigma_\eta &= \frac{\sqrt{\frac{\Sigma(x-\mu)^2}{N}}}{\sqrt{N}} \\ &= \sqrt{\frac{\eta(1-\eta)}{N}} \end{aligned} \tag{3.8}$$

We define the relative error of η as

$$\delta\eta = \sigma_\eta / \eta \tag{3.9}$$

and it can be expressed in,

$$\delta\eta = \sqrt{\frac{1}{N}\left(\frac{1}{\eta} - 1\right)} \tag{3.10}$$

Obviously, δη decreases with both N and η increasing. For example, if one simulation uses N=10,000 electrons normally incident on copper, and obtains

: $\eta \approx 0.3$, the error is about 0.015. If N=100,000 electrons are applied in another simulation, the error is reduced to 0.0046.

This method of error evaluation for one simulation results have been proved by the standard deviation for many times of simulations. Figure 3-8 shows the backscattering coefficient and its standard deviation for ten simulations. It indicates that the standard deviation obviously decreases with applied sample size (N) in the simulations. Figure 3-9 shows error evaluation for one simulation and standard deviation for ten simulations. The two curves are very close. It indicates that the error of one simulation-result can be evaluated by the incident electron number and backscattering coefficient using the formula (3.7).

By using formula (3.9) of relative error, we can also evaluate how large of N is necessary in order to get a specified relative error, for example 1%.

From the expression

$$\sqrt{\frac{1}{N}(\frac{1}{\eta}-1)} < 1\% \qquad (3.11)$$

if $\eta \approx 0.3$, N must be large than 23,300. In actual simulations, usually 100,000 incident electrons are used, so that the relative error of the backscattering coefficient is kept within 1%.

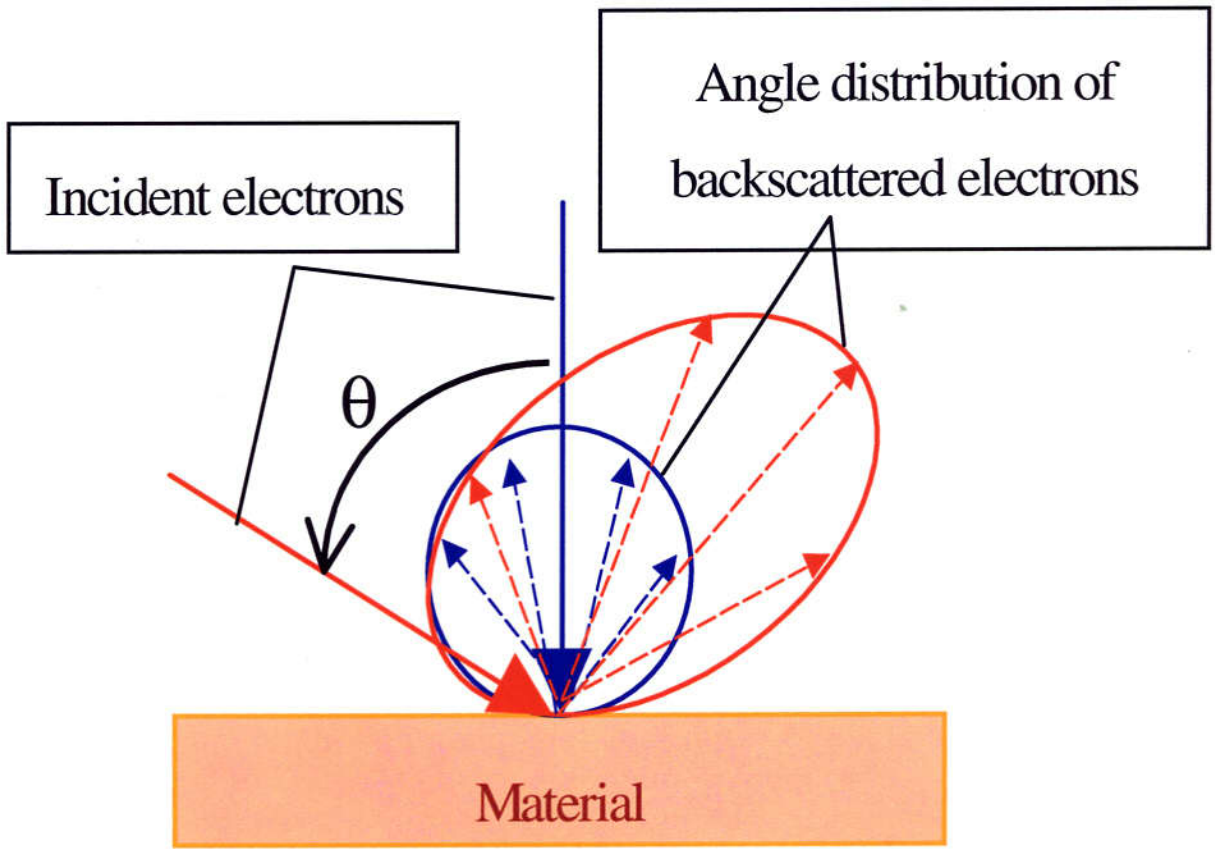

Figure 3-1: Sketch of electron backscattering on a plate.

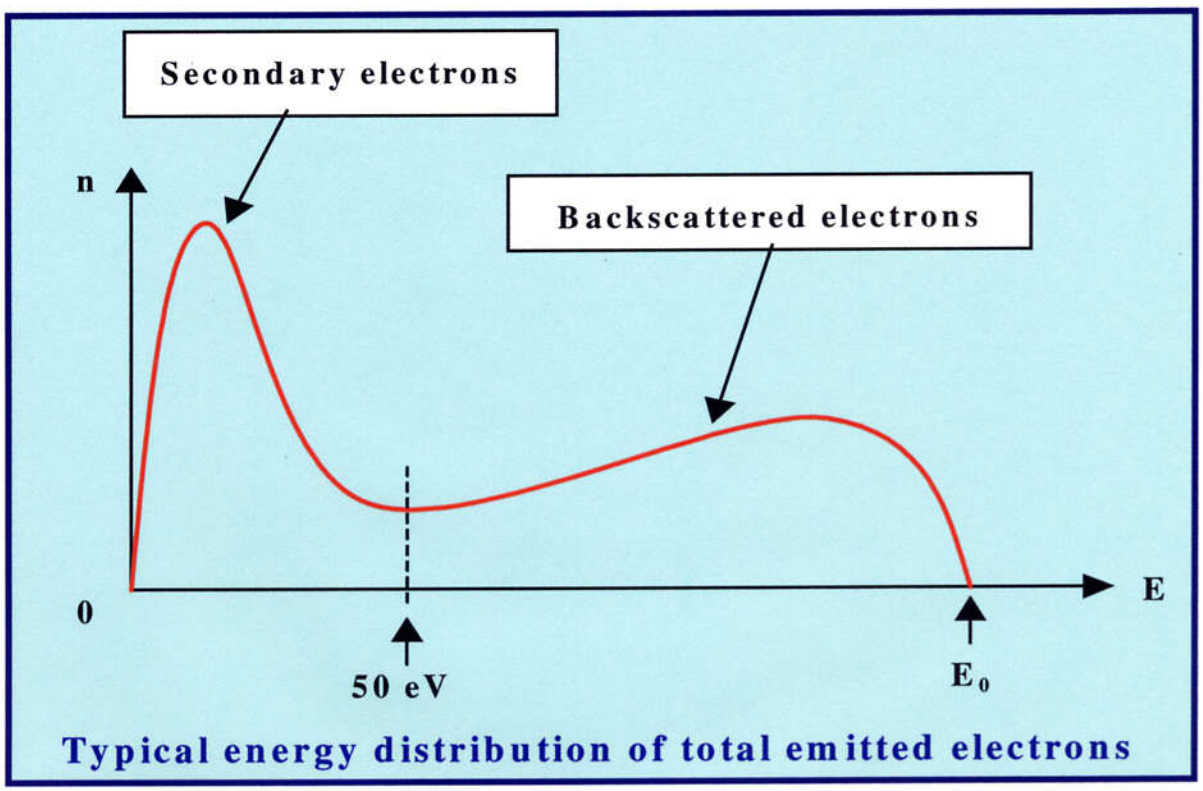

Figure 3-2: Typical energy distribution of total emitted electrons from a material surface bombarded by primary electrons.

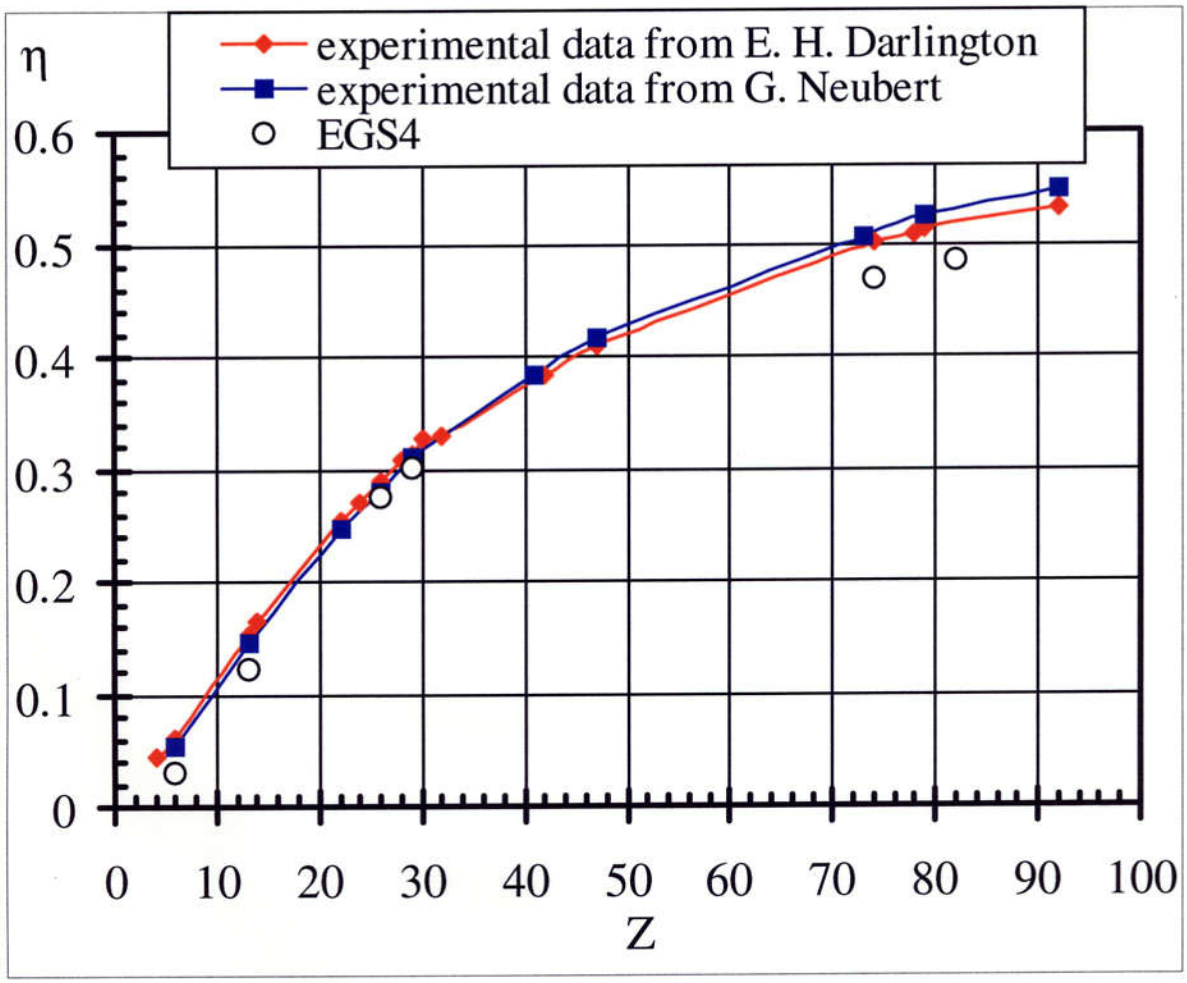

Figure 3-3: Backscattering coefficient (η) as a function of atomic number (Z) of material for normal incidence. (experimental data and EGS4 simulation results)

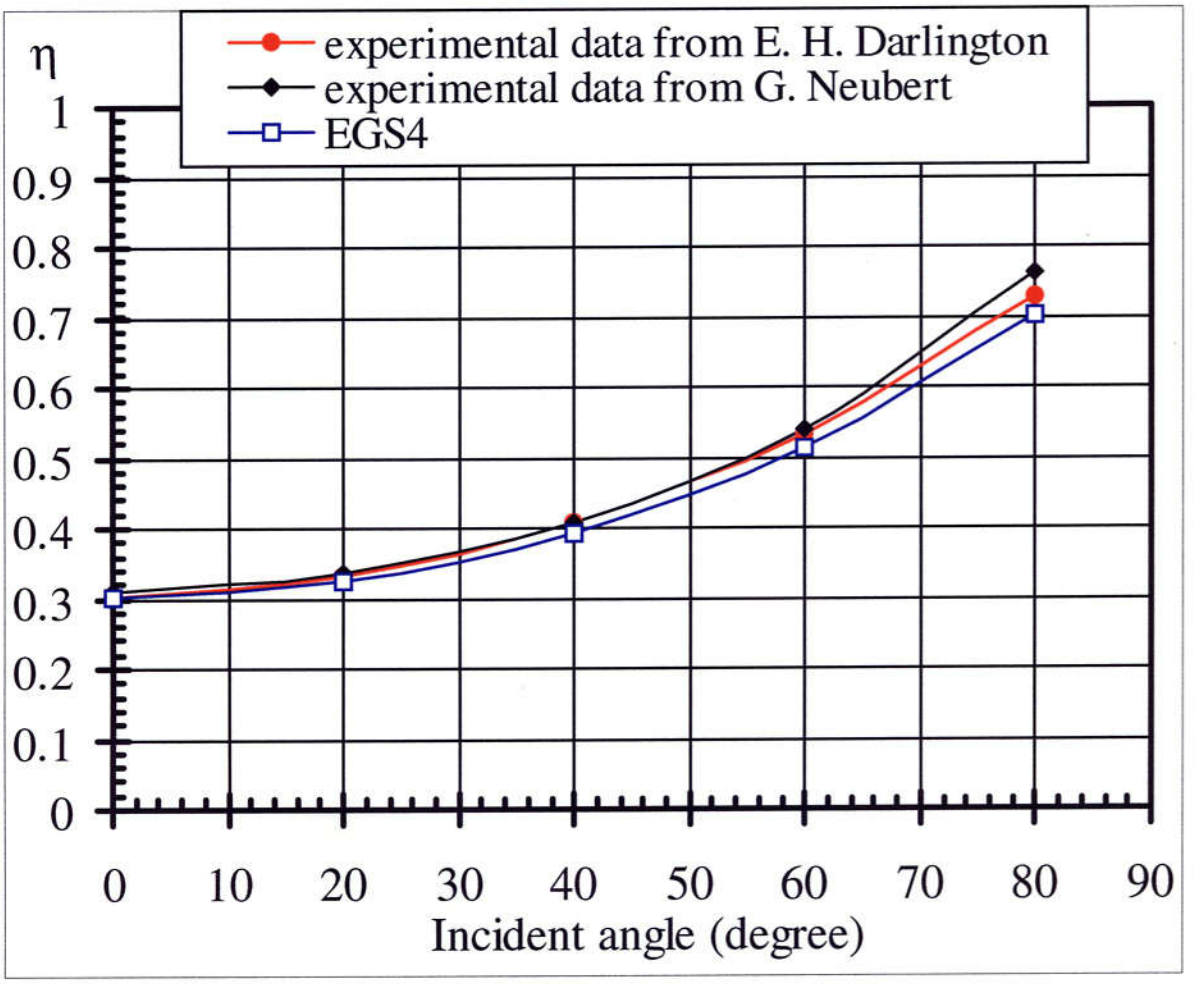

Figure 3-4: Backscattering coefficient (η) as a function of incident angle on a copper surface. (experimental data and EGS4 simulation results)

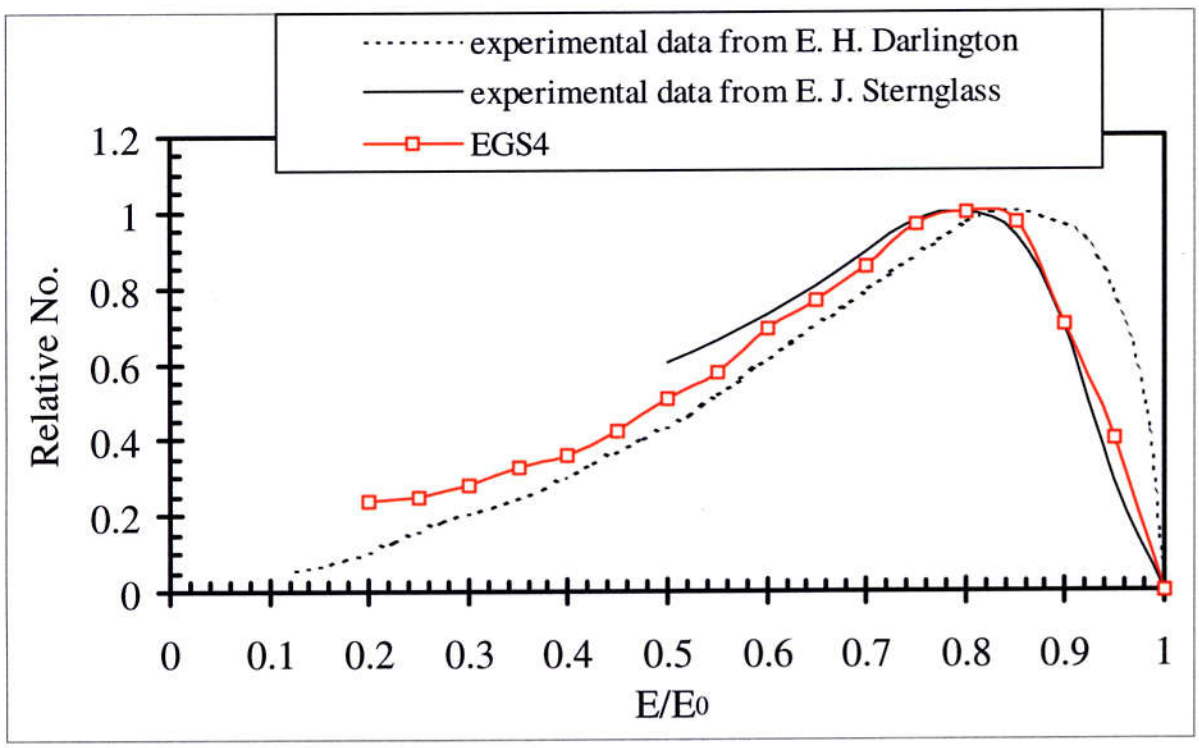

Figure 3-5: Energy distributions of backscattered electrons from a copper surface for normal incidence. (experimental data and EGS4 simulation results)

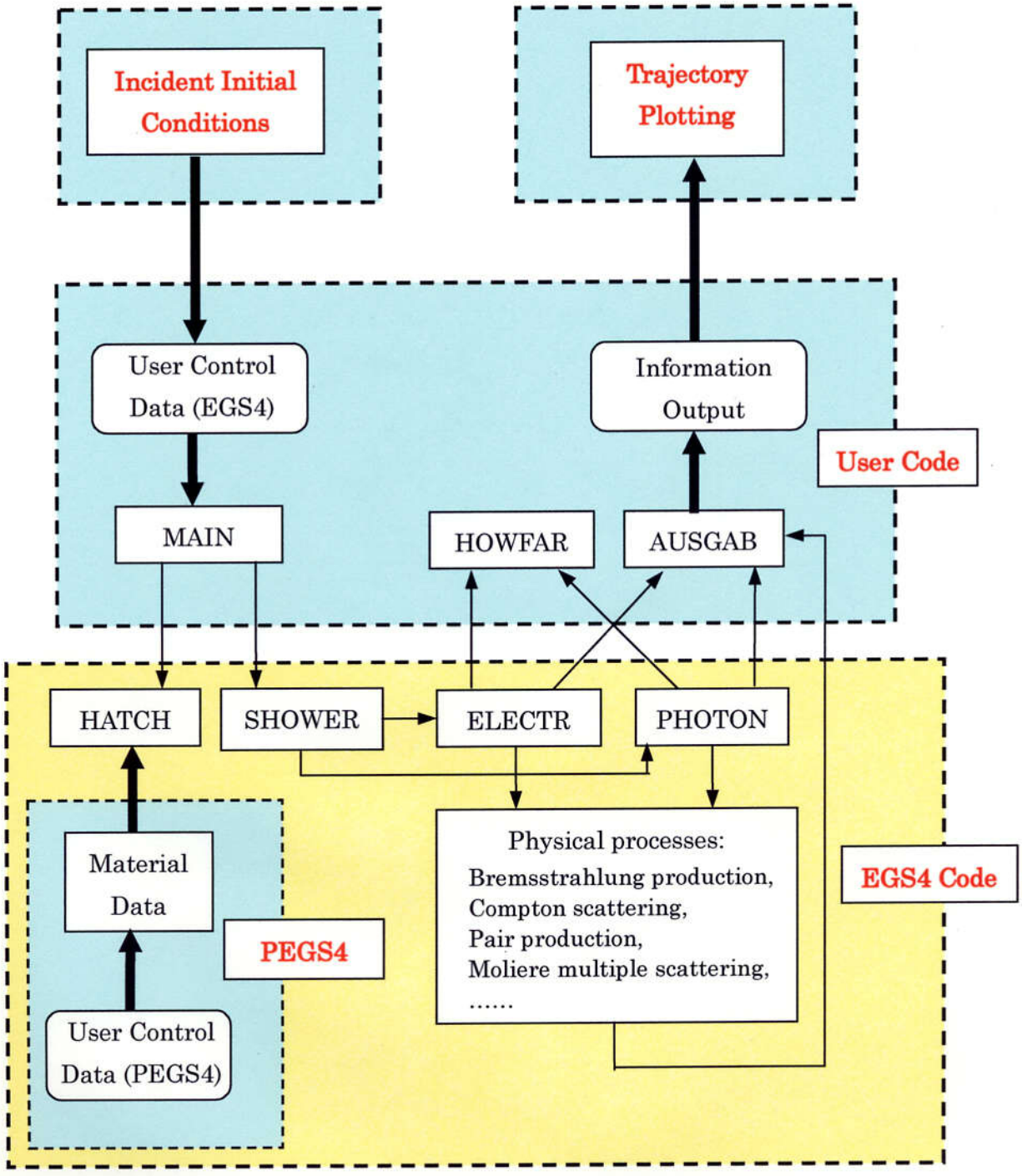

Figure 3-6: Flow control of simulation for electron backscattering using EGS4.

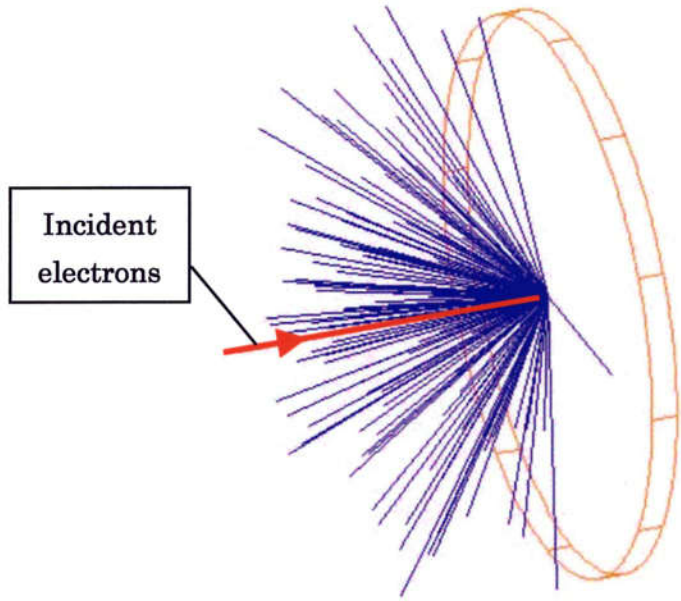

(a) incident angle, 0 degree.

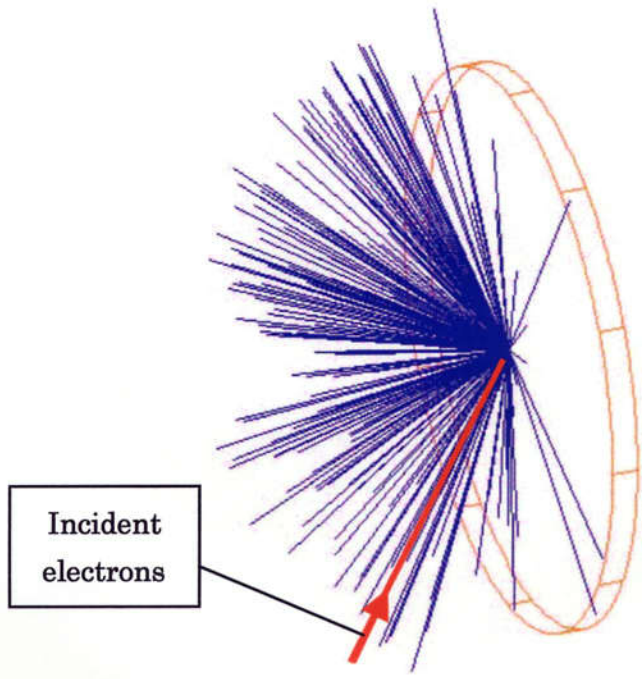

(b) incident angle, 60 degrees.

Figure 3-7: Trajectories of incident and backscattered electrons (60keV electrons incident on a copper plate).

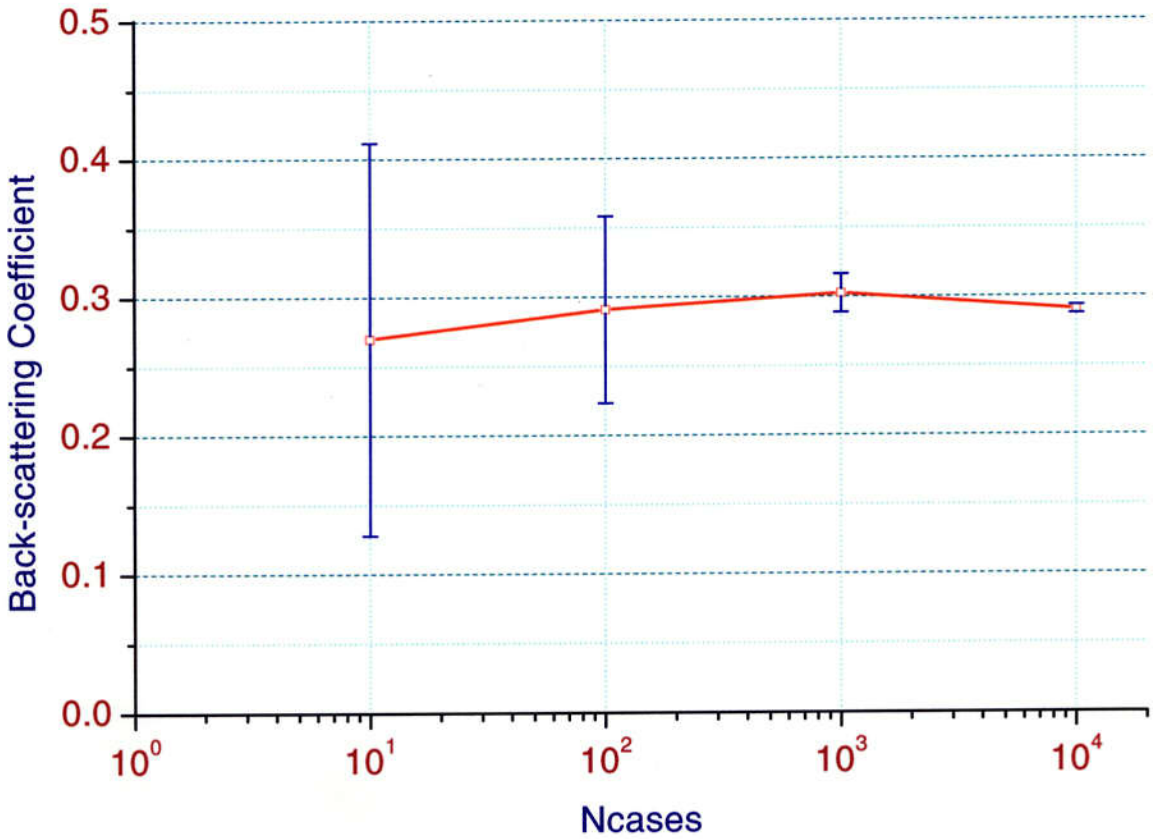

Figure 3-8: Backscattering coefficient and its standard deviation for ten simulations (60keV electrons normally incident on a copper plate; Ncases, incident electron number).

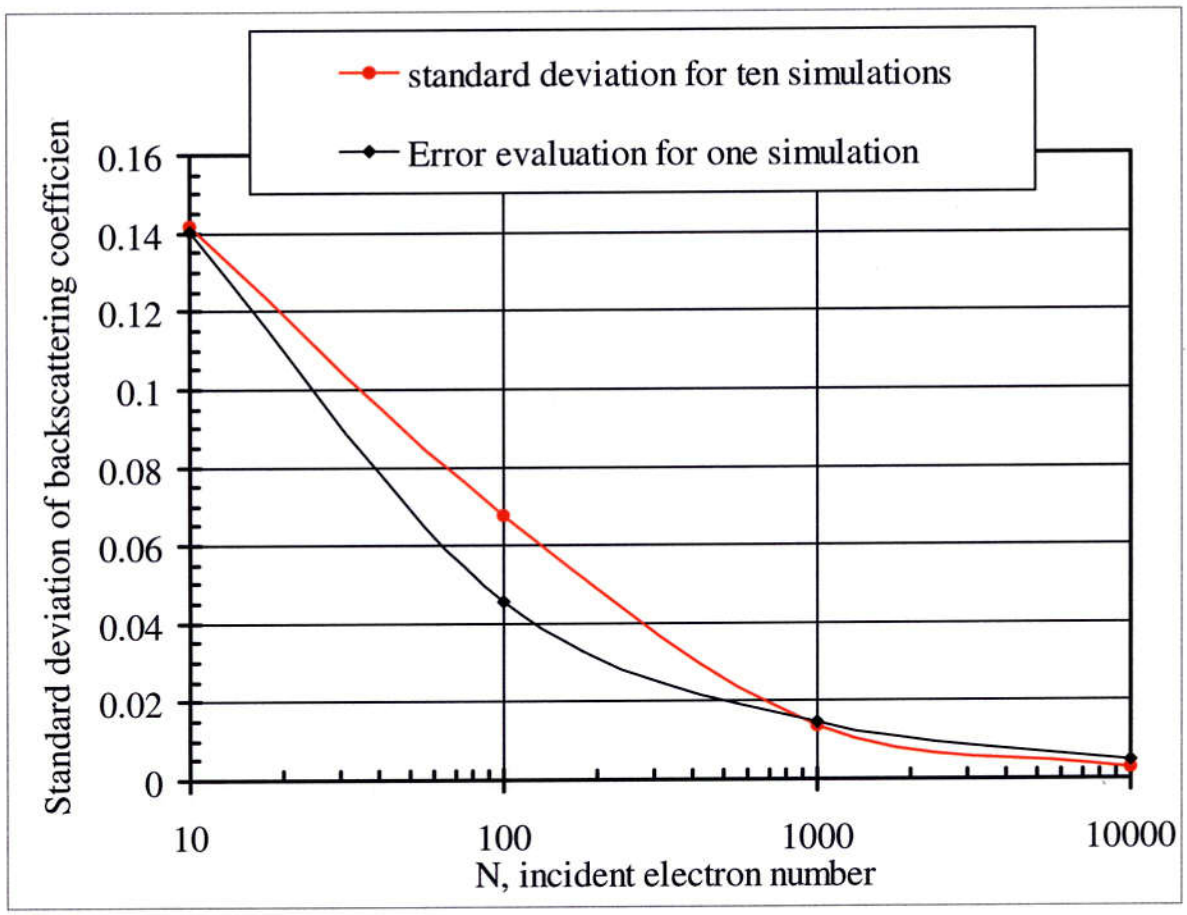

Figure 3-9: Backscattering-coefficient error evaluation for one simulation and standard deviation for ten simulations (60keV electrons normally incident on a copper plate; N, incident electron number).

Chapter 4

Backstreaming Electron Simulation from a Klystron Collector

4.1 Introduction

In the previous chapter, the process of electron backscattering has been calculated using EGS4. Good agreement between the calculation results and experiment results shows that the EGS4 code is reliable for the application of a klystron collector. Thus, a simulation of the backstreaming electrons from a klystron collector has been performed by designing a program using the EGS4 in this chapter. Descriptions of the calculation method and the application results to the klystron collector are given in this chapter. The simulation includes three steps. (1) The trajectory calculation for the incident beam in the collector up to the collector wall. (2) The simulation of the electron backscattering in the collector using the EGS4 Monte Carlo method. (3) The post-process for the backscattered and backstreaming electrons. The evaluation of the program has been achieved. The backstreaming electron coefficients and energy distributions have been obtained under different conditions of the klystron. The simulation results indicate that the backstreaming electrons are essentially independent of the beam voltage. The contributions to the backstreaming coefficients from the cylindrical surface and cone-shaped surface of the collector have also been investigated. The effects of the collector shape, i.e. its diameter and length, are discussed and physical phenomena are clarified. The dependence of the backstreaming electrons on various materials is also discussed in this chapter. Finally, the transmission of the backstreaming electrons in the drift tube is investigated.

4.2 Simulation method and three steps

In the klystron, the electron beam emitted from a gun is focused by external magnetic fields and transported in the drift tube. The focusing magnetic fields decrease rapidly at the entrance of the collector and the beam diverges in the collector due to the space-charge forces. After the beam bombards the collector surface, some of the electrons are backscattered, and the secondary electrons are also created. Since the energies of the secondary electrons are less than 50eV, we could neglect their effects as described in the previous chapter. Some of the backscattered electrons have a chance to go back to the drift tube directly, or undergo a few successive collisions with the collector wall. Some of them are reflected by the rapidly varying magnetic fields due to their mirror effects, and the electrons that are not reflected can be focused again by the magnetic fields in the drift tube and transferred to the upstream gun direction. These are called backstreaming electrons, and are considered to be harmful since they can cause instabilities. Here, we define the backstreaming electron coefficient (η_b) as the ratio of the number of backstreaming electrons (n) to the number of incident electrons (N),

$$\eta_b = n / N \tag{4.1}$$

The simulation of backstreaming electrons from a klystron collector is divided into three steps as shown in Figure 4-1. (1) The trajectory calculation for the incident beam in the collector up to the collector wall. This step is performed by a FORTRAN90 program. Besides space charge forces, relativistic effects, self-magnetic fields and external magnetic field effects are included in this calculation. The calculation results have shown a good agreement with the EGUN95 simulation results. (2) The simulation of the electron backscattering in the collector using the EGS4 Monte Carlo method. This step is performed by an EGS4 user code, which processes the initial conditions, collector geometry, electron motion in the magnetic fields, and output of the backscattered and backstreaming electrons. (3) The post-process for the backscattered and backstreaming electrons. This step includes two FORTRAN90 programs; one is for the electron trajectory plotting, and the other is for the calculation of the z-component energy distribution of the backstreaming electrons.

4.2.1 Trajectory calculation for incident beam in the collector

In order to simulate the electron backscattering in a klystron collector, it is necessary to prepare data for each incident electron, such as energy, direction, and position. Since there was no such suitable code, a program has been developed by using FORTRAN90. The flow control is shown in Figure 4-2.

The user control data, including klystron parameters, collector shape, and magnetic fields, will be used as the input of the trajectory calculation. For the klystron parameters, it is necessary to specify voltage (V_0), perveance (P_{er}), and beam radius (R_b). For the 324MHz klystron,

$V_0 = 110kV$

$P_{er} = 1.37\mu\ P_{er}$

$R_b = 0.035m.$

The collector shapers of the 324MHz klystron tubes are shown in Figure 2-6. The external focusing field has been simulated using POISSON as shown in Figure 4-3. The magnetic fields on the symmetrical Z-axis are shown in Figure 4-4; (a) is the fields in the whole region, (b) is the fields in the collector region, which starts from the center of the output cavity as the collector entrance. The maximum of the magnetic flux density on Z-axis is about 400Gauss at the input cavity region, where the beam is converged after emission from the cathode. In the downstream region of the input cavity, the magnetic fields decrease half, about 200Gauss till to the collector entrance. In the collector region, the magnetic fields fall rapidly. The permanent magnets attached at the collector region have also been simulated by PANDIRA, which will be described in section 4.3.2 of this Chapter. The data of these magnetic fields have been saved in text files, which are used in the calculation of step 1 and step 2.

At first, the initial conditions of the beam at the entrance of the collector are calculated. Here, because we assume there is no driving rf power in the input cavity, the electrons have a constant kinetic energy corresponding to the

applied voltage. A uniform-density beam is assumed, and the beam is divided into a large number of rays, as shown in Figure 4-5. Beam rotation due to the focusing magnetic fields is derived by using the Bush theorem, the angular-momentum conservation law in the electromagnetic fields.

$$\dot{\theta}_0 = \frac{\eta}{2\pi r^2}(\psi - \psi_c)$$
$$= \frac{\eta}{2}(B_z - B_c \frac{R_c^2}{R_b^2}) \qquad (4.2)$$

where $\eta = e / m$, the charge-to-mass ratio of an electron, e is the charge on the electron, and m is the relativistic mass of the electron. At the beam voltage V_0, the relativistic factor γ is,

$$\gamma = 1 + eV_0 / (m_0 c^2) \qquad (4.3)$$

where m_0 is the rest mass of the electron, and c is the velocity of light in vacuum. The electron mass is

$$m = \gamma m_0 \qquad (4.4)$$

In equation (4.2), R_c is the cathode radius, ψ_c is the magnetic flux on the cathode, B_c is the magnetic flux density on the cathode, R_b is the beam radius, and ψ is the magnetic flux on the beam, B_z is the magnetic flux density on the axis of electron beam. For the 324MHz klystrons,

R_c = 4.5cm

B_c = 130Gauss.

Therefore, for the electrons who have an initial position (r_0, θ_0) at the entrance of the collector in cylindrical coordinate, namely in Cartesian coordinate,

$$x_0 = r_0 \cos(\theta_0) \qquad (4.5)$$
$$y_0 = r_0 \sin(\theta_0) \qquad (4.6)$$
$$z_0 = 0$$

they will have an initial velocity as

$$v_x = r_0 \dot{\theta}_0 \sin(\theta_0) \qquad (4.7)$$
$$v_y = - r_0 \dot{\theta}_0 \cos(\theta_0) \qquad (4.8)$$
$$v_z = u_0 \qquad (4.9)$$

where, u_0 is the velocity of the electrons at the beam voltage V_0,

$$u_0 = c\sqrt{1-\frac{1}{\gamma^2}}$$
$$= c\sqrt{1-\frac{1}{(1+\frac{eV_0}{m_0c^2})^2}} \qquad (4.10$$

With the above initial conditions, each trajectory of the beam is calculated by solving the equation of motion numerically. In this calculation, space-charge forces, relativistic effects, self-magnetic fields and external magnetic field effects were included.

From Maxwell's equation,

$$\text{div } \mathbf{D} = \rho \qquad (4.11)$$

the space charge fields can be obtained,

$$\vec{E}_r^s = \frac{\pi r_0^2 \rho_0}{2\pi r \varepsilon_0}\vec{e}_r \qquad (4.12)$$

where, ε_0 is the permittivity of vacuum, $\varepsilon_0 = 8.854 \times 10^{-12}$ Farad/m, r_0 is the initial radial position, ρ_0 is the charge density,

$$\rho_0 = \frac{I_0}{\pi R_b^2 u_0} \qquad (4.13)$$

I_0 is the beam current. Then, the space-charge forces are calculated out by substituting equation (4.13) into (4.12),

$$\vec{F}_r^s = e\frac{I_0}{2\pi\varepsilon_0 u_0}(\frac{r_0}{R_b})^2\frac{1}{r}\vec{e}_r \qquad (4.14)$$

The x and y components of the space-charge forces are:

$$F_x^s = F_r^s\,(x/r) \qquad (4.15)$$

$$F_y^s = F_r^s\,(y/r) \qquad (4.16)$$

Again from Maxwell's equation,

$$\text{Curl } \mathbf{H} = \mathbf{J} + \partial \mathbf{D}/\partial t \qquad (4.17)$$

the self-magnetic fields are obtained,

$$B_\theta = \frac{\mu_0 I}{2\pi r}$$
$$= \frac{\mu_0}{2\pi r}\left(\frac{r_0}{R_b}\right)^2 \cdot I_0 \tag{4.18}$$

where μ_0 is the permeability of free space.

The forces due to the self-magnetic fields are calculated from Lorentz-force equation,

$$\vec{F}_B^s = e\vec{\upsilon}\times\vec{B} = eB_\theta \begin{vmatrix} \vec{e}_x & \vec{e}_y & \vec{e}_z \\ \upsilon_x & \upsilon_y & \upsilon_z \\ \frac{-y}{r} & \frac{x}{r} & 0 \end{vmatrix}$$
$$= eB_\theta\left[-\upsilon_z\frac{x}{r}\vec{e}_x - \upsilon_z\frac{y}{r}\vec{e}_y + (\upsilon_x\frac{x}{r} + \upsilon_y\frac{y}{r})\vec{e}_z\right] \tag{4.19}$$

After the simulations of the external focusing fields and attached permanent magnetic fields, the three direction components of the total fields, B_x, B_y, and B_z, are obtained. The forces due to the external fields are solved also by using Lorentz-force equation.

$$\vec{F}_B^e = e\vec{\upsilon}\times\vec{B} = e\begin{vmatrix} \vec{e}_x & \vec{e}_y & \vec{e}_z \\ \upsilon_x & \upsilon_y & \upsilon_z \\ B_x & B_y & B_z \end{vmatrix}$$
$$= e\left[(\upsilon_y B_z - \upsilon_z B_y)\vec{e}_x + (\upsilon_z B_x - \upsilon_x B_z)\vec{e}_y + (\upsilon_x B_y - \upsilon_y B_x)\vec{e}_z\right] \tag{4.20}$$

After getting the total forces, which are the vector summations of the space charge forces and the Lorentz forces due to self- and external magnetic fields, the beam trajectory can be calculated by using the motion equations:

$$\begin{cases} \vec{F} = \vec{F}_r^s + \vec{F}_B^e + \vec{F}_B^s \\ \vec{\upsilon} = \vec{\upsilon}_0 + \dfrac{\vec{F}}{m}dt \\ \vec{s} = \vec{s}_0 + \vec{\upsilon}\cdot dt \end{cases} \tag{4.21}$$

In our calculations, the time step (dt) in equation (4.21) is determined by a distance step over the velocity u_0. The distance step is set as 1/2000 ~ 1/3000 of the collector length so that the calculation results are converged.

This 3-dimensional calculation is different from the relaxation method solving the Poisson's equation with the fine mesh, for example, the recent 3-dimensilnal simulation on MDC [4-1]. In our method, the equation of motion is numerically solved 3-dimensionally for each ray with the rectangular coordinate (x, y, z). This is, in some senses, the perturbation method, and the space-charge potential is derived from the average potential, by assuming that the entire beam trajectory is not deviated largely from the axial symmetry. Thus the calculation of the orbit, when the asymmetric magnetic fields were applied externally, also employs this assumption. We didn't apply strong asymmetric magnetic fields to deflect the main beam largely, and this assumption remains a good approximation. For the axial-symmetric case, the calculation results showed a good agreement with that using the EGUN code [4-2].

Figure 4-6 shows the simulation results for 324MHz klystron #1 under beam voltage of 110kV without external magnetic fields. The beam edge hits the collector at the position in z-direction of 0.372m. The beam edge of the EGUN95 simulation results shown in (a) of Figure 4-7 is 0.378m, which is marked in Figure 4-6 also. These two points of the beam edge in the figure are almost same. The positions in z-direction of each ray when they hit the collector are shown in Figure 4-8. The results indicate that these two simulations of the spent beam agree very well. Figure 4-9 shows the kinetic energy of each ray when they hit the collector for 324MHz klystron #1 under beam voltage of 110kV without external magnetic fields. The kinetic energy of the beam edge increases 4.4%, from 110keV to 114.87keV. It results from the process of the beam divergence; the space-charge forces have done work to the electrons, while the potential energies decrease.

Figure 4-10 shows the simulation results of 324MHz klystron tubes #1, #1A, and #2, under beam voltage of 110kV with the focusing fields. Meanwhile comparisons with EGUN95 have been performed. Again they agree well. For example, for klystron #1, the beam edge is at 0.29m in our simulation; EGUN95 gives the beam edge at 0.28m, as shown in (b) of Figure 4-7.

After the calculations in this step, the output data, including the electron

energies, directions, and positions, are saved in memory for the next step, EGS4 simulation.

4.2.2 Simulation of backscattered electrons in the collector using EGS4

In the first step, the information data for each incident electron, including the energies, directions, and positions, are obtained. They will be used as the incident initial conditions for the second step, namely the EGS4 simulation of electron backscattering in the collector. After electrons of each ray bombarding the collector surface, some electrons are absorbed in the collector material and the other are backscattered. The tracks of the backscattered electrons are traced by solving motion equations including magnetic fields until they hit the wall again or until they go back to the drift tube. For the former case, again parts of them are backscattered, and the others are absorbed in the next collision. These procedures are repeated until all of the incident electrons are applied into the calculation. In this step, space-charge forces are neglected.

The flow control is same as the one shown in Figure 3-6. Again, at first the material data should be created using PEGS4 for a specified material and an energy boundary. Then a user code should be written by using MORTRAN in order to use the EGS4 code [4-3]. The incident initial conditions will be used as the input of the user code. The geometry of the collector, and the electron motions in the magnetic fields, are coded in the HOWFAR subroutine. In this subroutine, in order to use the combinatorial geometry with the EGS4 code, we divide the collector into 13 regions, as shown in Figure 4-11. Regions 3, 5, 7, 9, 10 and 11 are the collector material; other regions 1, 2, 4, 6, 8, 12, and 13 are defined as the vacuum. When the electrons go into the vacuum region within the collector, namely region 2, 4, 6, and 8, we change the user step length USTEP to a relatively short value and calculate the motion directions of the electrons after each step due to the magnetic fields using the formulas,

$$\begin{aligned}\vec{F} &= e\vec{\upsilon_0}\times\vec{B} \\ &= e\left[(\upsilon_y B_z - \upsilon_z B_y)\vec{e}_x + (\upsilon_z B_x - \upsilon_x B_z)\vec{e}_y + (\upsilon_x B_y - \upsilon_y B_x)\vec{e}_z\right]\end{aligned} \tag{4.22}$$

and

$$\vec{\upsilon} = \vec{\upsilon}_0 + \frac{\vec{F}}{m} dt \tag{4.23}$$

where v_0 is the electron velocity at certain moment, which is calculated from the kinetic energy (E_k) outputted by EGS4 simulation as intermediate results,

$$\upsilon_0 = c\sqrt{1 - \frac{1}{(1 + \frac{E_k}{m_0 c^2})^2}} \tag{4.24}$$

dt is the time step,

$$dt = USTEP / v_0 \tag{4.25}$$

A shorter step gives a more precise results, however the calculation time increases quickly as a shorter step is used. From the convergence of the calculation results with different short steps, a step of 0.2cm is adopted to use in our calculations.

The output information is specified in the AUSGAB subroutine. Here, the output information including: 1) the data of the positions of the backscattered electrons in the vacuum region within the collector, namely region 2, 4, 6, and 8; 2) the information of the electrons returning into the drift tube, namely from region 2 to region 1, including their energies, positions, and directions. Usually 1,000,000 electrons are employed for a calculation to obtain good statistics. After simulations are carried out for all of these incident electrons, the information concerning the backstreaming electrons is saved in memory, including their coefficient and energy distribution. The data of the positions of the backscattered electrons will be used in the last step, namely post-process, which plots the electron trajectories; The data of the directions of the backstreaming electrons also will be used in the last step to calculate the distribution of Z-component of the electron energies.

In this step, the program is executed using a personal-computer with a 333MHz Pentium processor; it takes about 2 hours for one simulation.

4.2.3 Post-process for backscattered and backstreaming electrons

This step includes two programs written by using FORTRAN90. One is plotting of the electron trajectories using the electron position data obtained in the second step. Figure 4-12 shows the trajectories of the backscattered and backstreaming electrons for 324MHz klystron tubes #1, #1A, and #2 under beam voltage of 110kV.

The other program is for the calculation of the distribution of the backstreaming electron energies in Z-direction. In the previous calculations, the total kinetic energies (E_k) of the backstreaming electrons and their directions ($\cos(\theta_x)$, $\cos(\theta_y)$, $\cos(\theta_z)$) are already obtained. Thus, the velocity is

$$\upsilon = c\sqrt{1-\frac{1}{(1+\frac{E_k}{m_0c^2})^2}} \tag{4.26}$$

and the z-component of the velocity is

$$v_z = v\cos(\theta_z) \tag{4.27}$$

Therefore the z-component of the kinetic energy is,

$$E_z = (\sqrt{\frac{1}{1-(\frac{\upsilon_z}{c})^2}}-1)m_0c^2 \tag{4.28}$$

After calculations for each backstreaming electron, the energy distributions in z-direction are obtained and will be used in the next chapter for the analyses and calculation of the oscillation conditions.

4.3 Simulation results

4.3.1 Beam voltage and energy distribution of backstreaming electrons

The backstreaming electron coefficients and energy distributions have been investigated under different beam voltages. It was found that they are almost same for a given collector. This agrees with the fact that the electron backscattering is essentially independent of the primary energy, as described in Chapter 3. For 324MHz klystron tube #1, the backstreaming coefficient is about 0.665%, and the energy distributions of the backstreaming electrons are shown in Figure 4-13 for beam voltages of 110kV, 100kV, 90kV, 80kV, and 70kV. In this figure, the energies of the backstreaming electrons are normalized by the incident-beam energy at the collector entrance. It indicates that the energy distribution curves for different beam voltages are almost same, and the energy peak is located around 0.75. Few of backscattered electrons have kinetic energies higher than the beam energy (E_0); this is due to the energy of incident beam increasing slightly during the spent process under the work of the space charge forces, which have mentioned in the Section 4.2.1.

Also simulations for different collectors have been performed. The energy distributions of the backstreaming electrons corresponding to the actual collector shapes of klystron #1, #1A, and #2, are shown in Figure 4-14; (a) is the distributions of the total energies, and (b) is the distributions of the Z-component energies. These figures show that for these three collectors, the energy distributions of the backstreaming electrons are very similar, while the backstreaming coefficients are quite different.

The distributions $\eta(x)$ of Z-component energies of the backstreaming electrons have been fitted by polynomial functions for klystrons #1, #1A, and #2. They are expressed as the followings, respectively.

$$\eta(x) = 2.53393\,x^4 - 1.12787\,x^3 - 6.38668\,x^2 + 4.97812\,x + 0.03794 \quad (4.29)$$

$$\eta(x) = -4.31901\,x^6 + 16.51592\,x^5 - 22.23838\,x^4 + 13.15166\,x^3 - 4.40450\,x^2 +$$

$$1.30383\ x + 0.00356 \qquad (4.30)$$

$$\eta(x) = 0.77337\ x^4 - 1.03569\ x^3 - 0.52646\ x^2 + 0.79273\ x + 0.01017 \qquad (4.31)$$

where x is the z-component of the kinetic energies (E_z) normalized by the beam energy (E_0), $x = E_z / E_0$. These energy distribution functions will be used in the next chapter for calculation of the oscillation conditions due to the backstreaming electrons.

4.3.2 Effects of attached permanent magnets and focusing magnetic fields

In Chapter 2, it was mentioned that the oscillations in klystron #1 were partially suppressed by the attached permanent magnets (see Figure 2-5, the sketch of the magnets). The effects of the deflecting magnets have been simulated. At first, the magnetic fields had been simulated by using PANDIRA, which are shown in Figure 4-15. The fields in the vertical direction are shown in Figure 4-16 for both the calculation and test results. They agree well with each other. It is shown that the fields increase from the collector center to position near the magnets. This simulation data of magnetic fields are used in the calculation of electron movements in the collector. From Figure 4-15, we can easily image that the magnets act as bending fields, which deflect the electron movements in the collector. The simulation results of the beam trajectories deflected by the attached permanent magnets are shown in Figure 4-17 for 324MHz klystron #1 under beam voltage of 110kV. Then based on these incident initial conditions, backstreaming electrons have been simulated by EGS4. The simulation results indicate that it become difficult for the backscattered electrons in the collector to return into the drift tube due to the deflecting fields. The backstreaming coefficient decreases from 0.66% to 0.56% in once simulation. That is why the oscillations were suppressed in the low voltage region.

The effects of the focusing magnetic fields to the backscattered electrons have also been simulated. It is well known when backscattered electrons go back to the drift tube under rapidly increased magnetic fields, some of them will be focused and others will be mirror-reflected. It can be easily understood

that for electrons of a certain energy, focusing will play an important role if the magnetic fields increase relatively gradually, and mirror reflection will play dominant role if the fields increase too rapidly. Figure 4-18 shows the motion of electrons of different energies (E) in magnetic fields of different strengths (B) comparing with the actual applied fields (B_0) in the 324MHz klystrons. It indicates that for the 100keV electrons in the magnetic fields B_0, there is no reflection, however for the 10keV electrons, some of them are reflected and the number of reflected electrons will increase in a stronger magnetic fields. Figure 4-19 shows the sketch of simulation for capture ratio of electrons in magnetic fields, where electrons of different positions and directions in the Y-Z plane are applied into the simulation. The capture ratio is defined as the ratio of the number of electrons which are captured by the magnetic fields and go back into the drift tube to the number of total applied electrons in the simulation. Figure 4-20 shows the simulation results of the capture ratio of electrons in magnetic fields. In this simulation, electrons of 20 Y-positions with Z=0.5m and 39 directions within ±45° to the reverse Z-direction are used. The simulation results show that as the magnetic fields become strong, the capture ratio increases at first due to the focusing effects, then arrives at a maximum value, and finally decreases due to the mirror reflections. For the actual applied fields in the 324MHz klystrons, focusing plays the dominant role to the electrons of energies higher than 10keV. Simulations also show that almost all of the secondary electrons can not go back to the drift tube due to the mirror reflections.

4.3.3 Collector shape and backstreaming electrons

A typical collector shape used in this simulation is shown in Figure 4-21; D_t is the diameter of the drift tube: D_c and L_c are the diameter and length of the collector, respectively. Backstreaming electrons have been calculated based on the various shapes of collector made of copper material. The results, including the actual klystron dimensions, are given in Table 4-1; the relative error in this table has a similar definition to (3.9), as the ratio of the standard deviation of the backstreaming coefficient to itself. It has been clarified that the number of backstreaming electrons strongly depends upon the ratio of the

drift-tube diameter to the collector diameter, as shown in Figure 4-22. In this figure, a collector dimension of klystron #2, L_c = 122.4cm, D_c = 23cm, is used. When the drift tube diameter changes from 10cm to 5cm, the backstreaming coefficient decreases quickly from 0.128% to 0.023%. It has also been clarified that the dimension of the collector has a large effect on the backstreaming electrons. These tendencies are given in Figure 4-23, where D_t =10cm is used in the simulation; (a) shows the backstreaming electron coefficient as a function of the collector length, L_c; (b) shows the backstreaming electron coefficient as a function of the collector diameter, D_c.

Table 4-1: Backstreaming electron coefficient for different dimensions of a copper collector

Tube	D_t (cm)	D_c (cm)	L_c (cm)	Backstreaming electron coefficient	Relative error
#1	10	13	62.4	0.00665	1.2%
#1A		23	92.4	0.00174	2.4%
#2		23	122.4	0.00128	2.7%
	7	23	122.4	0.00081	3.5%
	5			0.00023	6.6%

In order to analyze the features of backstreaming electrons from the collector, a sketch of three different typical collector shapes is shown in Figure 4-24, where the shaded lines on the collector boundary indicate the collector surfaces bombarded by the incident beam. From Figure 4-24 the contributions to the backstreaming coefficient can be divided into two parts: one from the cylindrical surface of the collector and the other from the cone shaped surface of the collector. The former contribution seems to come mainly from backscattering of the beam edge parts, since the coefficients remain constant for large L_c. On the other hand, it is natural that if the cone-shaped part of the collector is located near to the drift tube, a fairly large number of direct backscattering electrons contribute to the backstreaming electrons.

The contribution of the cylindrical surface has shown by the curve of the case L_c = 262.4cm in Figure 4-23 (b), since in this case the length can be regarded long enough. The coefficient is only determined by the collector

diameter, and it is approximately inversely proportional to the diameter square for the obtained results in the case of our simulations.

The beam-edge contributions have been demonstrated by the artificial setting of the incident initial conditions of EGS4 for two collectors of a relatively long length (in our simulations, a length of 262.4cm was used) and a diameter of 13cm and 23cm respectively. In this simulation D_t=10cm is used. A schematic view of the incident condition is shown in Figure 4-25. We divided the incident beam into 19 rays in the r-direction, and used the incident data of the outer 2, 5, 10, and 19 rays to calculate the contributions of these outer rays to the backstreaming coefficient. It is obvious that a beam edge including more rays will bombard the cylindrical surface up to a farther front position. The backstreaming-coefficient contribution of the beam edge as function of the front position of beam edge bombarding the collector surface are shown in Figure 4-26 for the case of collector diameter 13cm and 23cm. This figure indicates that, in the case of 13cm diameter, the beam edge of a length about 10% of the total collector length bombarded by beam gives about 96% contribution to the backstreaming coefficient. In the case of 23cm, the contribution of the beam edge reduces slightly, but still is relatively large; about 17% length gives 93% contribution.

Furthermore, in order to investigate the backscattering process in the collector, the collision process has also been investigated in three collectors; two of them have a long length (in our simulations, a length of 122.4cm was used) and a diameter of 13cm and 23cm respectively; and the other one has a short length of 62.4cm and a diameter of 23cm. The energy distributions of the backstreaming electrons undergoing successive collisions are shown in Figure 4-27 for these three collectors. It indicates that the peak of the energy distribution of the backstreaming electrons of single collision is obviously higher than that due to a successive multiple-collision process. Figure 4-28 shows the fractions of the backstreaming electrons undergoing successive collisions to the total backstreaming electrons. In the long collector cases, the fractions of single collision or two-successive collision are roughly the same around 30%. When the cone-shaped part of the collector is located near to the drift tube, the fraction of single collision increases apparently from 30% to 50%, as shown in (c) of Figure 4-28. This is due to the direct reflections of the incident electrons. The trajectories of the injection beam and the

backstreaming electrons undergoing different number of successive collisions for these three collectors are shown in Figure 4-29, Figure 4-30, and Figure 4-31, respectively. It indicates that, for a collector with a small diameter and a long length, the contribution of single collisions mainly comes from the beam edge bombarding the cylindrical surface. It seems that, for the backscattered electrons produced farther away from the collector entrance, they usually have to undergo a successive multiple-collision process to return into the drift tube. With the diameter increasing and the length shortening, the contribution of single collisions mainly comes from the cone-shaped part, which can be easily seen from Figure 4-31. From these simulation results, it is clear that the direct reflections usually take place in the collector surface close to the collector entrance: one is the cylindrical surface bombarded by the beam edge, the other is the cone-shaped surface if it is not far away from the entrance and bombarded by much of incident electrons. For the latter case, the contribution of direct reflections will be much higher than the former case, because in the former case, the emitted electrons in forward directions are much more than those in backward directions. Considering the multi-backscattering in the collector, two-successive collisions will give more contribution to the backstreaming coefficient than other-successive collisions, and their contribution is about the same as that of single collisions in case of long collectors. This can be understood qualitatively because there are more emitted electrons after one collision in directions other than direct reflection, and after they bombard the surface again in various directions, still a lot of electrons from the two-successive collision return to the collector entrance. However due to the backscattering coefficient smaller than unity, the total electron number after multi-scattering will decrease quickly. The fractions of backstreaming electrons due to more-than-three-successive collisions become apparently small.

For designing a suitable collector with a small backstreaming electron coefficient, a suitable ratio of the drift-tube diameter to the collector diameter should be determined for an acceptable backstreaming coefficient, which is derived by the oscillation condition described in the next chapter. If a longer collector shape can be chosen, only this diameter ratio determines the number of backstreaming electrons, as shown in the curve for the long collector case in Figure 4-23 (b). If a longer collector size is not allowed for some manufacturing

reason, compromising between the two factors mentioned above is necessary. This compromising can be assessed according to the tendency, as shown in Figure 4-23. A similar analysis is applicable to collectors of other microwave tube devices, a beam dump of accelerator, a secondary electron monitor (SEM) for beam current monitor, and a Faraday cup, if unwanted backstreaming electrons are desired to be eliminated.

4.3.4 Collector material and backstreaming electrons

Interesting features are obtained by changing the collector material. Figure 4-32 shows the backstreaming electron coefficient from a collector made of various materials, and Figure 4-33 gives the energy distribution of backstreaming electrons from a collector made of various materials. In the simulations, the same dimensions as the collector of klystron #2 are used. Obviously, a smaller number of backstreaming electrons are expected from lower atomic-number materials. This agrees with the feature of backscattered electron coefficient, which is a function of atomic number. The technology of using carbon and carbon-coated electrode for MDC had been reported in many references to reduce the backstreaming electrons especially due to true secondaries [4-4]. In reference [4-5], it was described that carbon material was effective for the reflected electrons. This analysis verifies those experimental results and furthermore it makes clear the relation between the backstreaming electron coefficient and the atomic number of used materials. Besides the carbon material, aluminum and its alloy are possible for the collector material. Another application is, for example, to use SiC as the collector material. This may be useful not only to reduce the backstreaming electrons but also to use it as the microwave absorber for unnecessary resonant modes in the collector. Since the penetration depth of the backscattered electrons into the materials for this energy region is very short, making a coating on the collector surface using the sputtering technique is also possible. If a manufacturing limitation prevents a suitable size of the collector, the material choice may be important.

4.4 Transmission of backstreaming electrons in drift tube

In the previous section, the backstreaming electron currents from the collector are carried out at the collector entrance. In order to have a study on the oscillations due to these backstreaming electrons, the behavior of the backstreaming electron transmission in the drift tube has also been simulated by calculating the motion of the electrons in the focusing magnetic fields. In this calculation we didn't include the production of new backscattered electrons after some of these electrons bombard the drift-tube surface. It was found that few of the backstreaming electrons can not pass through the drift tube and are intercepted mainly in the output cavity region, where the magnetic fields are not uniform. Thus the transmission of the electrons is precisely calculated in the region near the output cavity. The transmission ratio of the backstreaming electrons is shown in Figure 4-34. It indicates that the current of the backstreaming electrons decreases slightly after they pass through the output cavity, with a transmission ratio about 90%, and then the backstreaming electrons successfully pass to the upstream input-cavity direction under the focusing fields, which have an almost uniform pattern in the upstream region before the output cavity. The trajectories of the backstreaming electrons in the whole drift tube are shown in Figure 4-35. Same as the beam in the klystron, most of these backstreaming electrons will pass through the drift tube and move to the input cavity area under the focusing magnetic fields. Thus, it is estimated that the transmission ratio of backstreaming electrons is approximately 90%.

On the other hand, it was found that, in the EGS4 simulation using a USTEP of 0.02cm, which is one-tenth of the usually used USTEP of 0.2cm, the simulation result of backstreaming electron coefficient increases a little, for example, η_b increases about 7.4%, from 0.1273% to 0.1367%, for klystron #2. But it will take too much time for the calculation using the USTEP of 0.02cm. Therefore, this short step was not used in the previous calculations. It is

implied that the previous simulation results of η_b is slightly lower than actual value. Considering the transmission ratio, the backstreaming current derived from the previous calculation results will be close to the actual flowing current in the drift tube, within an error of 3%. It will be a proper approximation that the previous calculation result of the backstreaming-electron current at the collector entrance is regarded to be the reversibly flowing current that contributes to the oscillations.

4.5 Summary

This chapter has described the simulation method to calculate the backstreaming electrons from the klystron collector by applying the EGS4 code. Three steps have been executed, including (1) the trajectory calculation for the incident beam in the collector up to the collector wall, (2) the simulation of the electron backscattering in the collector using the EGS4 Monte Carlo method, and (3) the post-process for the backscattered and backstreaming electrons.

The backstreaming electron coefficient and energy distributions are obtained as function of beam voltages and collector shapes. Also the effect of the attached permanent magnets has been calculated. It is shown that the backstreaming electrons are essentially independent of the beam voltage. For klystron #1, #1A, and #2, the backstreaming electron coefficients are 0.66%, 0.17%, and 0.13%, respectively. The contributions to the backstreaming coefficients from the cylindrical surface and cone-shaped surface of the collector have also been investigated. The former contribution mainly comes from the backscattering of the beam edge, and the contribution is approximately inversely proportional to the square of the collector diameter. The latter contribution increases with the collector length shortening due to the direct reflection. The backstreaming coefficients as function of collector diameter and length have been carried out. The procedure for designing a collector with small backstreaming electron coefficients is also presented. Interesting features of backstreaming electrons concerning various materials have been investigated, as well as the possibility to use other materials, such

as carbon, instead of well-used copper material. The transmission of the backstreaming electrons in the drift tube has been investigated. It is shown that most of the backstreaming electrons can pass through to the input cavity region. These simulation results of the backstreaming electrons including the current and energy distribution will be applied to the study of the oscillation in the UHF klystrons caused by the backstreaming electrons; it will be described in the next chapter.

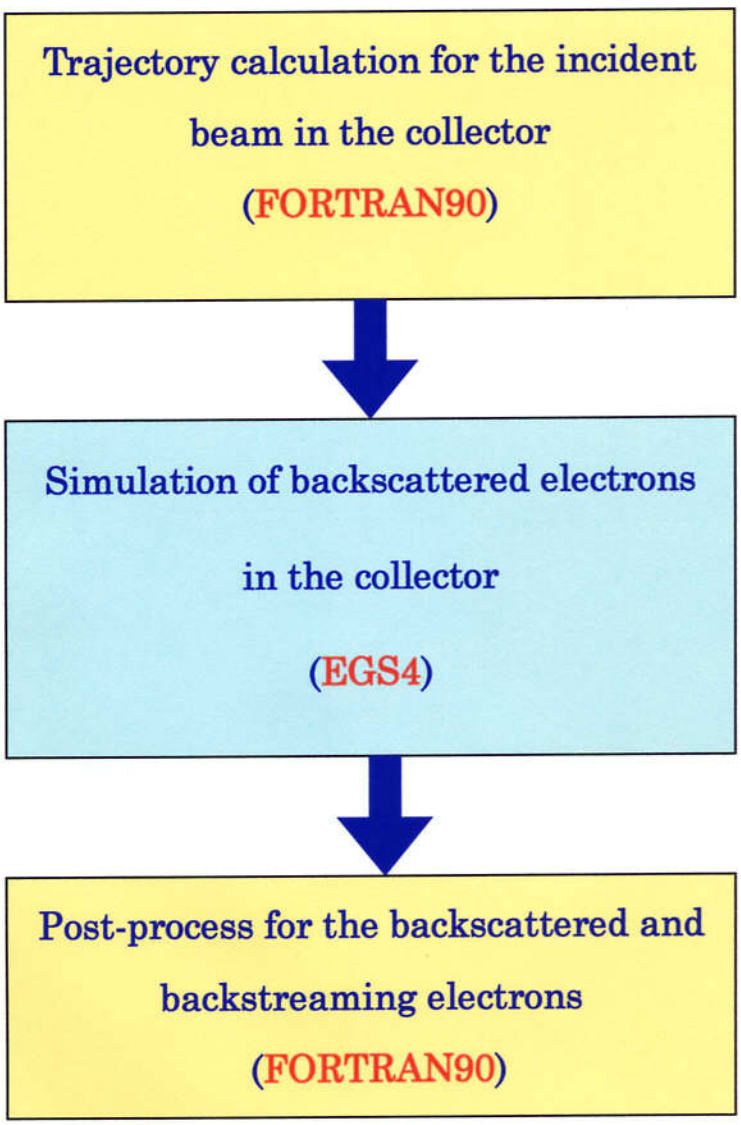

Figure 4-1: Three steps of simulation for backstreaming electrons from a klystron collector.

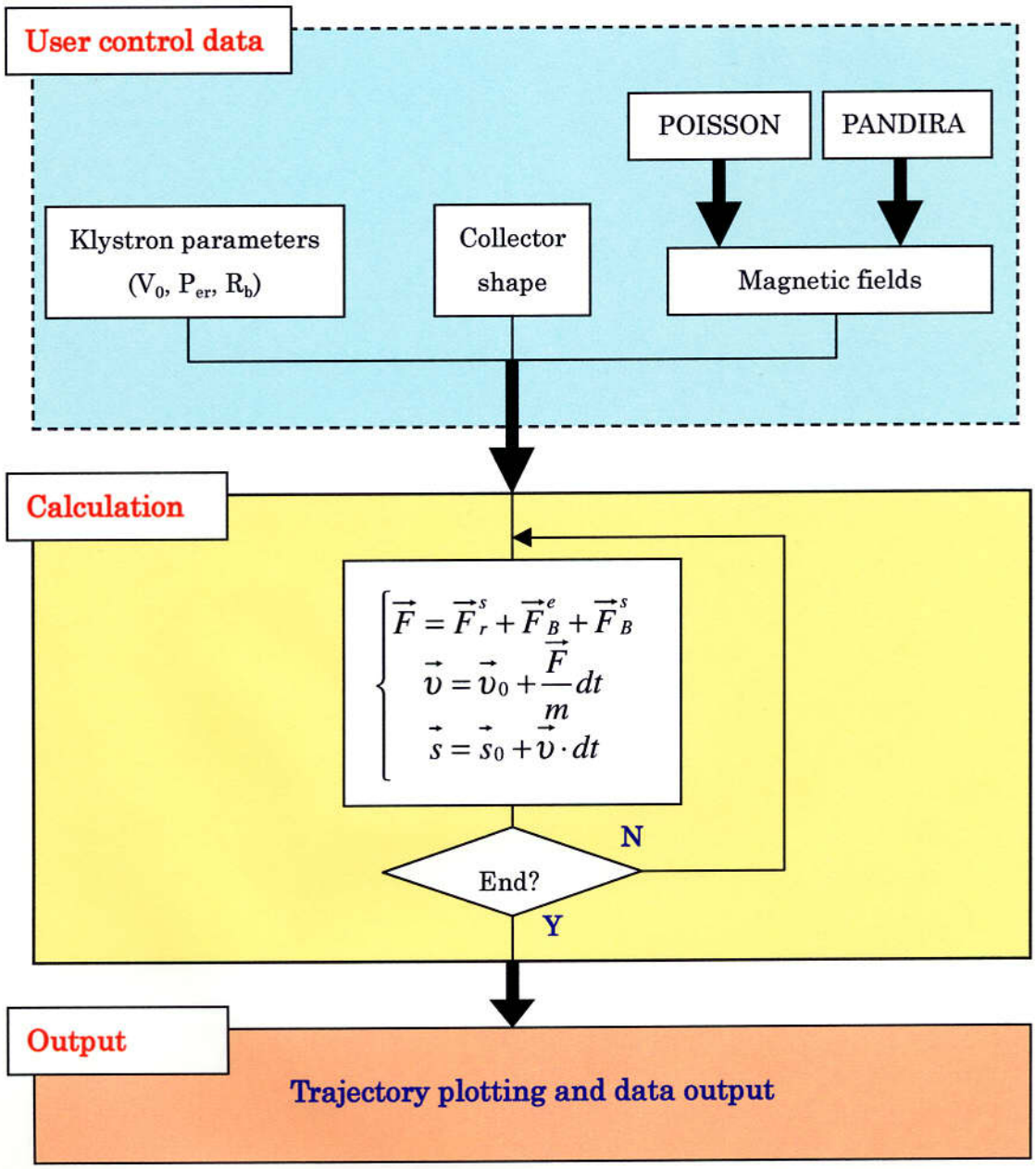

Figure 4-2: Flow control of trajectory calculation for incident beam in the collector.

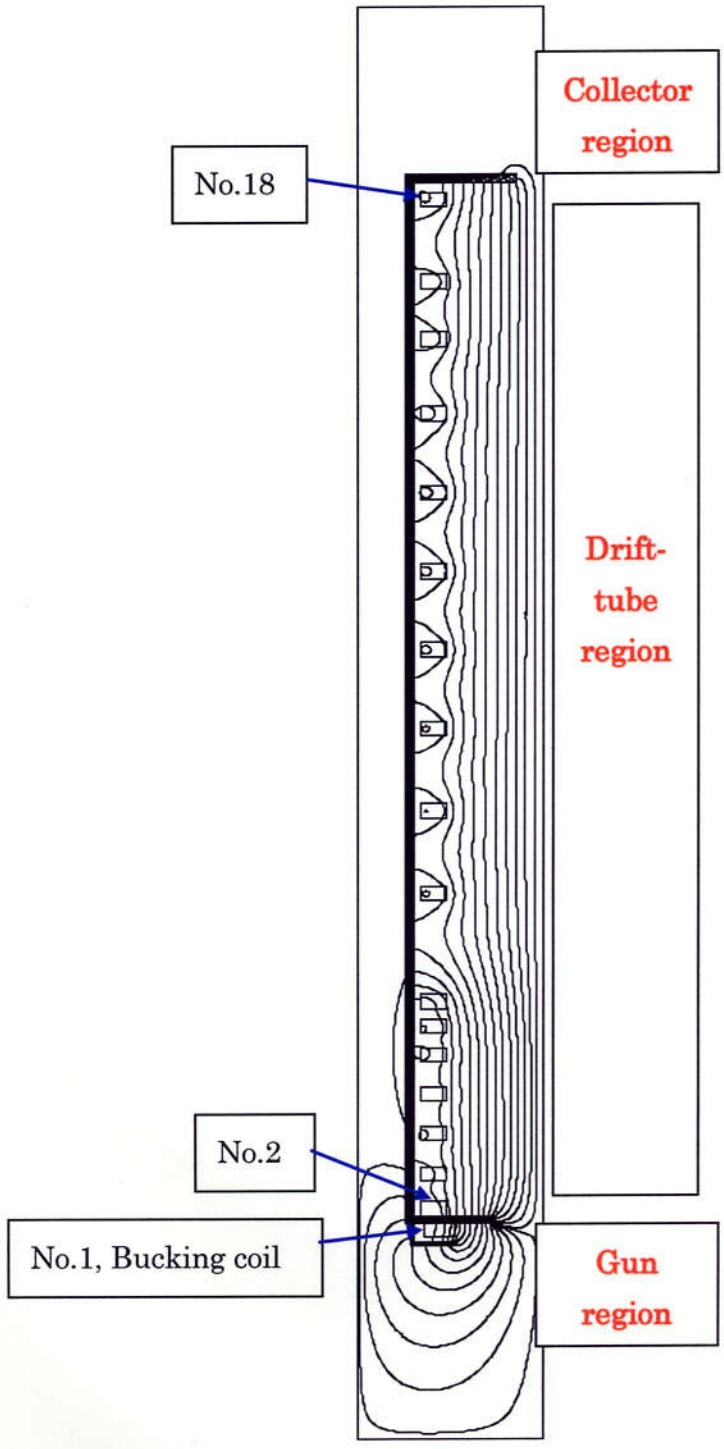

Figure 4-3: Simulation of the external focusing fields using POISSON.

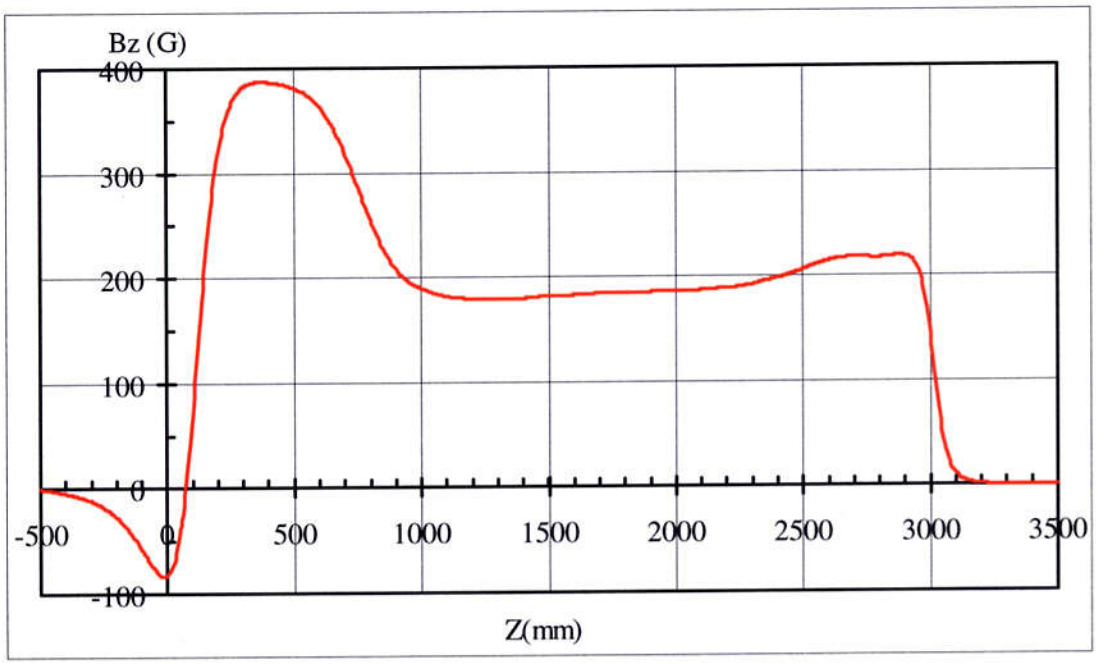

(a) in the whole region

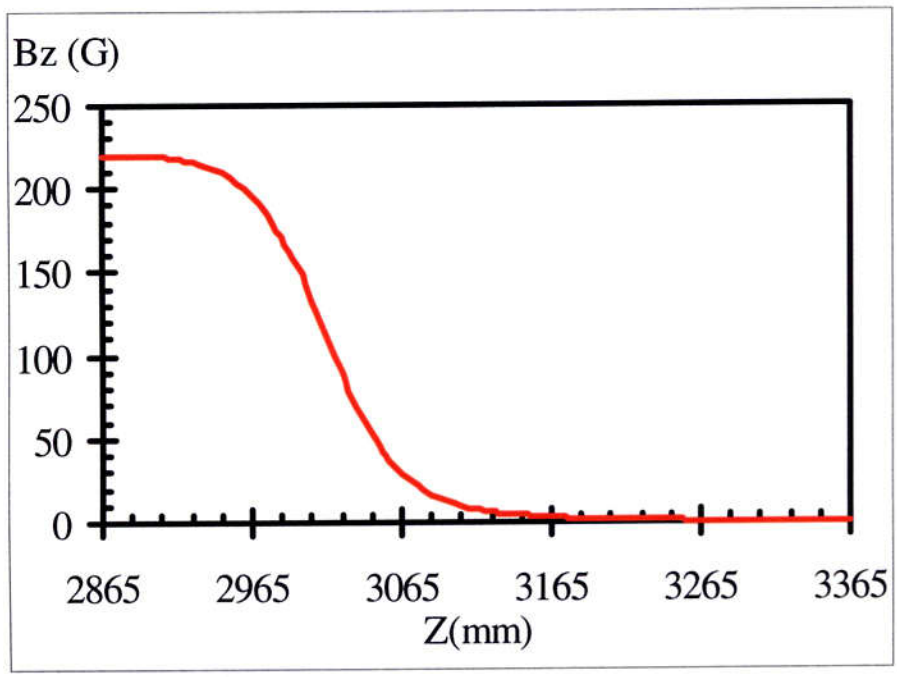

(b) in the collector region

Figure 4-4: Focusing magnetic fields on the symmetrical Z-axis.

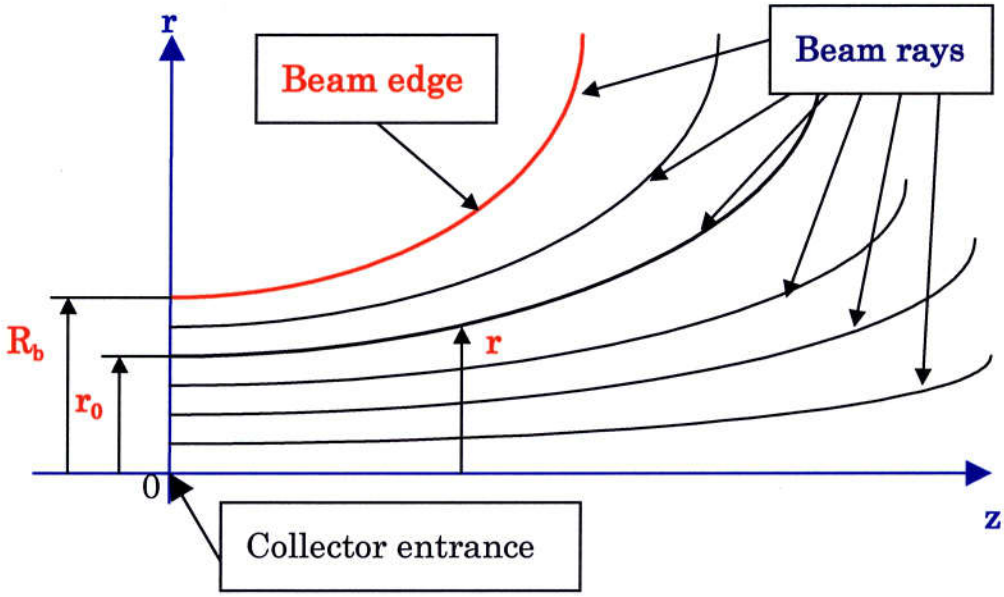

(a) beam rays in r-direction

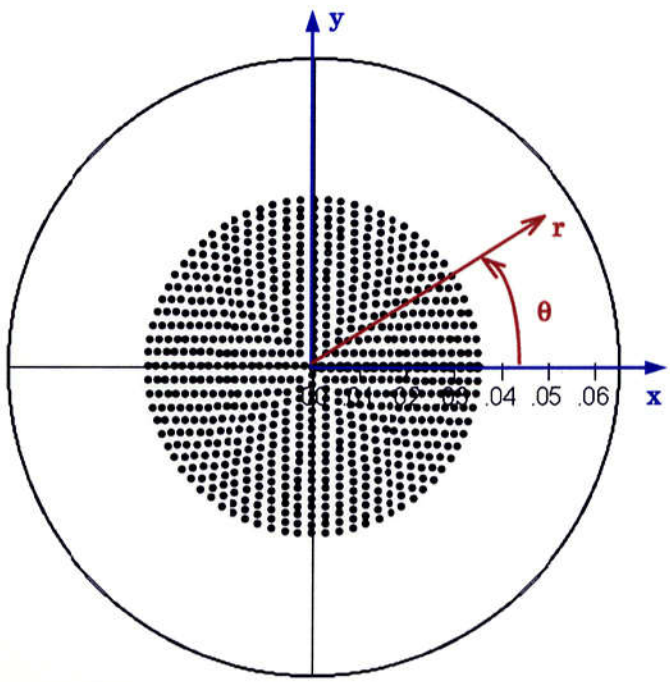

(b) beam rays in cross section at the collector entrance

Figure 4-5: Sketch of beam divided into a large number of rays.

Figure 4-6: Beam-trajectory simulation results for 324MHz klystron #1 under beam voltage of 110kV without external magnetic fields.

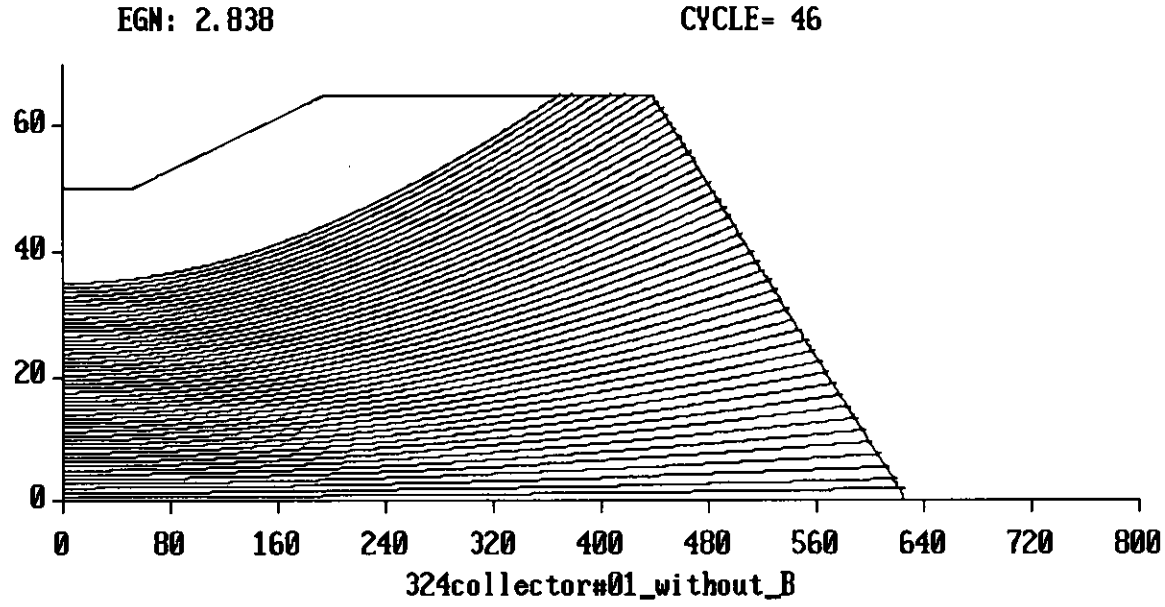

(a) without external magnetic fields

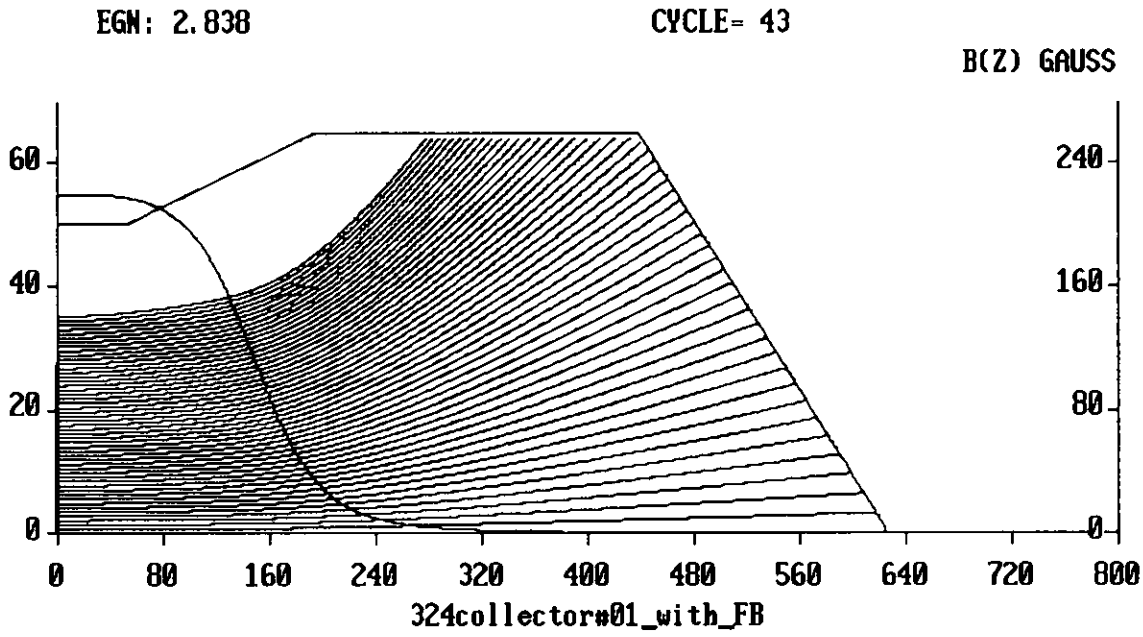

(b) with the focusing fields

Figure 4-7: EGUN95 simulation results of beam-trajectories for 324MHz klystron #1 under beam voltage of 110kV.

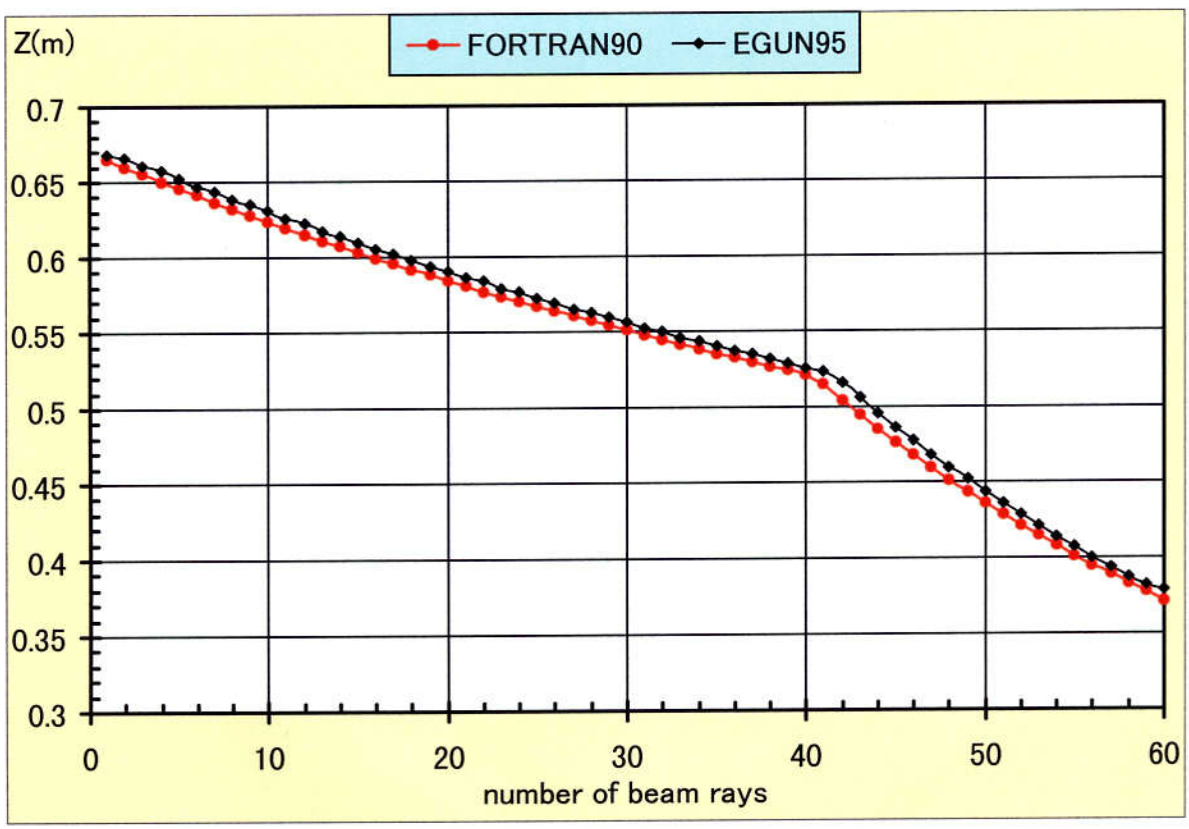

Figure 4-8: Positions in z-direction of each ray when they hit the collector for 324MHz klystron #1 under beam voltage of 110kV without external magnetic fields.

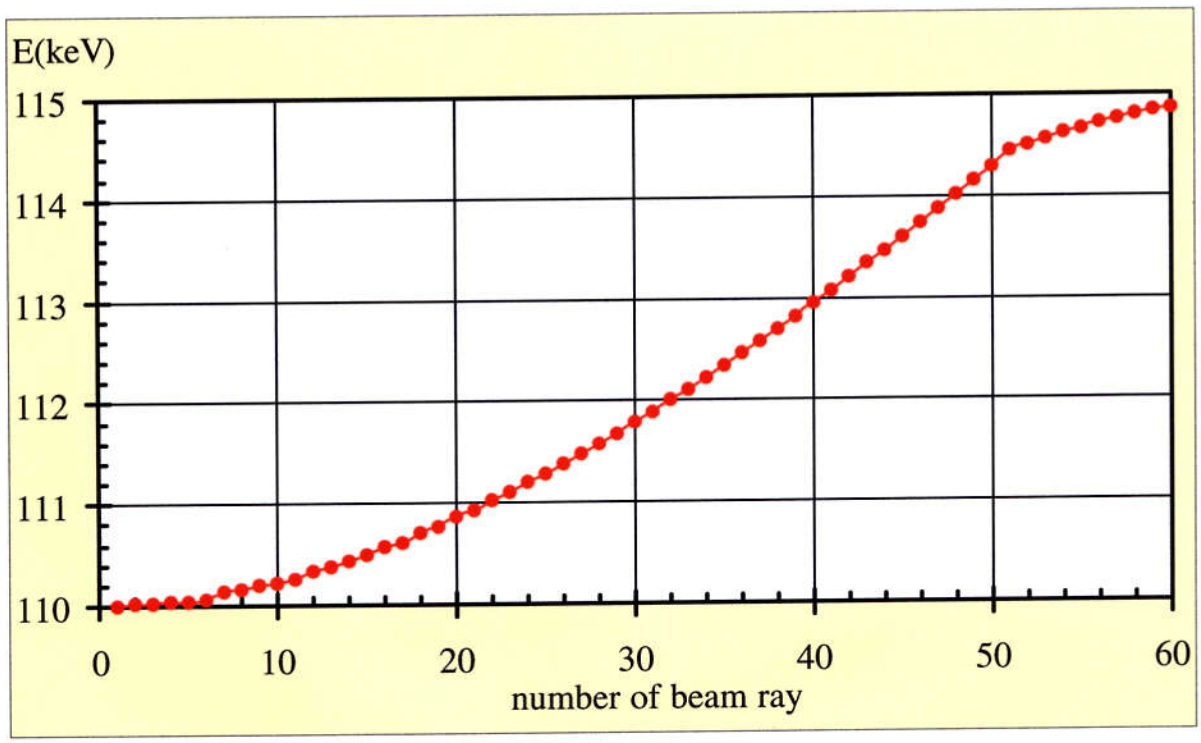

Figure 4-9: Energy of each ray when they hit the collector for 324MHz klystron #1 under beam voltage of 110kV without external magnetic fields.

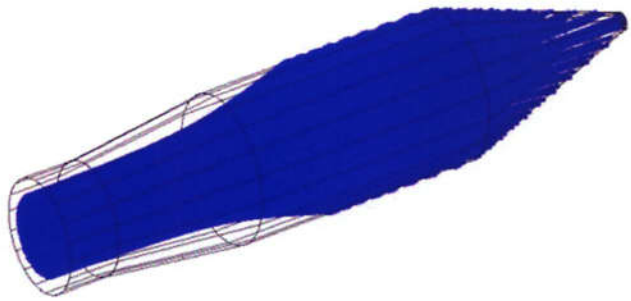

(a) tube #1

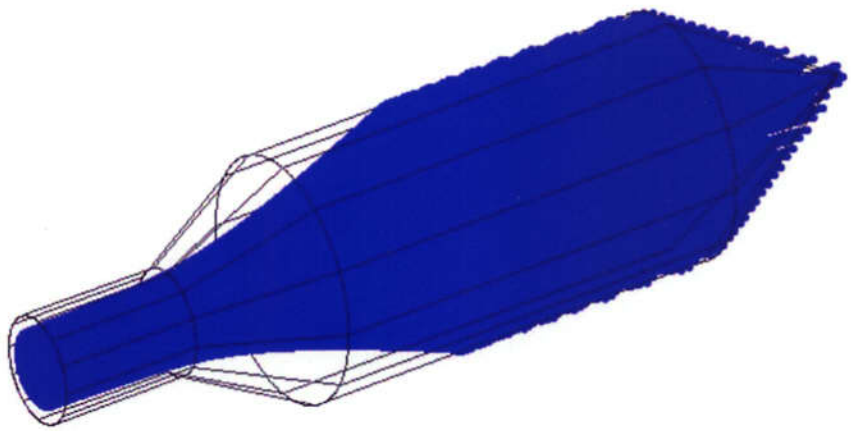

(b) tube #1A

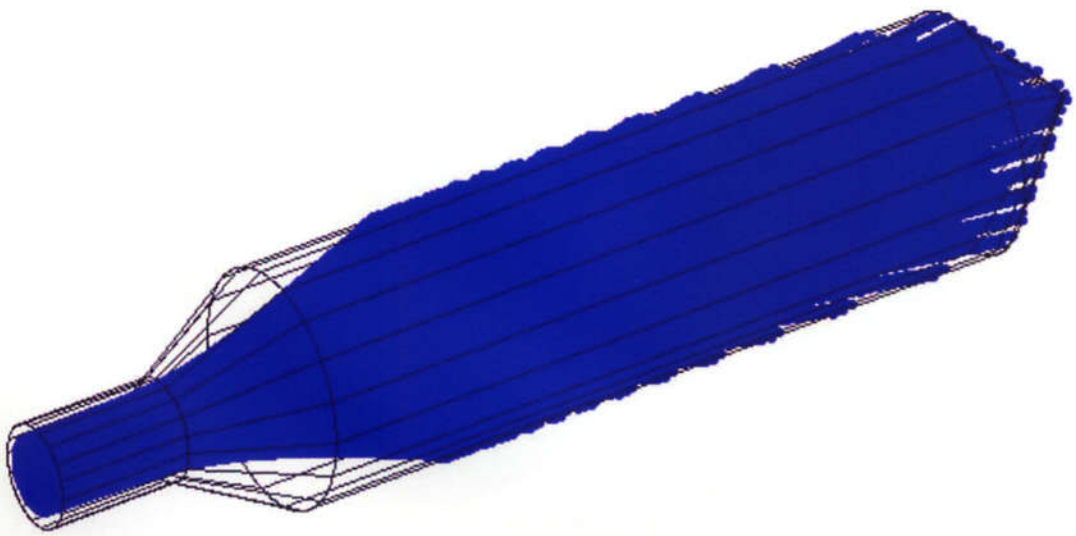

(c) tube #2

Figure 4-10: Beam-trajectory simulation results for 324MHz klystrons #1, #1A, and #2, under beam voltage of 110kV with the focusing fields.

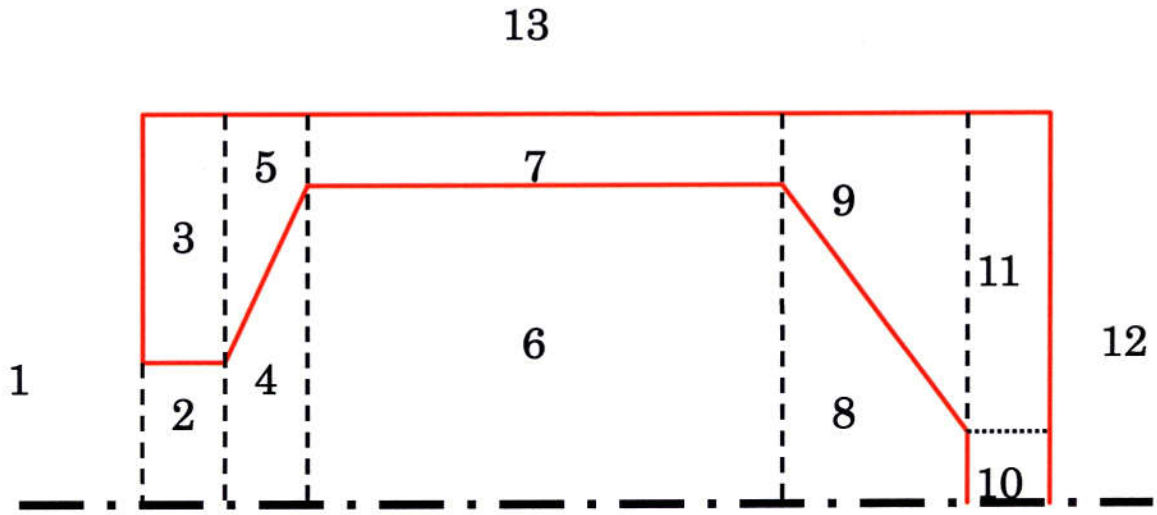

Figure 4-11: Collector of divided 13 regions for using the combinatorial geometry with the EGS4 code.

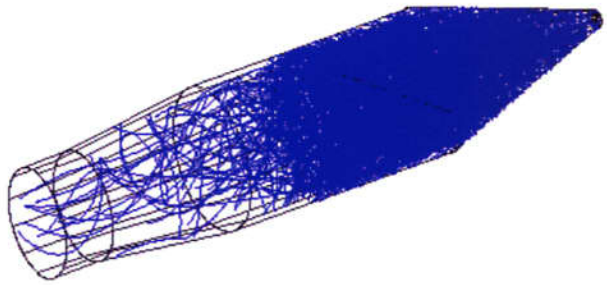

(a) tube #1

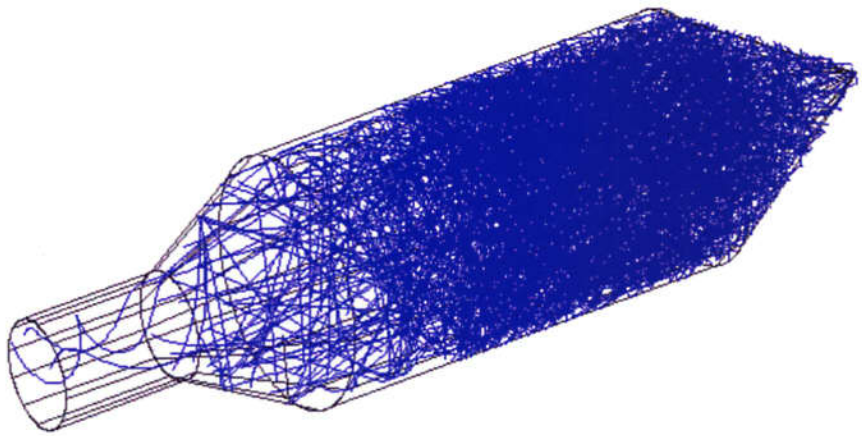

(b) tube #1A

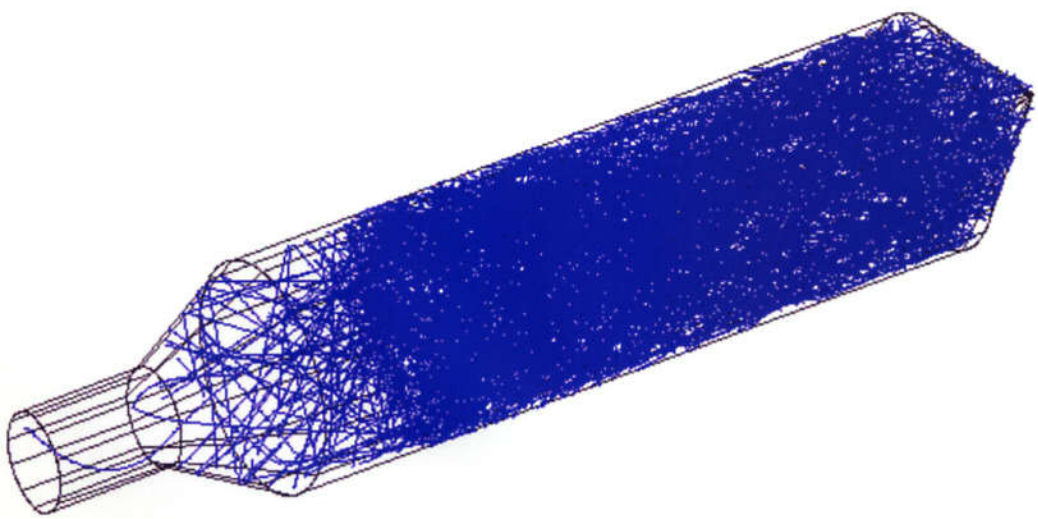

(c) tube #2

Figure 4-12: Trajectories of the backscattered and backstreaming electrons for 324MHz klystrons #1, #1A, and #2 under beam voltage of 110kV.

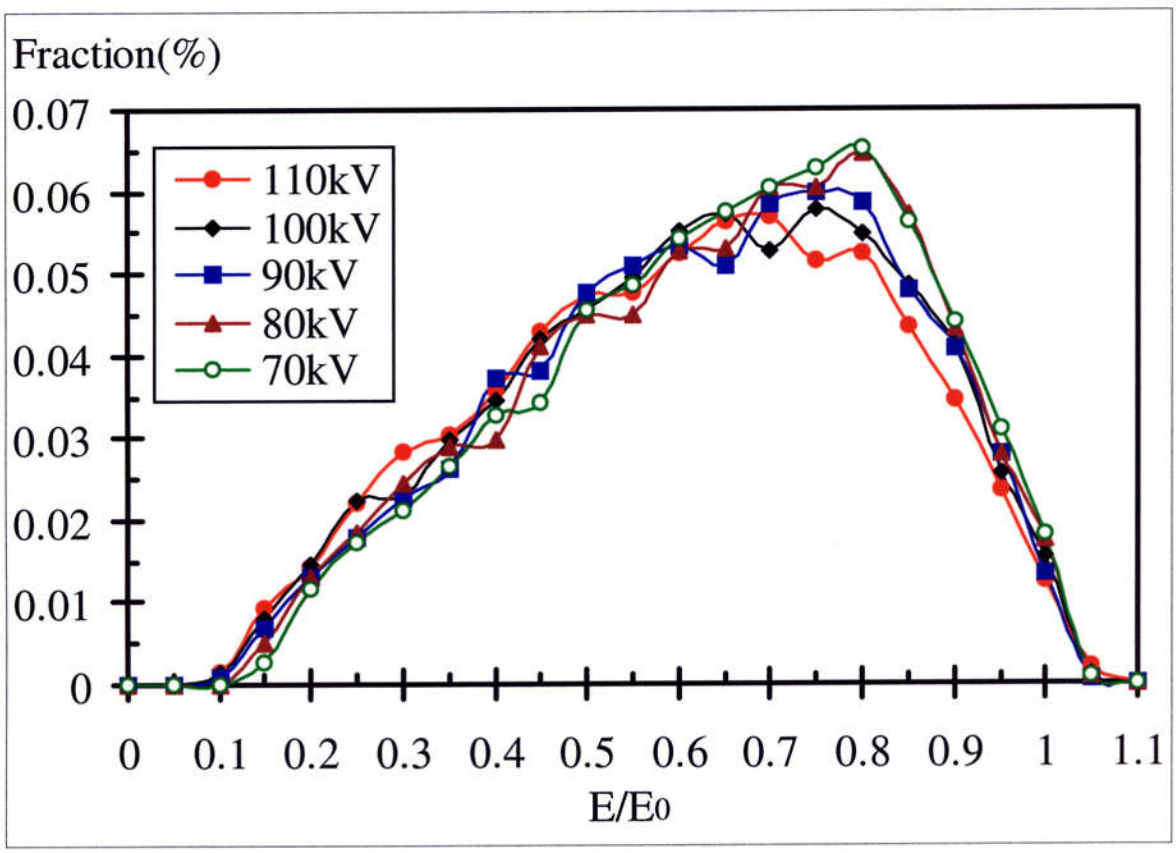

Figure 4-13: Energy distributions of the backstreaming electrons for different beam-voltages for 324MHz klystron tube #1.

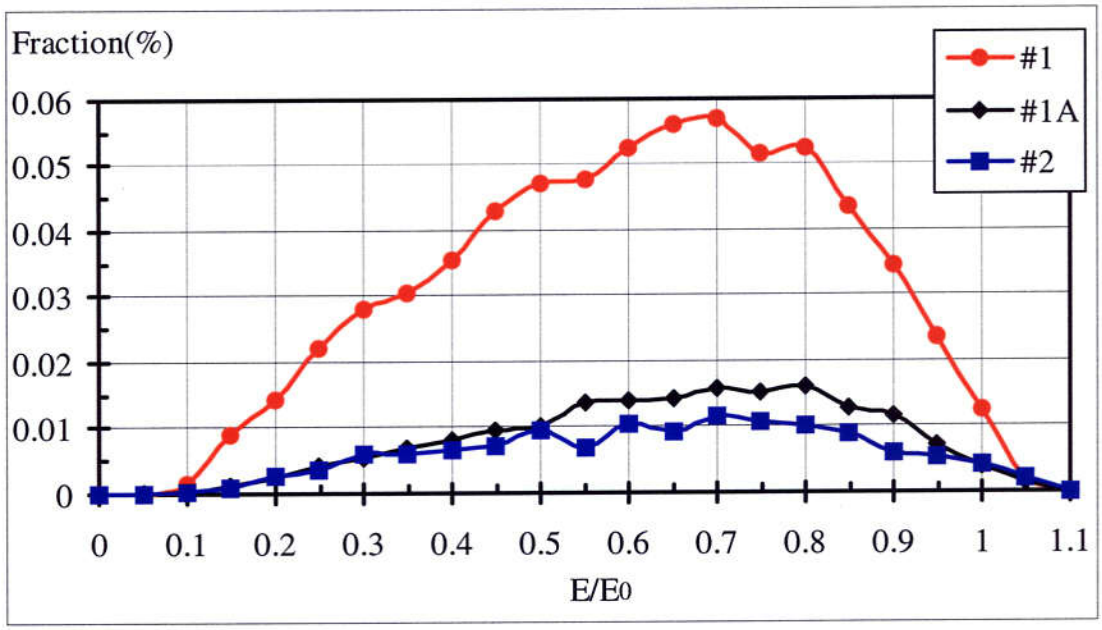

(a) distribution of the total energy

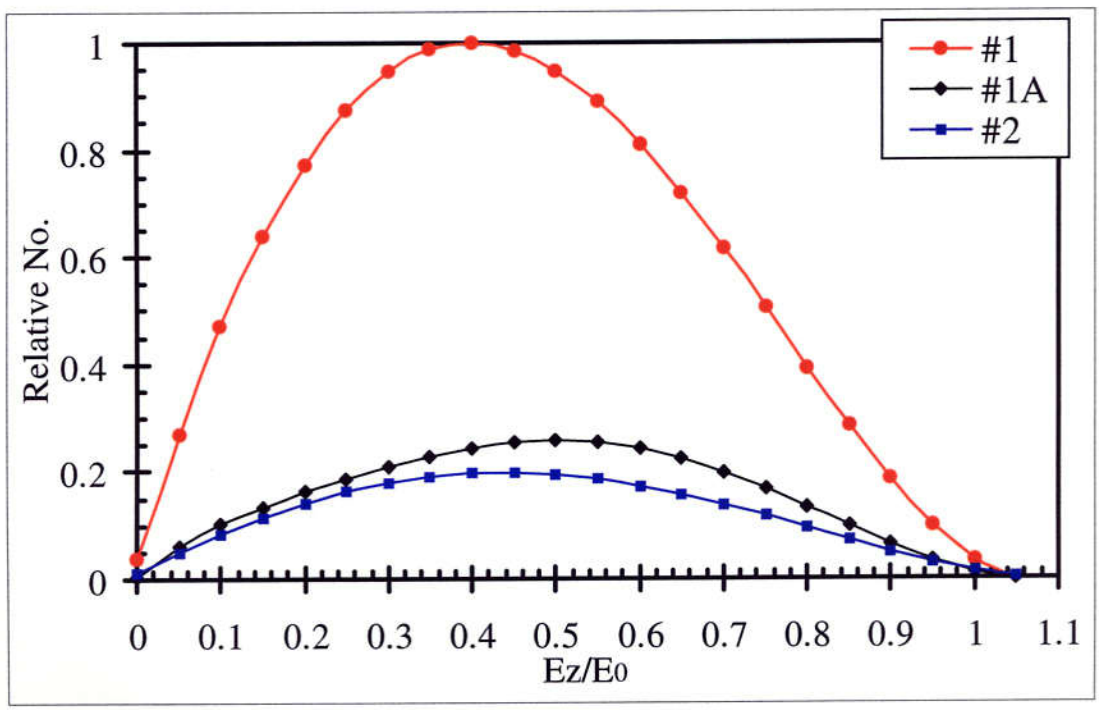

(b) distribution of the Z-component energy

Figure 4-14: Energy distributions of backstreaming electrons for 324MHz klystron tubes #1, #1A, and #2.

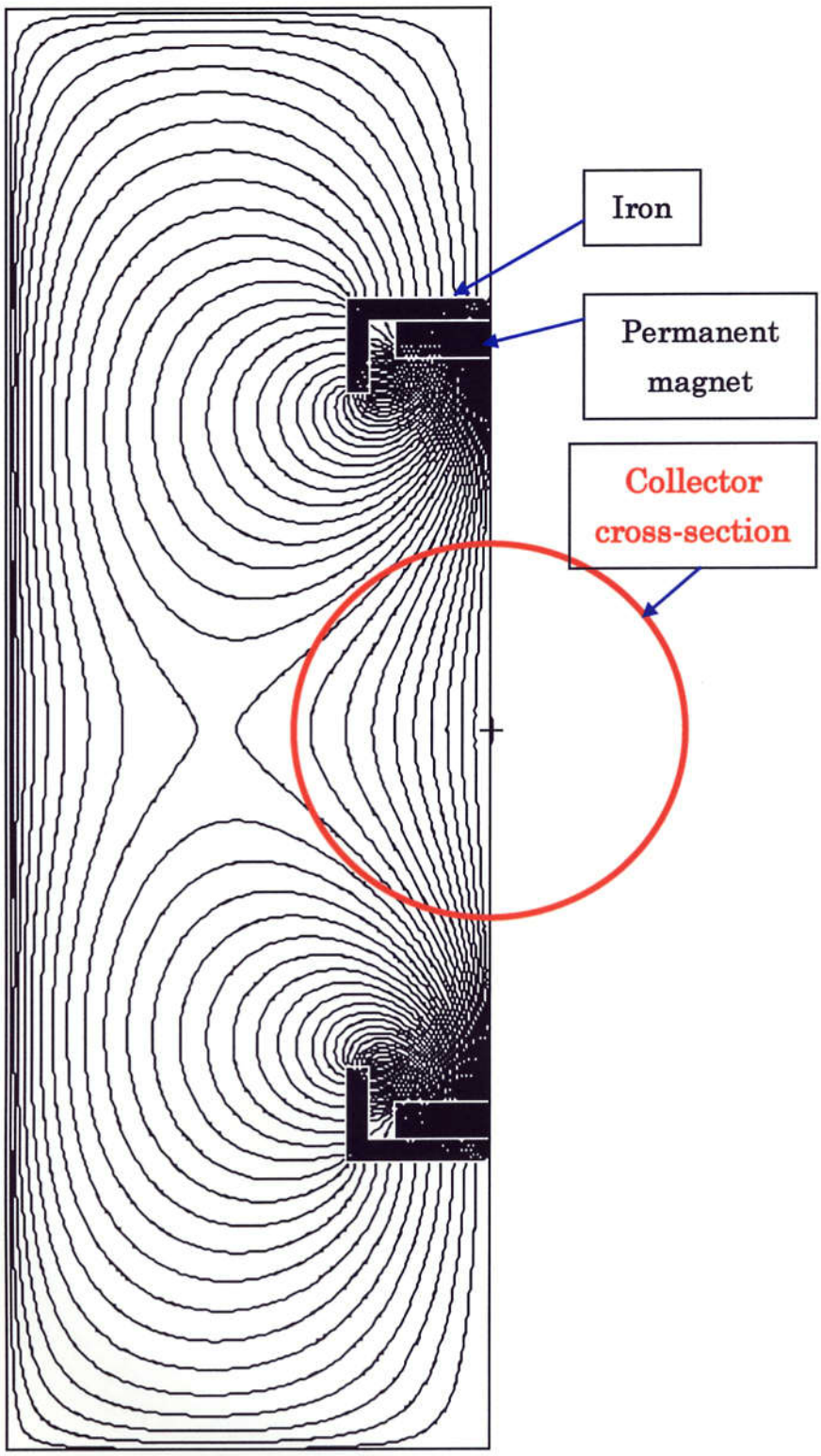

Figure 4-15: Simulation of the permanent magnets by using PANDIRA.

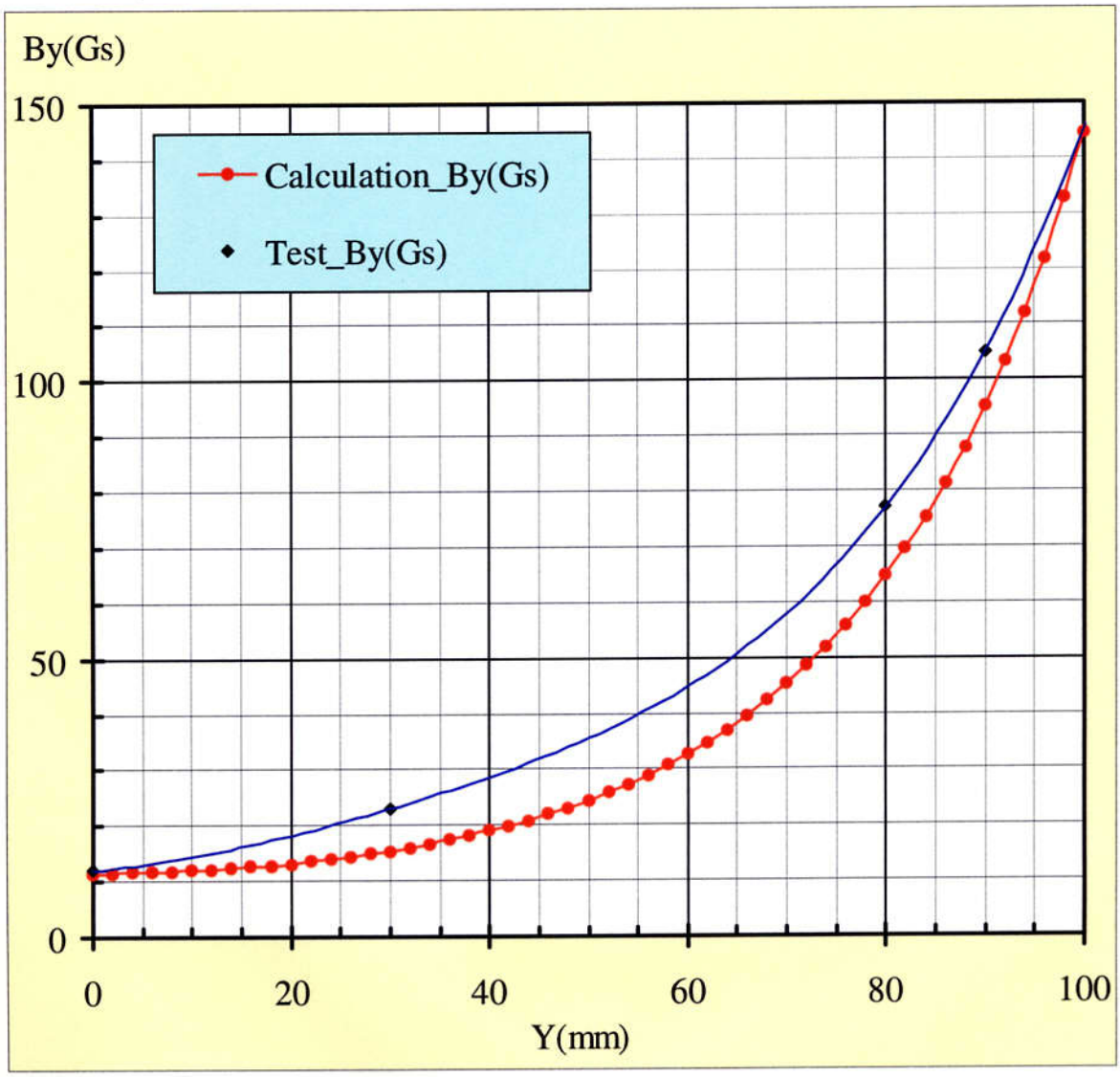

Figure 4-16: Magnetic fields in the vertical direction of the permanent magnets attached at the collector.

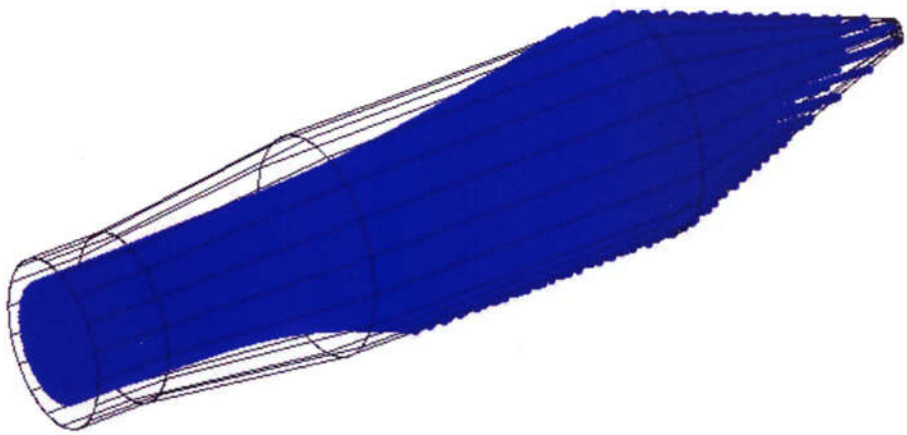

Figure 4-17: Incident beam deflected by the attached permanent magnets in the collector of 324MHz klystron #1 under beam voltage of 110kV.

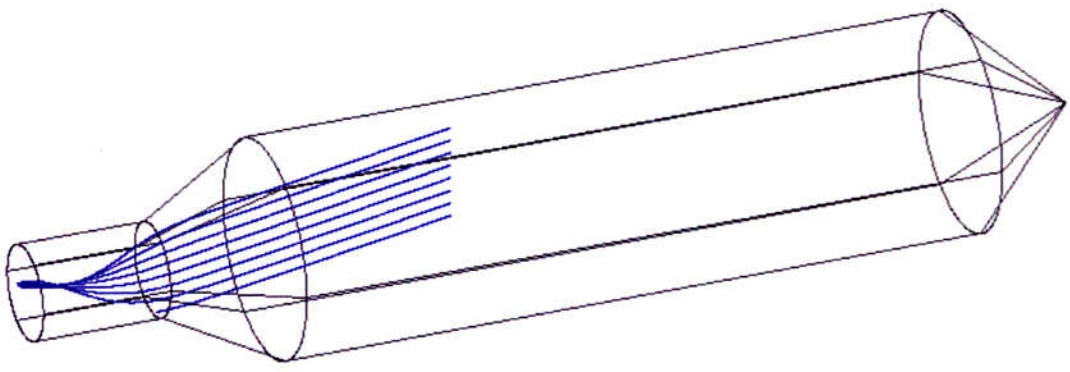

(a) E=100keV, $\mathbf{B}=1.0\times\mathbf{B_0}$

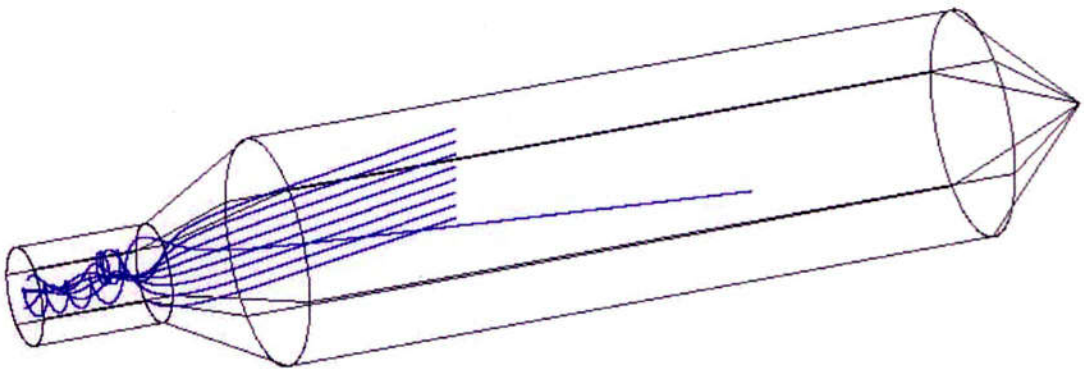

(b) E=10keV, $\mathbf{B}=1.0\times\mathbf{B_0}$

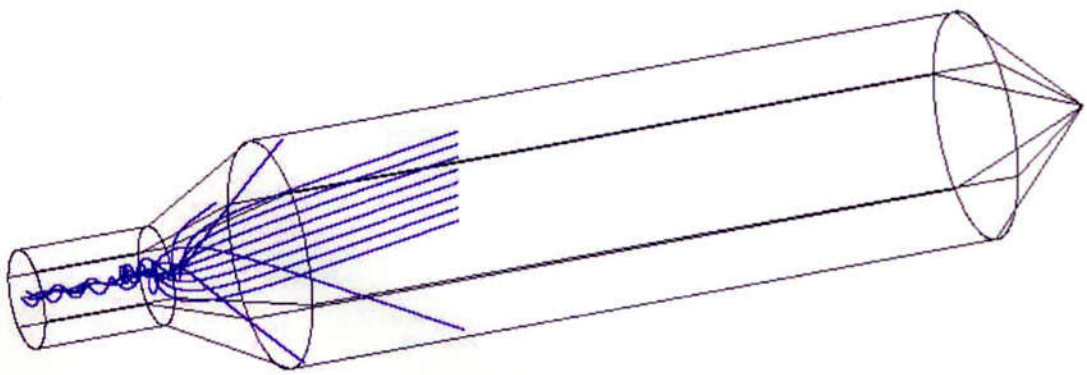

(c) E=10keV, $\mathbf{B}=2.0\times\mathbf{B_0}$

Figure 4-18: Motion of electrons of different energies (E) in magnetic fields of different strength (**B**). ($\mathbf{B_0}$, the actual applied magnetic fields in the 324MHz klystrons.)

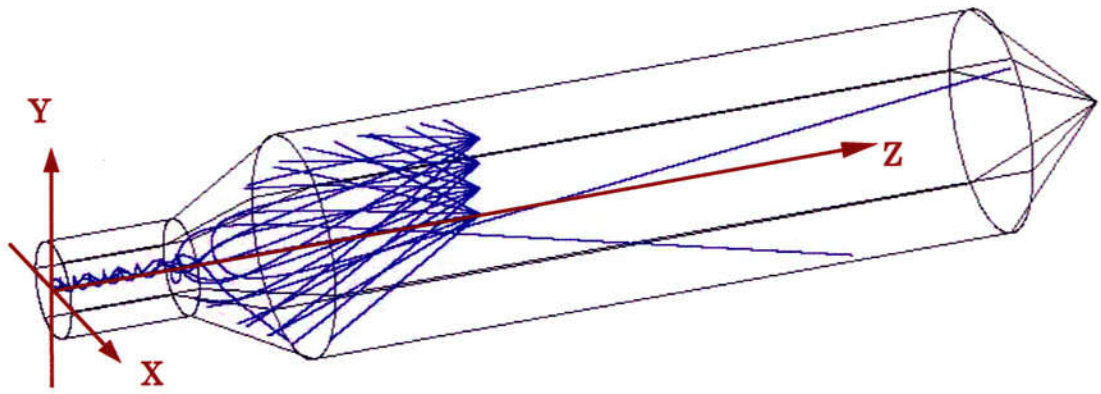

Figure 4-19: Sketch of simulation for capture ratio of electrons in magnetic fields in collector.

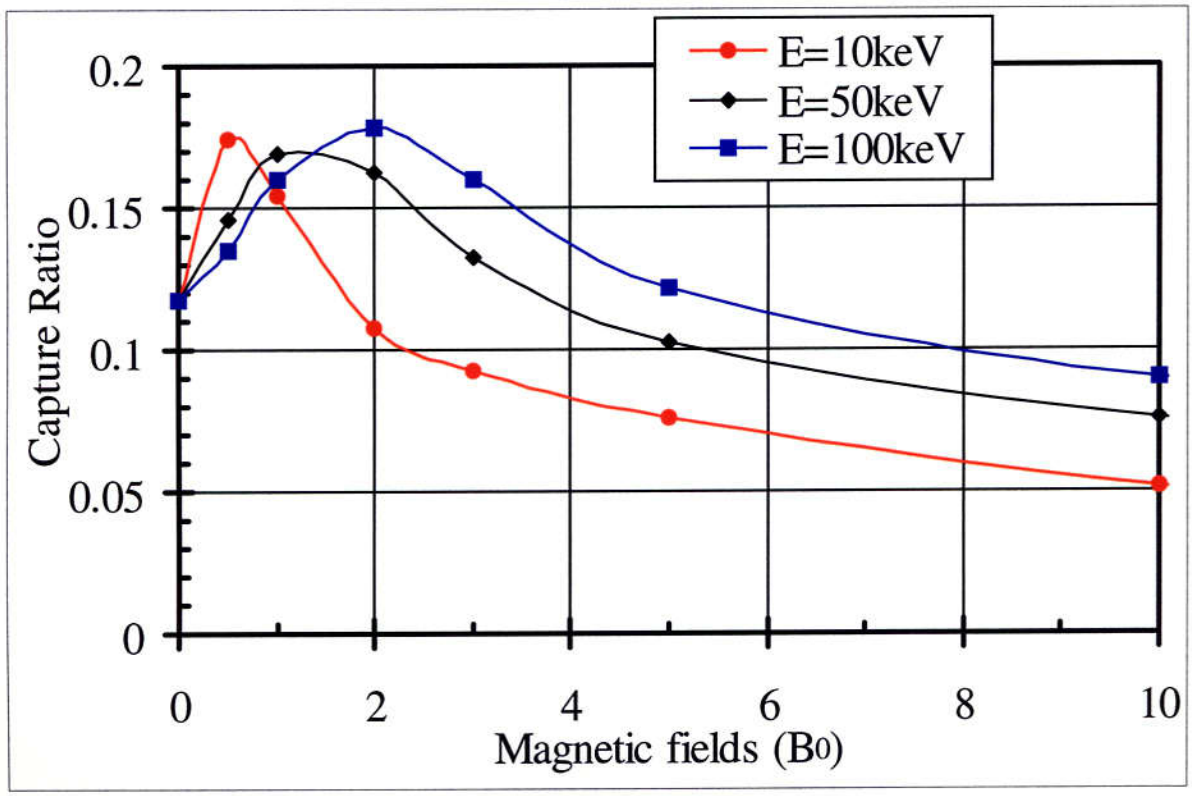

Figure 4-20: Capture ratio of electrons of different energies (E) in magnetic fields of different strength (B). (B_0, the actual applied magnetic fields in the 324MHz klystrons.)

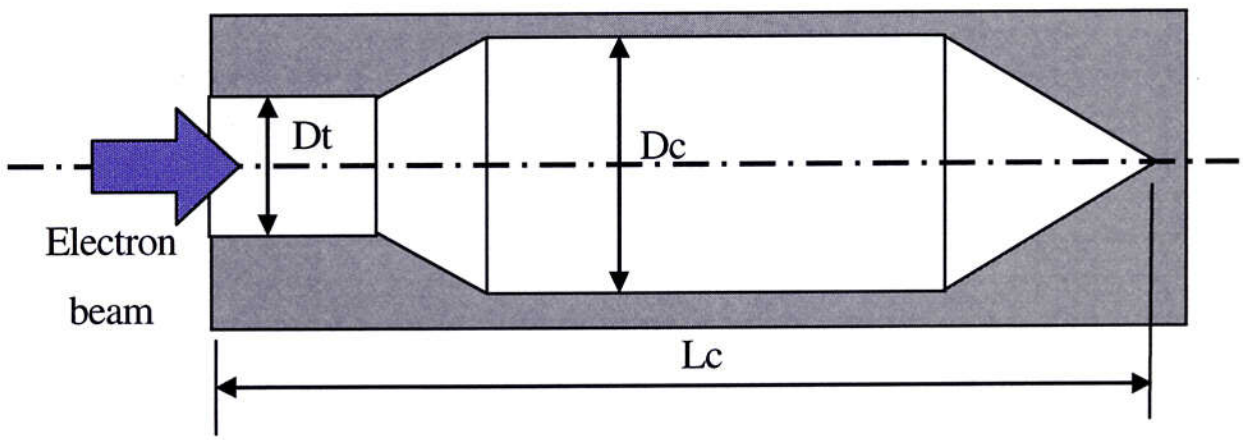

Figure 4-21: Typical collector shape.

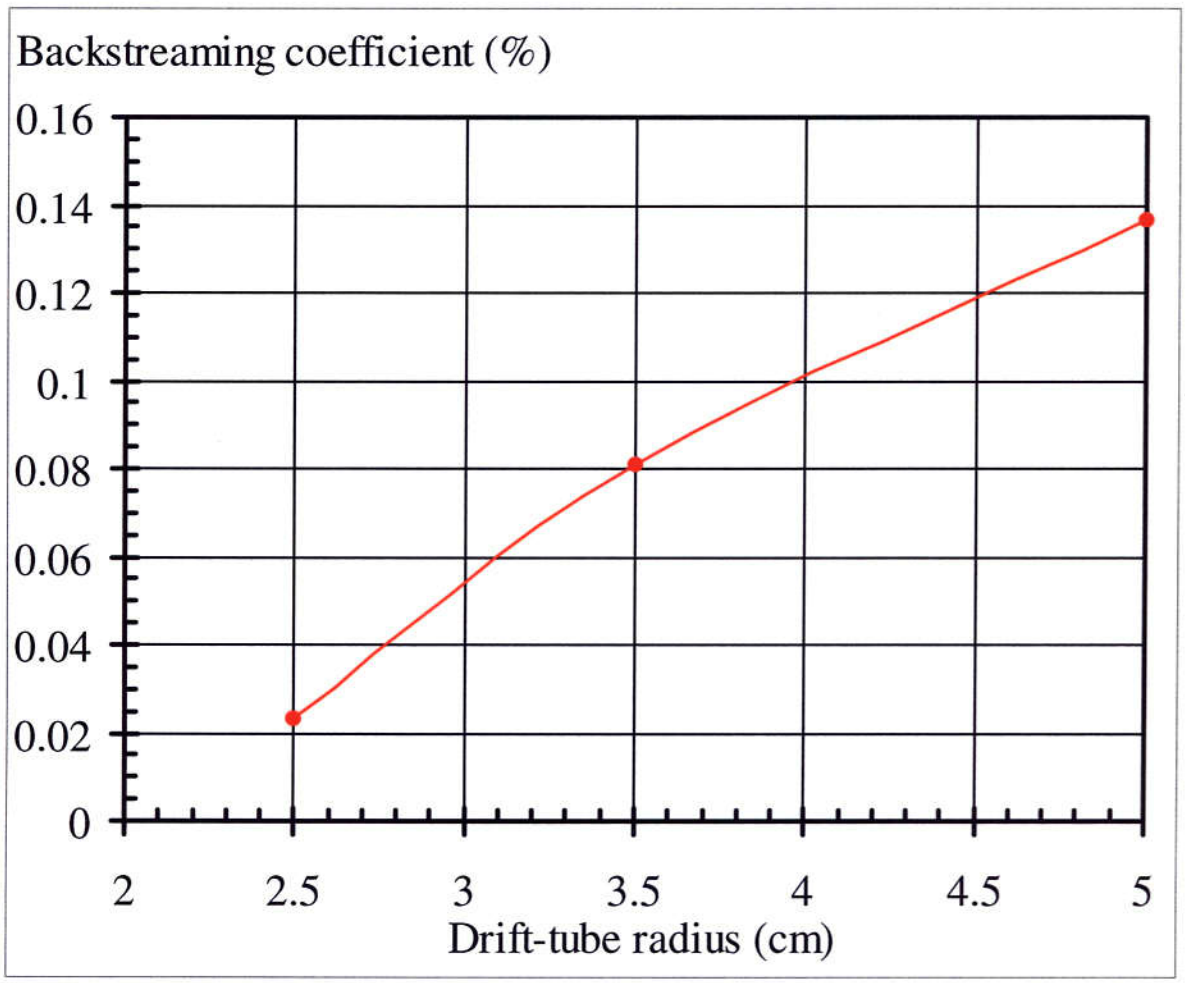

Figure 4-22: Backstreaming electron coefficient as function of the drift-tube radius. (L_c = 122.4cm, D_c = 23cm)

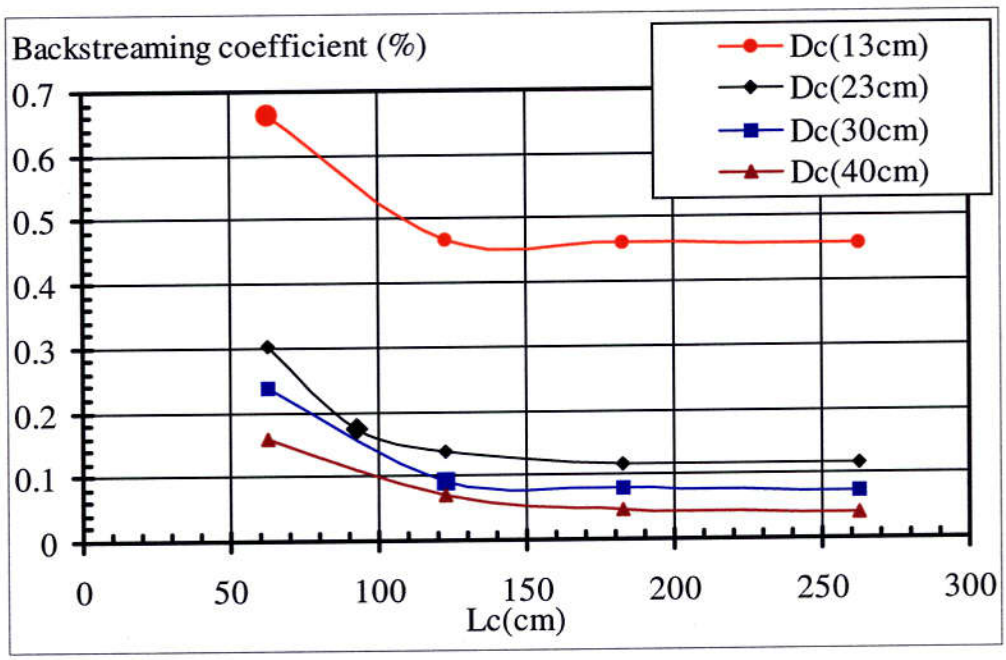

(a)

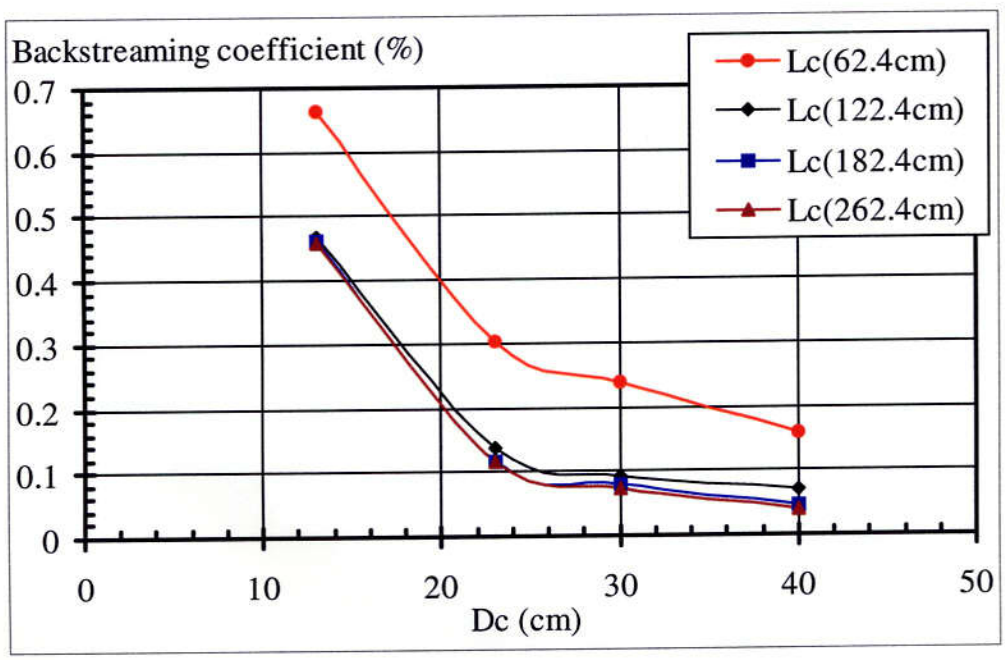

(b)

Figure 4-23: Backstreaming electron coefficient as function of the collector length (L_c) and diameter (D_c). (D_t=10cm)

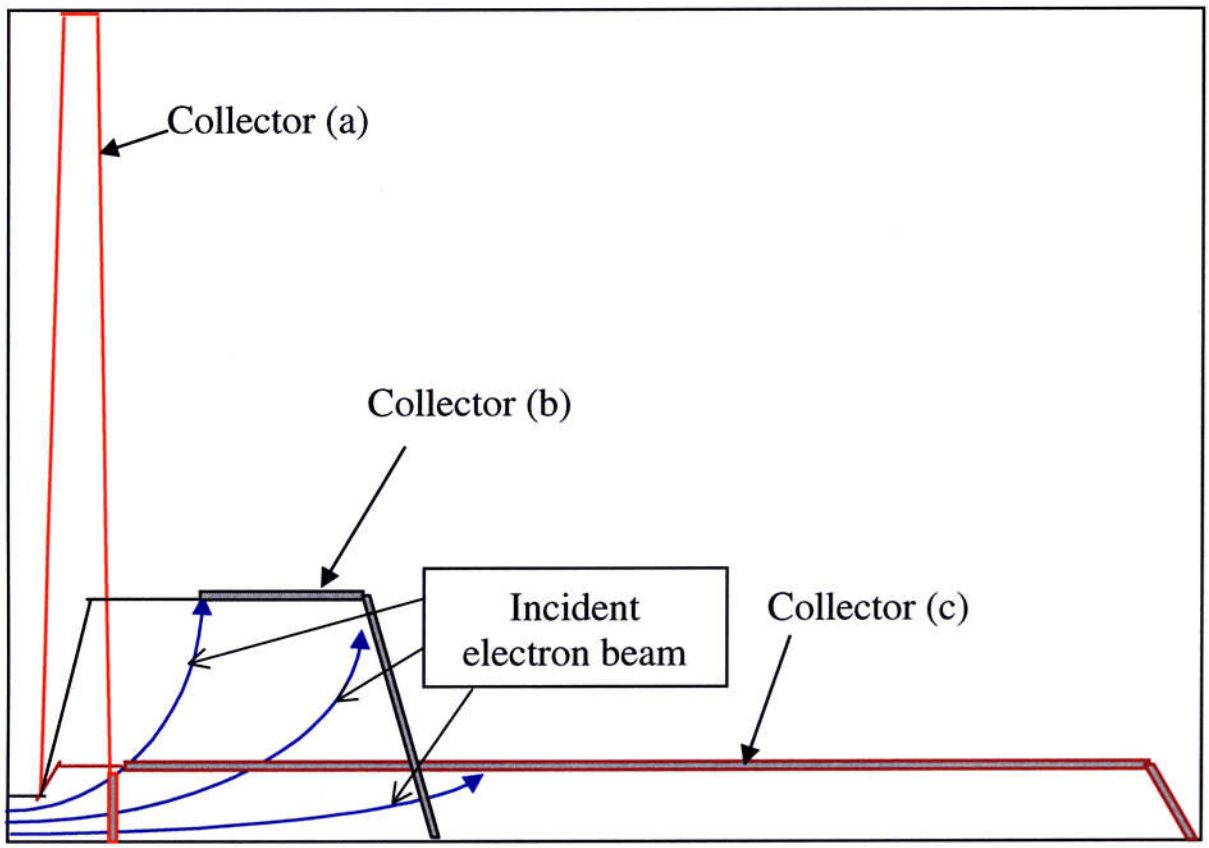

Figure 4-24: Sketch of three different typical collector shapes.

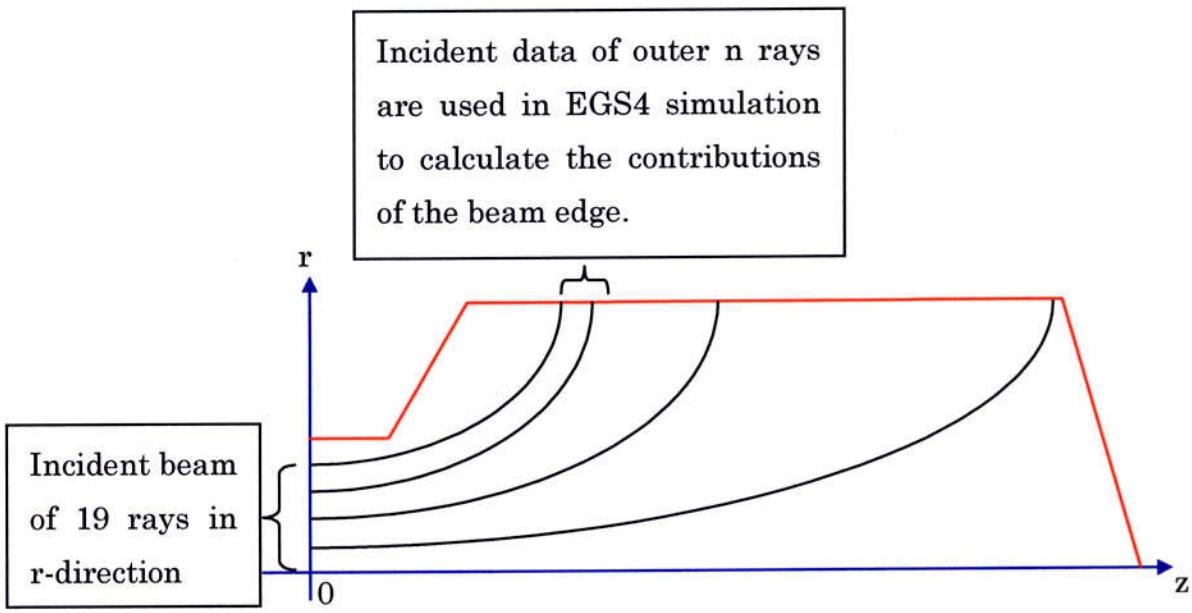

Figure 4-25: Schematic view of the incident condition for evaluation of the beam-edge contribution to the backstreaming coefficient.

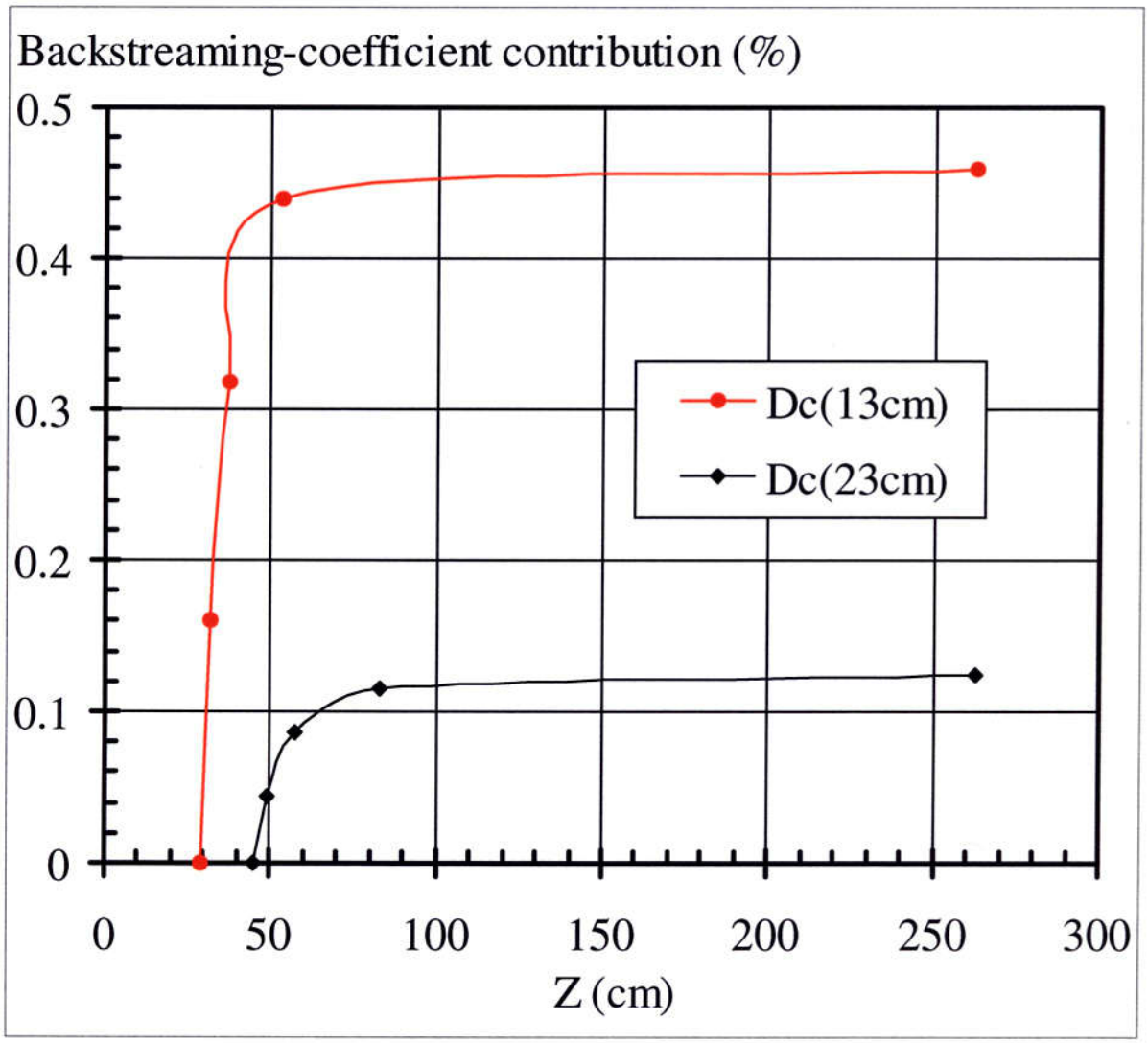

Figure 4-26: Backstreaming-coefficient contribution of the beam edge as function of the front position of beam edge bombarding the collector surface by using an incident condition shown in Figure 4-25. (L_c=262.4cm, D_t=10cm)

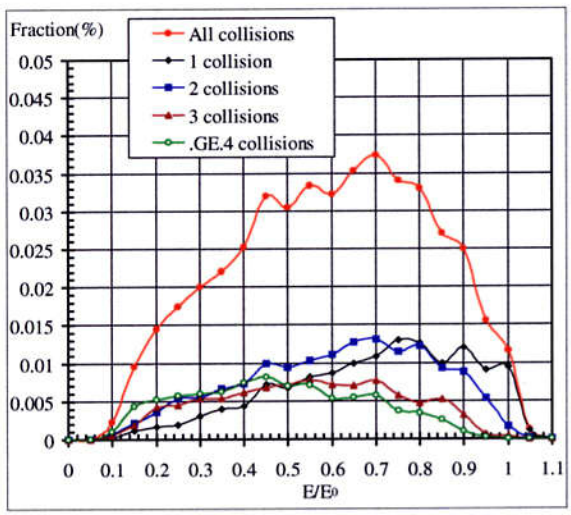

(a) L_c=122.4cm, D_c=13cm, D_t=10cm.

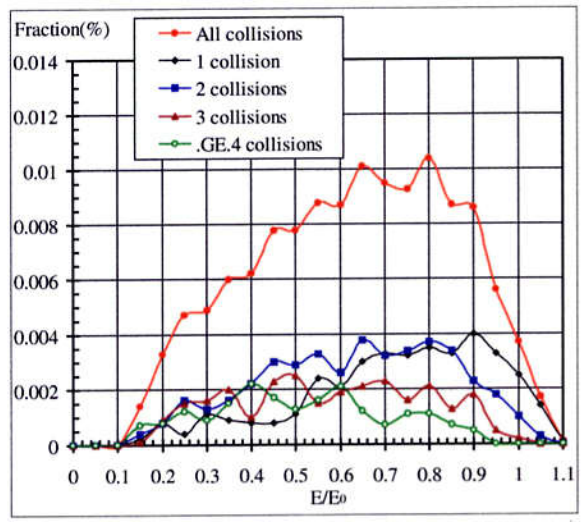

(b) L_c=122.4cm, D_c=23cm, D_t=10cm.

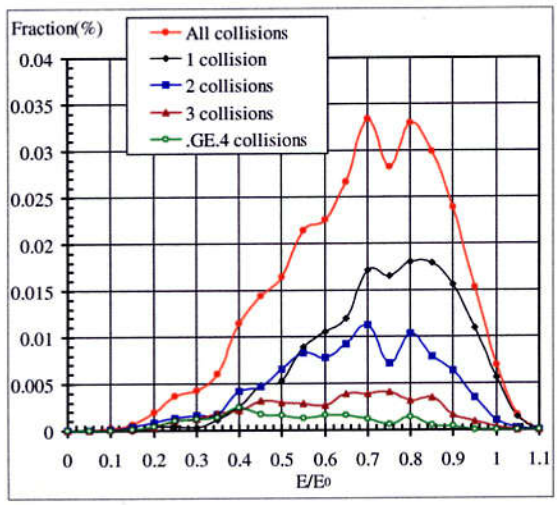

(c) L_c=62.4cm, D_c=23cm, D_t=10cm.

Figure 4-27: Energy distributions of the backstreaming electrons undergoing successive collisions. (GE., more than or equal to.)

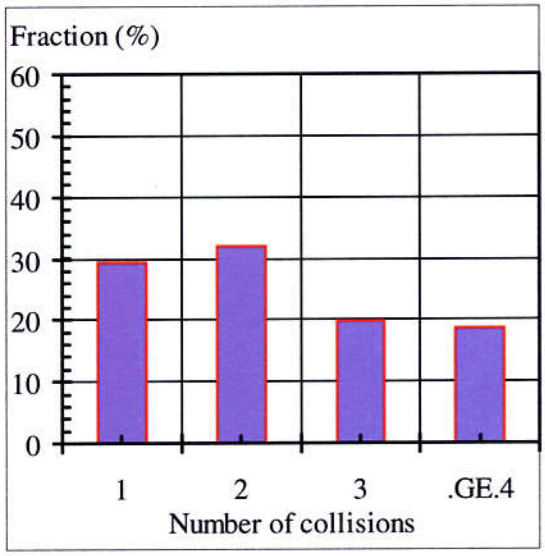

(a) L_c=122.4cm, D_c=13cm, D_t=10cm.

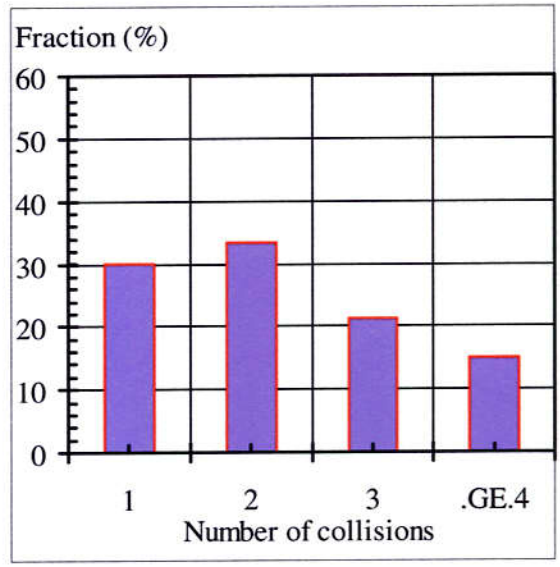

(b) L_c=122.4cm, D_c=23cm, D_t=10cm.

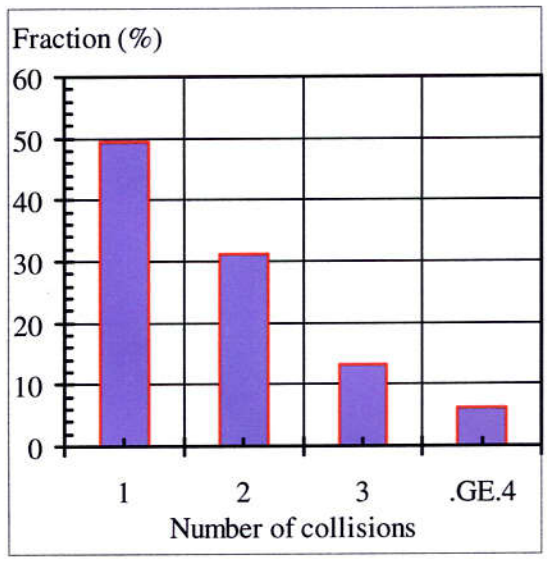

(c) L_c=62.4cm, D_c=23cm, D_t=10cm.

Figure 4-28: Fractions of the backstreaming electrons undergoing successive collisions. (GE., more than or equal to.)

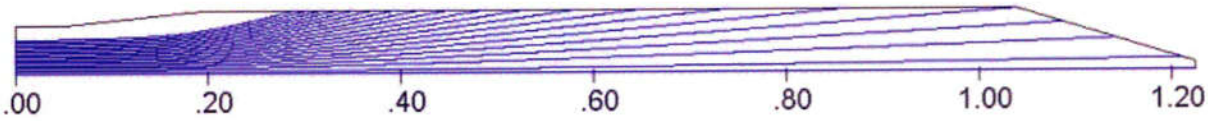

(a) Trajectories of the injection beam.

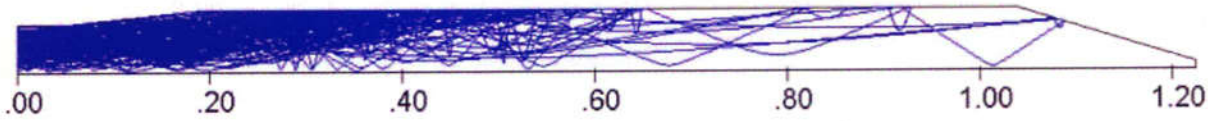

(b) Trajectories of the total backstreaming electrons.

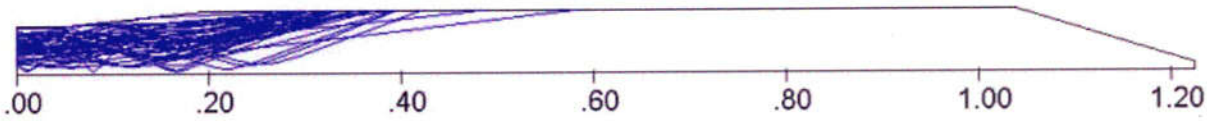

(c) Trajectories of the backstreaming electrons undergoing single collision.

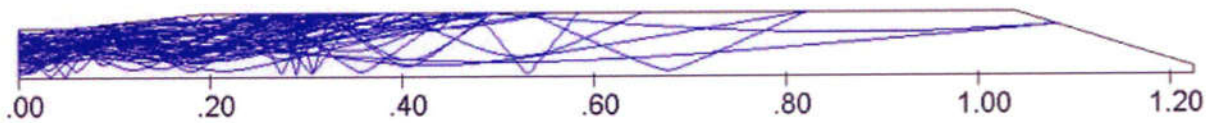

(d) Trajectories of the backstreaming electrons undergoing two-successive collisions.

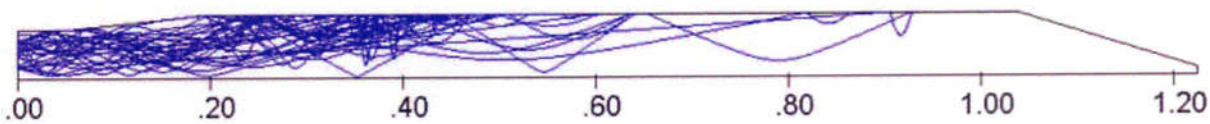

(e) Trajectories of the backstreaming electrons undergoing three-successive collisions.

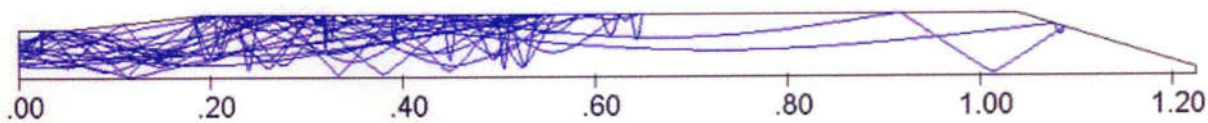

(f) Trajectories of the backstreaming electrons undergoing more-than-four-successive collisions.

Figure 4-29: Trajectories of the injection beam and the backstreaming electrons undergoing successive collisions for the collector of L_c=122.4cm, D_c=13cm, and D_t=10cm.

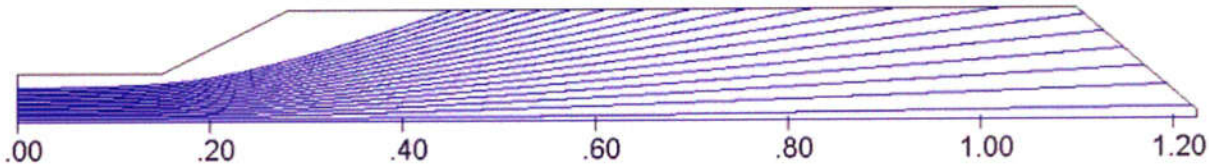

(a) Trajectories of the injection beam.

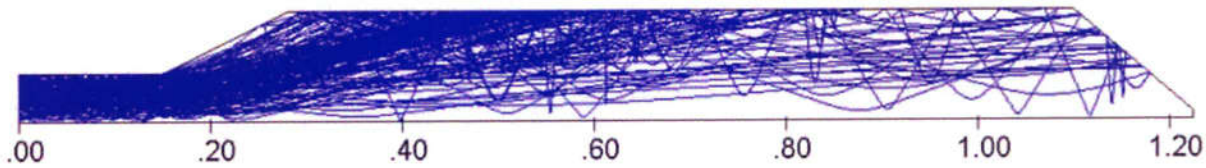

(b) Trajectories of the total backstreaming electrons.

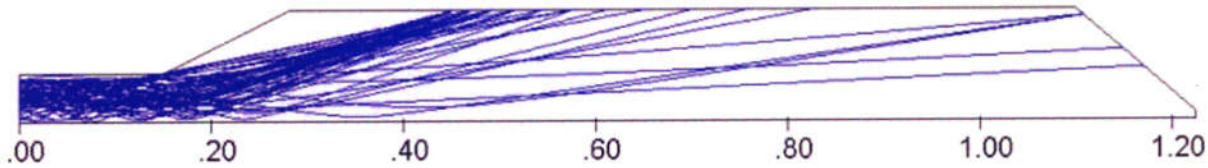

(c) Trajectories of the backstreaming electrons undergoing single collision.

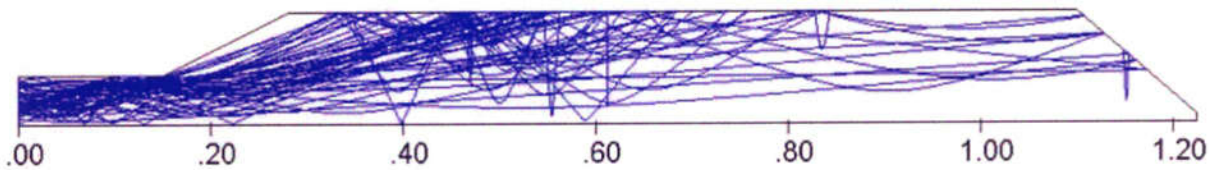

(d) Trajectories of the backstreaming electrons undergoing two-successive collisions.

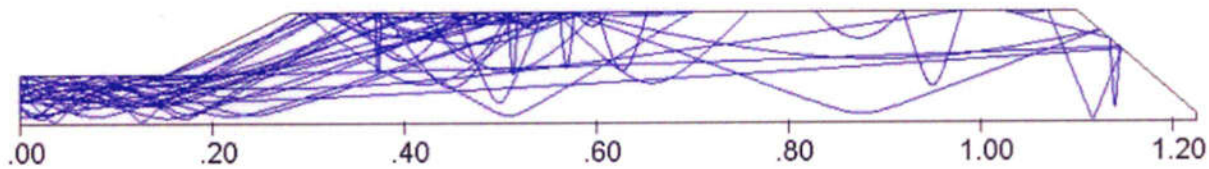

(e) Trajectories of the backstreaming electrons undergoing three-successive collisions.

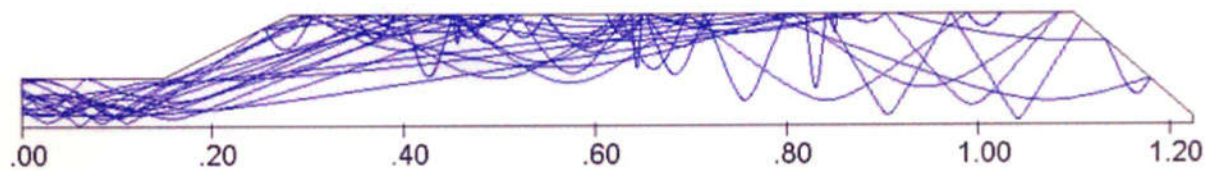

(f) Trajectories of the backstreaming electrons undergoing more-than-four-successive collisions.

Figure 4-30: Trajectories of the injection beam and the backstreaming electrons undergoing successive collisions for the collector of L_c=122.4cm, D_c=23cm, and D_t=10cm.

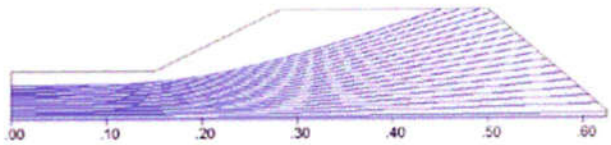

(a) Trajectories of the injection beam.

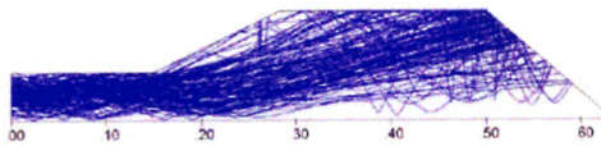

(b) Trajectories of the total backstreaming electrons.

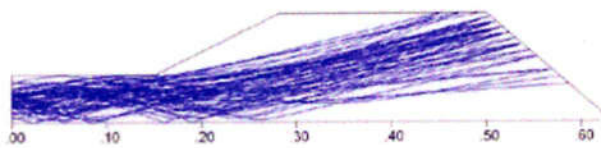

(c) Trajectories of the backstreaming electrons undergoing single collision.

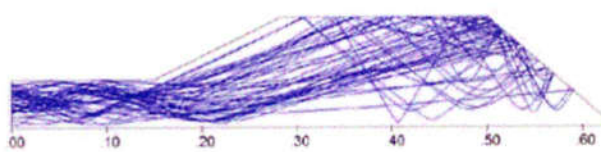

(d) Trajectories of the backstreaming electrons undergoing two-successive collisions.

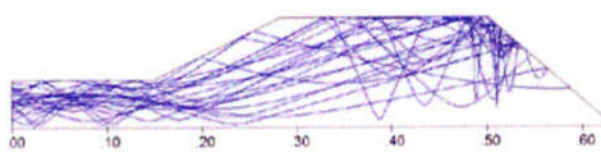

(e) Trajectories of the backstreaming electrons undergoing three-successive collisions.

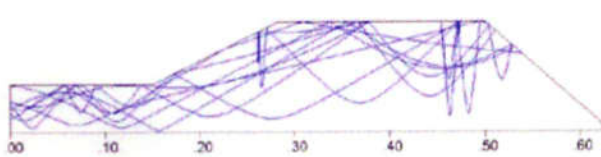

(f) Trajectories of the backstreaming electrons undergoing more-than-four-successive collisions.

Figure 4-31: Trajectories of the injection beam and the backstreaming electrons undergoing successive collisions for the collector of L_c=62.4cm, D_c=23cm, and D_t=10cm.

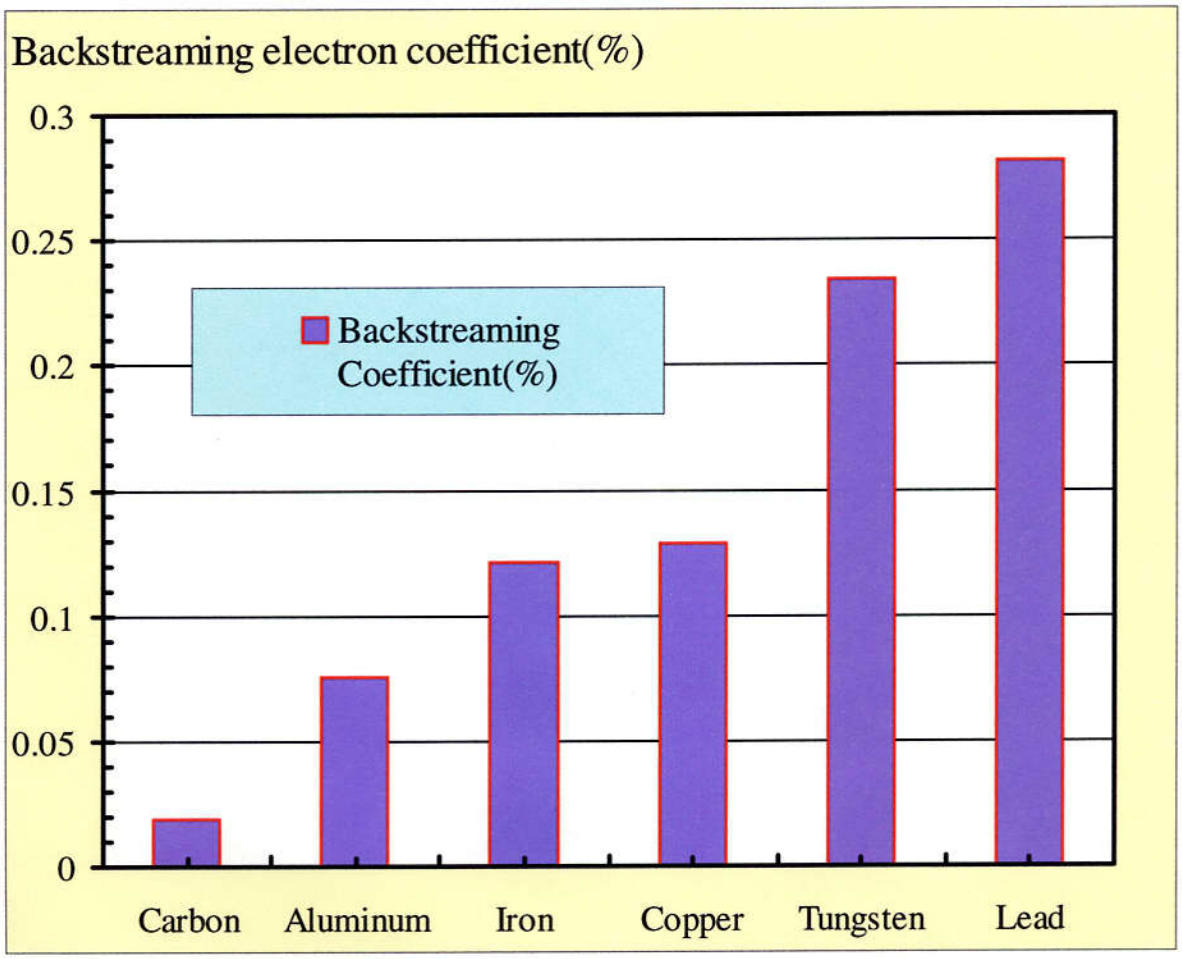

Figure 4-32: Backstreaming electron coefficient as a function of the collector material. (The same dimensions as the collector of klystron #2 are used.)

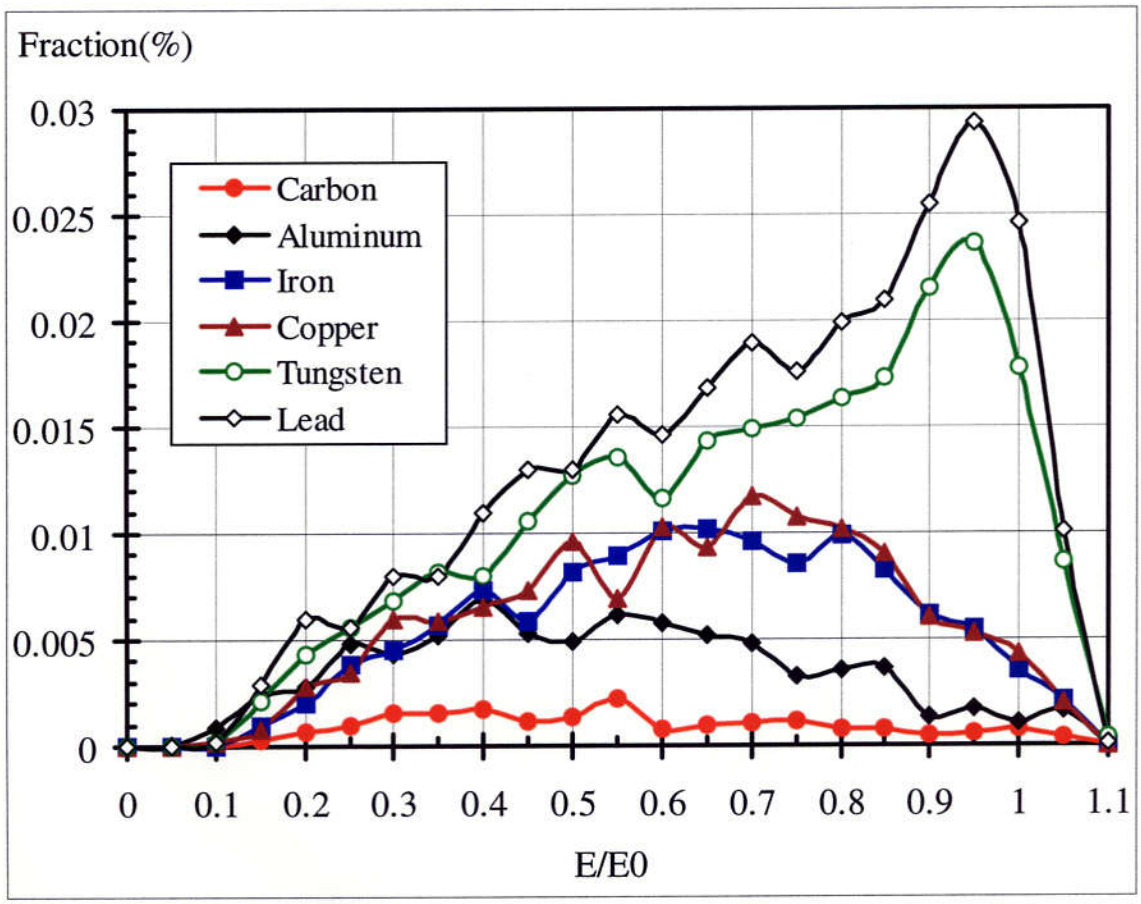

Figure 4-33: Backstreaming electron energy distribution as function of the collector material. (The same dimensions as the collector of klystron #2 are used.)

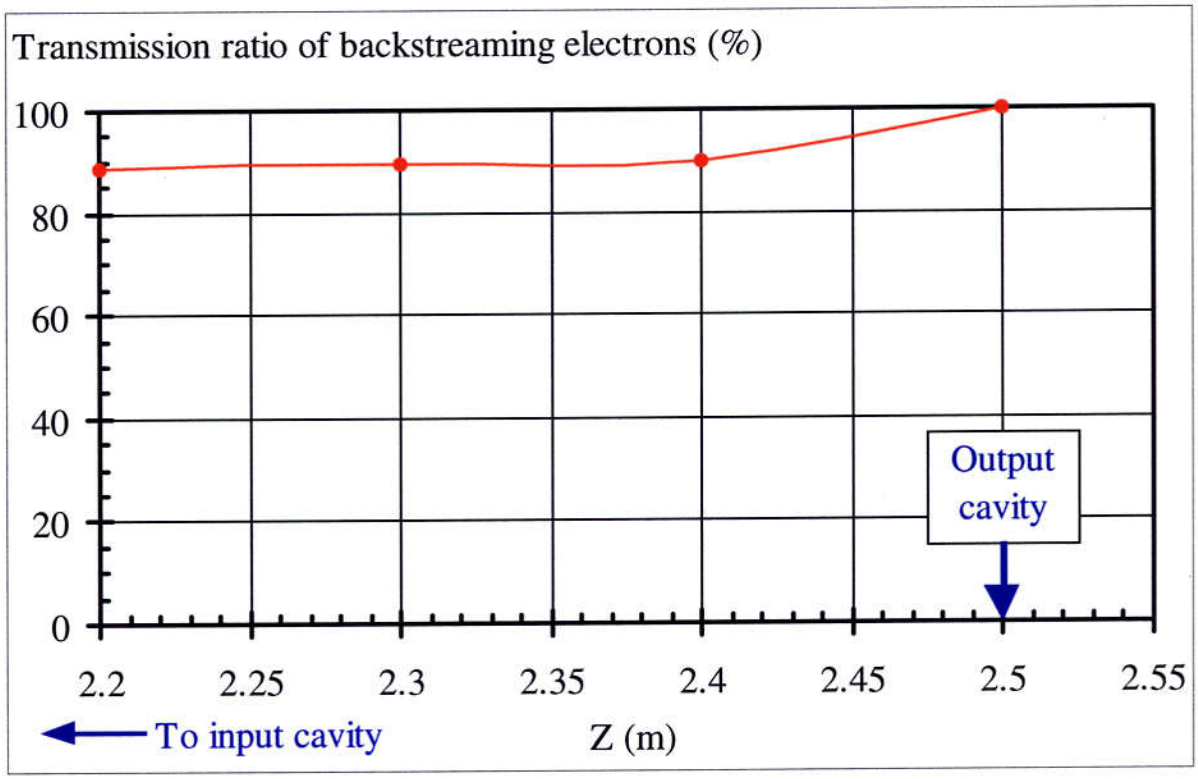

Figure 4-34: Transmission ratio of backstreaming electrons in a drift tube near the collector entrance.

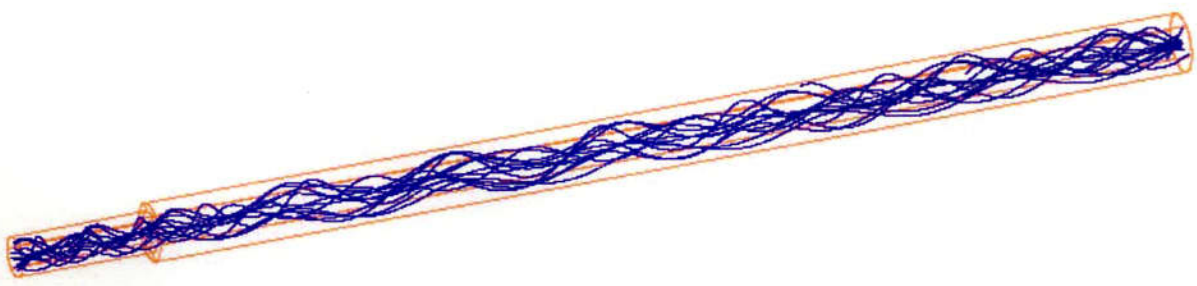

Figure 4-35: Trajectories of backstreaming electrons passing through the whole drift tube.

Chapter 5

Oscillation Mechanism and Conditions Due to Backstreaming Electrons

5.1 Introduction

The simulations of the backstreaming electrons from the collector into drift tube have been performed in Chapter 4, and the information of backstreaming electrons has been carried out, including the backstreaming electron current and their energy distribution under different conditions of the klystron. In this chapter, these simulation results of the backstreaming electrons are applied to the study of the oscillation mechanism and conditions. At first, analyses of the mechanism and conditions are performed for these electrons causing the spurious oscillations. Since the backstreaming electrons can carry the rf signals from the output cavity to the input cavity, they result in a formation of a feedback loop inside the tube. From the feedback theory, the oscillation conditions can be expressed by the complex product of the klystron voltage-gain and feedback coefficient caused by the backstreaming electrons: (1) the amplitude of the product should be larger than unity, and (2) the phase of the product should be zero or integral times of 2π. Then relevant calculations of the oscillation conditions are also executed using the simulation results of the backstreaming electrons from the collector. The voltage gain of the klystron is simulated by JPNDISK, and the feedback coefficient due to the backstreaming electrons is calculated by a FORTRAN90 program applying the ballistic theory. Based on the calculations of the oscillation conditions, the beam-voltage regions of the oscillations for the 324MHz klystrons are worked out, and a good agreement is shown with the experiments.

5.2 Analyses of oscillation mechanism and conditions

In the klystron, after electrons of the main beam bombard the surface of the collector, back-scattered electrons are produced by elastic and inelastic process with atomic electrons, and some of these back-scattered electrons return into the drift tube of the klystron. Same as the main beam of a klystron, when the backstreaming electrons go into and pass through the drift tube under the same focusing magnetic field, a reverse 'klystron' comes out. Thus the backstreaming electrons will carry the rf signals from the output cavity to the input cavity. Since these backstreaming electrons are modulated by a complex gap voltage V_o of the output cavity, they induce a complex rf voltage V_f in the input cavity after drifting the drift tube toward the upstream. In this way, the backstreaming electrons and the main beam of the klystron form a feedback loop as shown in Figure 5-1, and it's possible to cause spurious oscillations. In Figure 5-1, A is the complex voltage gain of the klystron;

$$A = V_o / V_d \tag{5.1}$$

where V_d is the complex input cavity voltage modulating the main beam. β is a complex feedback coefficient caused by the backstreaming electrons. The feedback coefficient is a voltage gain of the reverse 'klystron' made up of the backstreaming electrons, and can be expressed as

$$\beta = V_f / V_o \tag{5.2}$$

From the feedback theory on stability and oscillators, if the input cavity voltage could be regenerated by the backstreaming electrons, oscillations will occur. In this case, if the phase of the induced voltage by the backstreaming electrons is the same as the phase of the voltage modulating the main beam, and the amplitude of the induced voltage is larger than that of the modulation voltage, then the input cavity voltage is regenerated by the backstreaming electrons and spurious oscillations will occur. In other words, the oscillation conditions are

$$|A\beta| > 1 \tag{5.3}$$

and

$$\arg(A\beta) = \arg(A) + \arg(\beta) = 2n\pi, \qquad n = 0, 1, 2... \qquad (5.4)$$

where the complex variable A is expressed as the product of delayed function and the factor analogous to the gain function of a number of amplifying stage in cascade from Chapter 3 of the reference [5-1]. If the phase of the delayed function is θ_0, this phase is considered to be nearly the dc transit angle from the input cavity to the output cavity. Therefore, it is written as,

$$A \equiv |A| \angle \arg(A)$$
$$= |V_o / V_d| \angle -\theta_0 \qquad (5.5)$$

where θ_0 is a delayed angle corresponding to the DC transit time, which is a function of the angle frequency ω, the distance Z between the input and output cavities, and the Z-component of the electron velocity, u_0 .

$$\theta_0 = \omega Z / u_0 \qquad (5.6)$$

In order to evaluate the complex variable A, the one-dimensional simulation code, JPNDISK [5-2] is applied to the UHF klystrons with the actual parameters. Though 2.5-dimensional PIC code, such as ARSENAL [5-3] and FCI [5-4] are often used for designing the klystron, one-dimensional code is very convenient and it saves lots of time for our analysis. In the same manner,

$$\beta = |V_f / V_o| \angle -\theta_0' \qquad (5.7)$$

where θ_0' is the delayed angle corresponding to the dc transit angle for the backstreaming electrons. In order to calculate β using the backstreaming-electron current derived in the previous chapter, a modulation process is considered for the backstreaming electrons at the output cavity. This process is similar as that of the main beam modulated at the input cavity of the klystron. For the backstreaming electrons, considering only the output cavity contribution is enough. If the backstreaming electron coefficient is η_b, the backstreaming current is I_b, and forward current is I_0,

$$I_b = \eta_b I_0 \qquad (5.8)$$

From Figure 4-14, the backstreaming electrons have a broad energy distribution $\eta(x)$, which is different from the forward beam with a well-defined energy. However there is no suitable simulation code to treat the modulation process for electrons with a wide energy distribution. Hence a FORTRAN90 program is designed to evaluate the effects of the backstreaming electrons. From the results of Table 4-1, the current of the backstreaming electrons is very weak, typically only 0.66%~0.12% of the forward beam for the 324MHz klystrons. Considering the beginning of the oscillations, a small modulation is

applied to the backstreaming electrons. Therefore, the small-signal linear theory is a good approximation to evaluate the β. Since the current is weak and strong bunching is not formed, the small signal ballistic theory [5-5] is applicable to this case. It is necessary to modify the formula for the rf current in the ballistic theory for the returning electrons, to take into account energy distribution $\eta(x)$ of the backstreaming electrons, which is a polynomial function fitted to the distribution shape for each of the collectors, as shown in Figure 4-14. Considering the axial direction z, let E_z as the energy of the backstreaming electrons, E_0 as the energy of the forward beam, and its ration as $x = E_z / E_0$, modified rf current of backstreaming electrons is derived by

$$I_1 = \frac{2I_b \int \eta(x) J_1(X') \cos(\omega t - \theta') dx}{\int \eta(x) dx} \qquad (5.9)$$

where $J_1(X')$ is the first order Bessel function, and X' is the bunching parameter for backstreaming electrons. From the simple analysis using the ballistic theory, we can get that β is proportional to the rf current I_1, hence it is proportional to the backstreaming-electron current I_b. Therefore the oscillation conditions determined by the equation (5.3) strongly depend upon the backstreaming-electron current I_b. Let's consider the phase condition of equation (5.4). Generally A and β are functions of frequency, and can be expressed as $A(\omega)$ and $\beta(\omega)$, whose phases are sensitive functions of frequency and beam voltage. We notice that if once the relation $|A\beta|>1$ is satisfied, it will be possible for some frequency components at the certain voltage to satisfy the relation of $\arg(A\beta) = 2n\pi$. Thus, both of the two oscillation conditions are satisfied. So in order to suppress the oscillations completely, we must reduce the total DC current of the backstreaming electrons, I_b, to keep $|A\beta|<1$ in the whole beam-voltage region of the klystron.

Based on these analyses, the calculations for evaluating the effects of the backstreaming electrons are performed for the 324MHz klystrons as described in the following section.

5.3 Calculations of oscillation conditions

From the previous analyses, for the oscillations occurring in the klystron, it is necessary to meet simultaneously the two conditions: $|A\beta|>1$ and $\arg(A\beta) = 2n\pi$. In order to study the oscillations of the 324MHz klystrons, the calculations of $A(\omega)$ and $\beta(\omega)$ are performed at the different voltage to find the oscillation regions of beam voltage.

In the beginning of the oscillations, just a small modulation exists for the forward beam. Also for the backstreaming electrons, the modulation index is small at the initial moment. Due to the feedback from the output to input by the backstreaming electrons, a larger modulation is added to the beam. By this way, the modulation will be enhanced after each loop for both the forward beam and backstreaming electrons, and the oscillation power increases steadily. However, it is well know, the voltage gain of the klystron decreases with the modulation index. A balance will be reached for the oscillation power and voltage gain; the oscillation power will stop increasing at a certain modulation index, which is a critical point of the oscillation conditions. In this thesis, we are interested in understanding the oscillation mechanism and evaluating the beam voltage region of the oscillations by numerical calculation. Small modulations are applied for both the forward beam and backstreaming electrons considering the beginning of the oscillations. The JPNDISK code and a FORTRAN90 program are used in the calculations.

5.3.1 Voltage gain of klystron

The simulation code JPNDISK was used to obtain the voltage gain $A(\omega)$ as mentioned in the previous section. For the 324MHz klystrons, the input parameters for the simulation are shown in Table 1-2. Figure 5-2 shows the phase diagram of the JPNDISK simulation results of 324MHz klystron #1 with different driving power at beam voltage of 110kV. The driving power is 0.1W, 1W, and 10W, for figure (a), (b), and (c), respectively. It indicates that with the driving power increasing, the beam bunch becomes stronger, and output power gets higher. From the ballistic theory, assuming the input cavity

voltage is

$$V_d = V_d \sin(\omega t) \tag{5.10}$$

after the modulation, the fundamental rf current of the beam is

$$I_1 = 2I_0 J_1(X) \cos(\omega t - \theta) \tag{5.11}$$

where X is a bunching parameter, and θ is a DC transit angle.

$$X = \frac{V_d}{V_0} \cdot M\theta \cdot \frac{1}{\gamma_0(\gamma_0 + 1)} \tag{5.12}$$

where γ_0 is the relativistic factor. For the small signal region, I_1 is proportional to V_d, it means that voltage gain is a constant at small signal region, and decreases with the driving power increasing. Figure 5-3 shows the voltage gain and the efficiency of 324MHz klystron #1 at the beam voltage 110kV. This figure clearly shows that the voltage gain is a approximate constant within driving power of 1W, and decreases rapidly with the input power larger than 1W. The efficiency arrived at the maximum value about 64% at the saturation point around 10W input power. Figure 5-4 shows the phase of 324MHz klystron #1 at the beam voltage 110kV. It indicates that the phase is almost a constant in the small-signal linear region, and it slightly shift in the larger signal region.

In order to investigate the oscillation conditions, the klystron has been simulated in the small signal region for different beam voltages and frequencies. In these calculations, small driving powers of 0.02W, 0.1W, and 0.5W are applied to the input cavity. The obtained voltage gains are almost same for these three cases; an average value is worked out. Figure 5-5 shows the calculation results of the frequency response of the voltage gain |A| of tube #1 at the beam voltages 70kV, 90kV, and 110kV. It indicates that |A| increases with the beam voltage and the klystron has a bandwidth less than 2MHz.

5.3.2 Feedback coefficient caused by backstreaming electrons

In order to calculate the feedback coefficient β, which is a voltage gain of

the reverse 'klystron' made up of the backstreaming electrons, the current I_b and energy distribution $\eta(x)$ of the backstreaming electrons are calculated at first, which have been investigated as shown in Table 4-1 and (b) of Figure 4-14 for tubes #1, #1A, and #2. Then using the small signal ballistic theory, we calculated the rf current in the backstreaming electrons through equation (5.9), and work out the feedback coefficient β.

In equation (5.9), the bunching parameter (X') for backstreaming electrons is expressed by,

$$X' = 0.5\,\alpha\,M\,\theta' \tag{5.13}$$

where α is a modulation index, M is a gap coupling coefficient, and θ' is a DC transit angle. For the backstreaming electrons with an energy distribution of $\eta(x)$, where $x = E_z / E_0$, considering those electrons with energy of $E_{be} = x\,E_0$,the modulation index is

$$\alpha = \frac{V_o}{V_{be}} \cdot \frac{2}{\gamma(\gamma+1)} \tag{5.14}$$

where V_o is the gap voltage at the output cavity, V_{be} is the voltage corresponding to E_{be}, $V_{be} = x\,V_0$, and $2/(\gamma(\gamma+1))$ is a relativistic correction coefficient. γ is the relativistic factor corresponding to E_{be}. In the calculations, a very small gap voltage of V_o is applied at the output cavity for modulating the backstreaming electrons. Typically, in our calculations, 0.001 times of beam voltage (V_0) is used to ensure the small modulation for almost all of the backstreaming electrons. In this case,

$$\alpha = \frac{0.001V_0}{V_{be}} \cdot \frac{2}{\gamma(\gamma+1)} = \frac{0.001}{x} \cdot \frac{2}{\gamma(\gamma+1)} \tag{5.15}$$

The gap transit angle is calculated from

$$\theta_g = \omega\,D_g / u_{be} \tag{5.16}$$

where ω is the angular frequency, D_g is the gap distance of the output cavity, and u_{be} is the velocity of the backstreaming electrons corresponding to the energy E_{be}. Thus, the gap-coupling coefficient is

$$M = \frac{\sin(\theta_g/2)}{\theta_g/2} \tag{5.17}$$

The DC transit angle is

$$\theta' = \omega Z / u_{be} \tag{5.18}$$

where Z is the distance from the output to input cavity. By substituting equations (5.15), (5.17) and (5.18) into (5.13), the bunching parameter is obtained,

$$X' = \frac{0.001}{x} \cdot \frac{\sin(\theta_g/2)}{\theta_g/2} \cdot \frac{\omega Z}{u_{be}} \cdot \frac{1}{\gamma(\gamma+1)} \tag{5.19}$$

By substituting this equation into equation (5.9), the rf current I_1 of the backstreaming electrons at the input cavity can be carried out for different moment. Thus, the phase can also be determined from the variation of the amplitude of I_1. Therefore, a complex value of the rf current (I_1) is obtained. It is assumed that the induced current in the cavity I_{ind} is approximately equate to $-I_1$. Then, the induced gap voltage is calculated out by

$$V_1 = I_{ind}\ Z_1 \tag{5.20}$$

where Z_1 is the impedance of the input cavity. This cavity impedance should be calculated with the consideration of the forward beam loading. The forward beam loading conductance G_B and susceptance B_B are

$$G_B = G_0 \frac{\sin(\theta_g/2)}{\theta_g/2}\left(\frac{\sin(\theta_g/2)}{\theta_g/2} - \cos(\theta_g/2)\right) \cdot \frac{1}{\gamma_0(\gamma_0+1)} \tag{5.21}$$

$$B_B = G_0 \frac{\cos(\theta_g/2)}{\theta_g/2}\left(\frac{\sin(\theta_g/2)}{\theta_g/2} - \cos(\theta_g/2)\right) \cdot \frac{1}{\gamma_0(\gamma_0+1)} \tag{5.22}$$

where G_0 is the DC conductance, $G_0 = I_0 / V_0$, θ_g is the gap transit angle,

$$\theta_g = \frac{\omega}{u_0} d \tag{5.23}$$

and γ_0 is the relativistic factor. Thus the loaded Q is,

$$Q_L = \frac{Q_e}{1 + (R/Q) \cdot Q_e \cdot G_B} \tag{5.24}$$

where R/Q is the shunting impedance of the cavity, and Q_e is the external Q of the cavity. The loaded frequency is

$$f_L = \frac{f_r}{\sqrt{1+(R/Q)\cdot B_B}} \tag{5.25}$$

The gap impedance is calculated by

$$\overrightarrow{Z_1} = \frac{Q_L \cdot (R/Q)}{1+j\cdot Q_L \cdot (\frac{f}{f_L} - \frac{f_L}{f})} \tag{5.26}$$

Then the induced gap voltage can be calculated out by equation (5.20). Finally, the feedback coefficient β is calculated out, $\beta = V_1 / V_0$.

Also in order to study the oscillation conditions, the feedback coefficient β has been carried out for different beam voltages and frequencies. Figure 5-6 shows the frequency response of the feedback coefficient |β| of tube #1 at the beam voltages 70kV, 90kV, and 110kV. We can see that the shape of the curves of the frequency response of |β| are similar to the ones of |A|, and the amplitudes are much smaller than |A| due to the weak current of the backstreaming electrons and their broad energy distributions. The bandwidth is also less than 2MHz.

5.3.3 Product of klystron voltage gain and feedback coefficient

After working out both the amplitude and phase of A and β, we plot the product Aβ in the complex plane. Figure 5-7 shows the calculation results of the phases for the complex values A, β ,and Aβ as functions of the frequency for tube #1 at the beam voltage of 70kV. Figure 5-8 shows the curves of $A(\omega)\beta(\omega)$ as function of frequency of 322 ~326MHz for tube #1 under beam voltages of 65kV, 70kV, and 75kV. We can see that, between 65 and 70kV, there are some frequency components satisfying the oscillation conditions, $|A\beta|>1$ and $\arg(A\beta) = 2n\pi$. This agrees with the test results of the klystron.

Similar calculations were performed varying the beam voltage and the frequency in the vicinity of 324MHz for the three klystron tubes. Based on the calculations of the oscillation conditions, the beam-voltage regions of the oscillations for the 324MHz klystrons have been worked out. For klystron #1, the beam-voltage regions are 65~70kV and higher than 79kV. For the collector of #1A and #2, the regions are higher than 100kV and 105kV, respectively. From Table 2-1 summarizing the experimental results, for the tube with the collector shape #1, the oscillations occurred at the voltage from 63kV to 71kV and more than 90kV. For the collector shapes #1A and #2, the oscillations occurred at the beam voltage of more than 95kV and 104kV, respectively. These results show a good agreement with the calculation values.

5.4 Discussions

The analyses and calculations in the previous two sections indicate that the our results of the oscillation regions of the beam voltages for these three tubes agree with the experiment results very well by applying the criteria of the oscillation conditions. And the oscillation features and phenomena observed in the our klystrons can be explained by the analyses and calculations presented in this thesis.

5.4.1 Oscillation voltage region

After the previous work, the oscillation feature of voltage threshold is understood. As the beam voltage increases, the beam current and the current of the backstreaming electrons will become high, and $|A|$ and $|\beta|$ will become large as shown in Figure 5-5 and Figure 5-6. That is the reason why the oscillations occurred in the high-voltage regions. Because these klystrons are designed with a center working frequency of 324MHz, the voltage gain $|A|$ and $|\beta|$ are much higher around this frequency than other frequencies, which can be seen from Figure 5-5 and Figure 5-6. Therefore, it is quite natural that the oscillations always have a frequency almost same as the

working frequency.

From Figure 5-7 and Figure 5-8, we can see that the phase of $A\beta$ easily varies under different beam voltages and frequencies. It means, as said before, once $|A\beta|>1$, it will be possible for some frequency components at certain high voltages to satisfy the equation $\arg(A\beta)=2n\pi$. Thus, both of the two oscillation conditions are satisfied. Therefore in order to suppress the oscillation completely, it is necessary to satisfy the relation, $|A\beta|<1$, in the whole beam-voltage region of the klystron. One possible way is lowering the forward voltage gain $|A|$. As described in chapter 2, it was found that oscillations were partially avoided if we adjusted the focusing field distribution and external Q at the input cavity so as to decrease the total gain of the klystron. However it is not recommended to adjust the klystron parameters in normal operation. The other way is to lower the $|\beta|$. As described in chapter 4, we can decrease the current due to backstreaming electrons by choosing the proper collector shape; hence we can lower $|\beta|$ and achieve $|A\beta|<1$. In fact in the collector shape #2, we could suppress the oscillation successfully by developing the suitable collector shape.

5.4.2 Oscillation enhancement

If the oscillation conditions, $\arg(A\beta) = 2n\pi$ and $|A\beta|>1$, are satisfied at certain beam voltage, the process of the oscillation enhancement is considered as the following. At the moment of the beam voltage being turned on, supposing there are very weak oscillations in the output cavity, the backstreaming electrons will feedback the rf signal from the output to input cavity, and this regenerated rf signal in the input cavity will be amplified by the main beam. After one round trip, the oscillations will be enhanced by the factor $|A\beta|$, and after n round trips, enhanced by $|A\beta|^n$. The oscillation power will be enlarged due to this feedback loop. However, the amplitude of the oscillations can not increase without limit, because of nonlinearity associated with the amplifying process as shown in Figure 5-3, which indicates the voltage gain of the klystron decreases with the modulation index. For the backstreaming electrons, similar nonlinearity can be derived from equation (5.9). Such kind of nonlinearity becomes more marked as the

amplitude of oscillation increases. Finally, a balance will be reached, where the oscillation power arrives at the maximum point for that beam voltage and voltage gains are located at the critical points of the oscillation conditions, $\arg(A\beta) = 2n\pi$ and $|A\beta| = 1$. Thus, for a higher beam voltage and a larger $|A\beta|$, the oscillation power tends to arrive at a higher value. Therefore, the oscillation power shown in Figure 2-3 can be qualitatively understood from the process of the oscillation enhancement.

The time delay of oscillation waveform might also be associated with this process of the oscillation enhancement. Experiment results for tube #1 shown in Figure 2-1 indicated that, as the beam voltage went into and went out of the oscillation beam-voltage regions, the time delay of the oscillations changed from long to short, and then to long again, which is shown in Figure 2-4. As mentioned above, the oscillations will be enhanced by the factor $|A\beta|^n$ after n round trips. Therefore, for a large $|A\beta|$, it will take a short time to reach a relatively high level, while for a small $|A\beta|$, it will take a long time. From the calculation results (Figure 5-8) for tube #1, with the beam voltage increasing, $|A\beta|$ just exceeds 1 around 64kV. Consequently, the oscillations started, however, with a long time delay. As the beam voltage increases furthermore, the delayed time becomes short due to increase of $|A\beta|$. Again when the beam voltage arrived at 70kV, $|A\beta|$ was reduced, which will cause a long delayed time which was also observed in the experiments shown in Figure 2-1. It indicates that for the oscillation occurring, it will always take a time of enhancement. Therefore, the possibility of the oscillations occurring in long-pulsed or CW klystrons will be much higher than in short-pulsed klystron tubes.

5.4.3 Proposals for collector of 324MHz klystron

As described previously, sometimes an irregularity in the input-to-output power relations and an instability in the waveform of the output power envelop were still observed even in klystron tube #2. From the previous analysis, in order to suppress the oscillation completely, it is necessary to satisfy the relation, $|A\beta|<1$, in the whole beam-voltage region of the klystron. However, once main parameters, such as beam voltage and cavity parameters,

are optimized to reach designed performance, the voltage gain A is fixed and will not be changed easily. In order develop a 324MHz klystron to suppress the oscillations completely, a suitable collector shape or drift tube size should be designed and adopted for the klystron to reduce the feedback coefficient β caused by the backstreaming electrons.

One possible way is to enlarge the collector size a little. However due to the manufacture limitation, the collector length cannot be increased further. Thus, the purpose of reducing backstreaming electrons is realized by using an increased collector diameter of 30cm instead of 23cm in klystron #2. Proposal 1 of collector shape is shown in (a) of Figure 5-9. The backstreaming electron coefficient is reduced from 0.13% for klystron #2 to 0.093%. The maximum of $|A\beta|$ in the whole voltage region is smaller than 0.75. Another way is to use a small drift-tube diameter. Proposal 2 of collector shape is shown in (b) of Figure 5-9. The drift-tube diameter is decreased to 7cm instead of 10cm in klystron #2. The backstreaming electron coefficient is reduced from 0.13% for klystron #2 to 0.081%. The maximum of $|A\beta|$ in the whole voltage region is smaller than 0.66. So, by using each of proposed collectors for the 324Mhz klystron, the oscillations due to backstreaming electrons will be completely suppressed.

5.4.4 Nyquist criterion

The oscillations occurring in the 324MHz klystrons can also be understood from the point of general feedback theory. For a feedback loop shown in Figure 5-1,

$$V_d = V_i + V_f \tag{5.27}$$

$$V_o = V_d A \tag{5.28}$$

$$V_f = V_o \beta \tag{5.29}$$

The above equations reduce to

$$V_d = V_i + V_f = V_i + V_o \beta = V_i + V_d A\beta \tag{5.30}$$

Solving for V_i yields,

$$V_i = (1-A\beta)\, V_d \tag{5.31}$$

Thus, the closed loop gain is

$$\overrightarrow{A_f} = \frac{\overrightarrow{V_o}}{\overrightarrow{V_i}} = \frac{\overrightarrow{V_o}}{(1-\vec{A}\cdot\vec{\beta})\cdot\overrightarrow{V_d}} = \frac{\vec{A}}{1-\vec{A}\cdot\vec{\beta}} \tag{5.32}$$

In this case, the Nyquist criterion tells us that the amplifier is unstable if the curve of Aβ in the complex plane encloses the point 1+ j0 as frequency changes from - ∞ to + ∞. The oscillation can be illustrated with positive feedback: No signal is applied, but because of some transient disturbance, a signal V appears at the output port. A portion of this signal will be fed back to the input port, and will appear in the output as an increased signal AβV. Thus, the amplifier may start spontaneous oscillations. Also from the closed loop gain formula (5.32), for Aβ =1+ j0, $A_f \rightarrow \infty$, which may be interpreted to mean that there exists an output voltage even in the absence of an externally applied signal voltage. In the 324MHz klystrons, a similar closed loop is formed by the main beam and backstreaming electrons, and the oscillation mechanism obeys the Nyquist criterion too. However the feedback loop made up of the backstreaming electrons depends on many factors, such as beam voltage, collector dimensions, and rf interaction relations. These effects have been successfully worked out with curves of Aβ plotted in the complex plane, from which the oscillation voltage region is evaluated.

5.5 Future proposals

Considering study in the future, some proposals are pointed out for the following three problems:

(1) We have considered the oscillations caused by the backstreaming electrons in the case of no drive power in the input cavity. In the future, we should investigate the case with drive power. In this case, spent beam has a complicated feature. It has a strong scalloping envelope with a transverse oscillation due to the large signal behavior. Also it has a complicated energy distribution from near $2V_0$ to lower energies. Masuda [5-6] developed the 2.5-dimensional PIC code and applied it to MDC in the klystron collector. If the electron dynamics in the collector is combined with the EGS4, the dynamic simulation is possible.

(2) Besides backstreaming electrons produced in the collector, sometimes

they are created at the output cavity due to the dynamic interaction between the beam and rf fields. Usually in the design stage we had an effort to avoid the backstreaming electrons, observing the simulation result in the output cavity. It might be possible to estimate the backstreaming electrons through the code, for example, the PIC code. On the other hand, if the secondary electrons, produced at the gap nose of the output cavity, play an important role, the situation becomes very complicated. These investigations are also interesting for the study on klystron instabilities.

(3) As discussed before, the ratio of the diameter of the drift tube to collector determines the backstreaming electrons and hence determines the oscillations, but strictly speaking, it is not completely right. At KEK, for example, we have used S-band high-power pulsed klystrons and their driver klystrons, whose ratio of the diameter of the drift tube to collector is small, and they have been operated stably. This stability came from their short pulse operation. On the other hand, there are CW 1MW klystrons at KEK and their ratio of the drift tube diameter to collector diameter is larger than the pulsed tube, but some oscillations and the instability were reported [5-7]. It is necessary to investigate the built-up mechanism of the oscillations. From Figure 2-1, the start time of the oscillation was changed complicatedly and these may suggest the difference between the short pulse operation and the long pulse/cw operation.

5.6 Summary

In this chapter, the oscillation mechanism due to the backstreaming electrons is described. The backstreaming electrons carrying rf signal from the output to input cavity form a feedback loop inside the tube, which can cause the oscillations. From the feedback theory, the oscillation conditions due to the backstreaming electrons are obtained: $\arg(A\beta) = 2n\pi$ and $|A\beta| > 1$. Based on the calculations of the oscillation conditions, the beam-voltage regions of the oscillations for the 324MHz klystrons have been worked out. For klystron #1, the beam-voltage regions are 65~70kV and higher than 79kV. For the collector of #1A and #2, the regions are higher than 100kV and 105kV, respectively.

These results show a good agreement with the experiments. With these analyses and calculations, the oscillation mechanism including oscillation phenomena has been clarified physically and numerically. Furthermore, some discussions and directions for future investigation on the oscillations are presented.

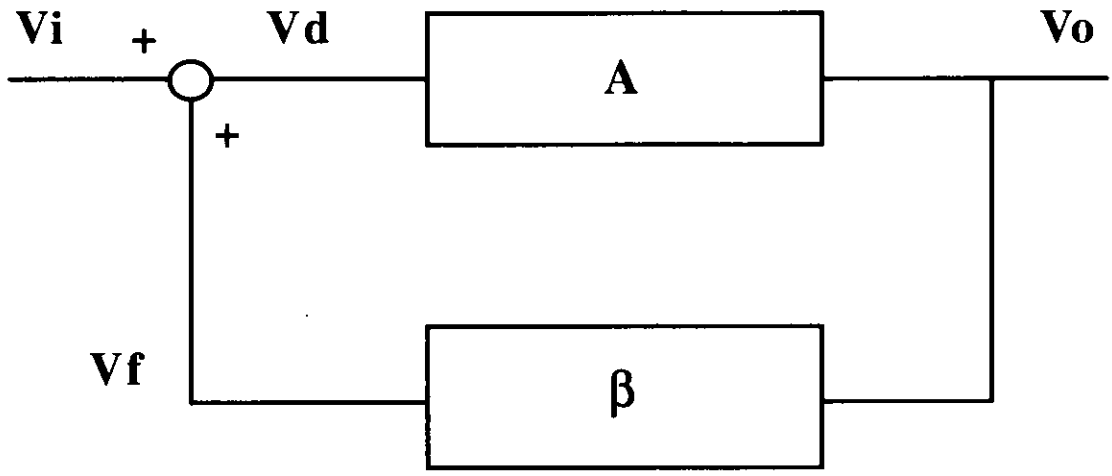

Figure 5-1: Block diagram of the feedback loop of the klystron due to the backstreaming electrons. (**A** is the complex voltage gain of the klystron; β is a complex feedback coefficient caused by the backstreaming electrons.)

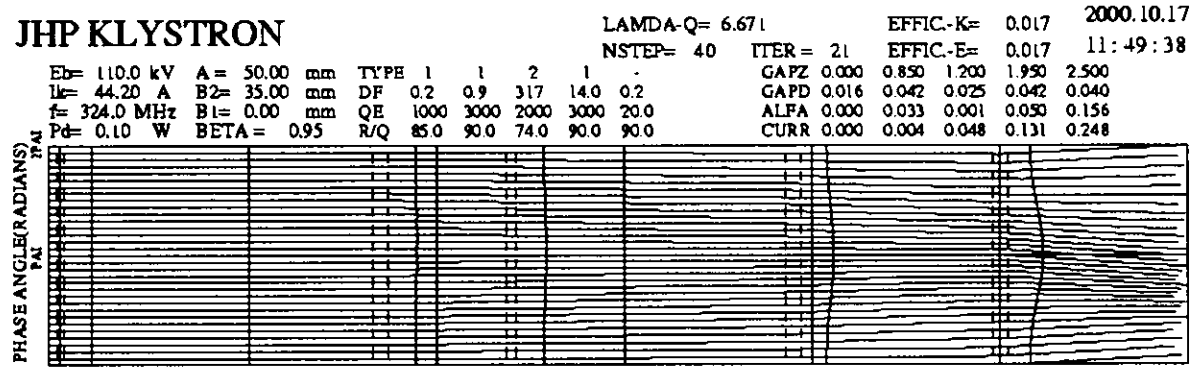

(a) P_d = 0.1W

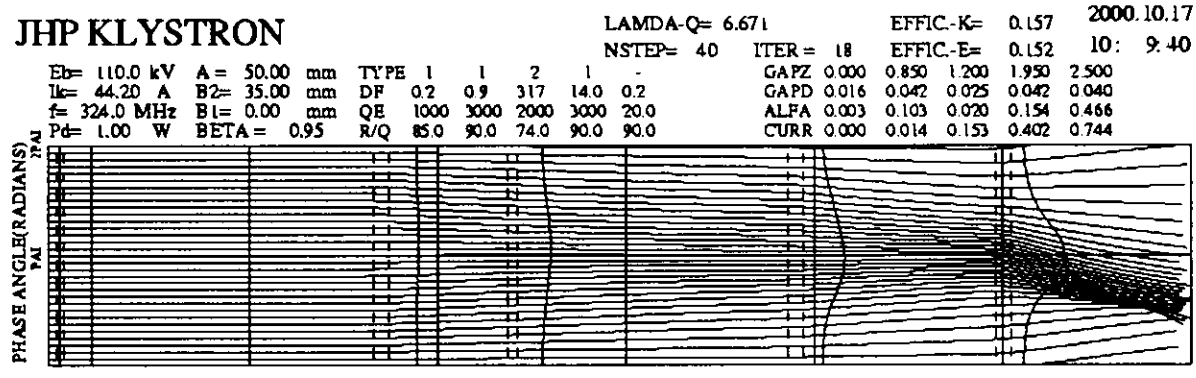

(b) P_d = 1W

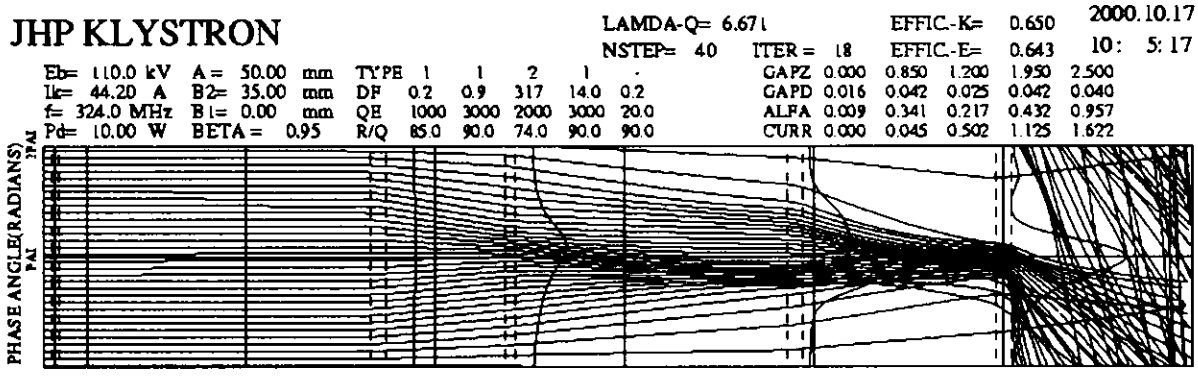

(c) P_d = 10W

Figure 5-2: Phase diagram of the JPNDISK simulation results of 324MHz klystron #1 with different driving power at beam voltage of 110kV.

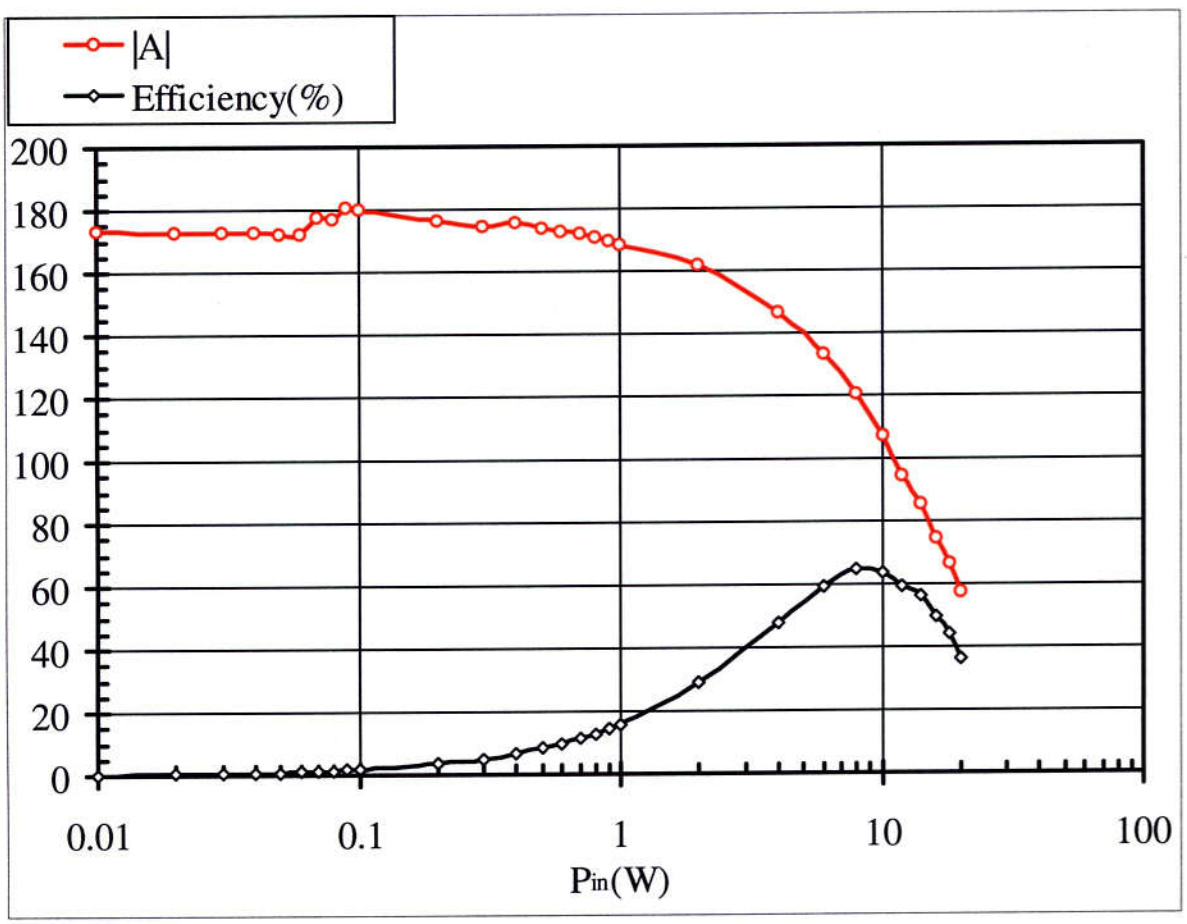

Figure 5-3: Voltage gain and efficiency of 324MHz klystron #1 at the beam voltage 110kV.

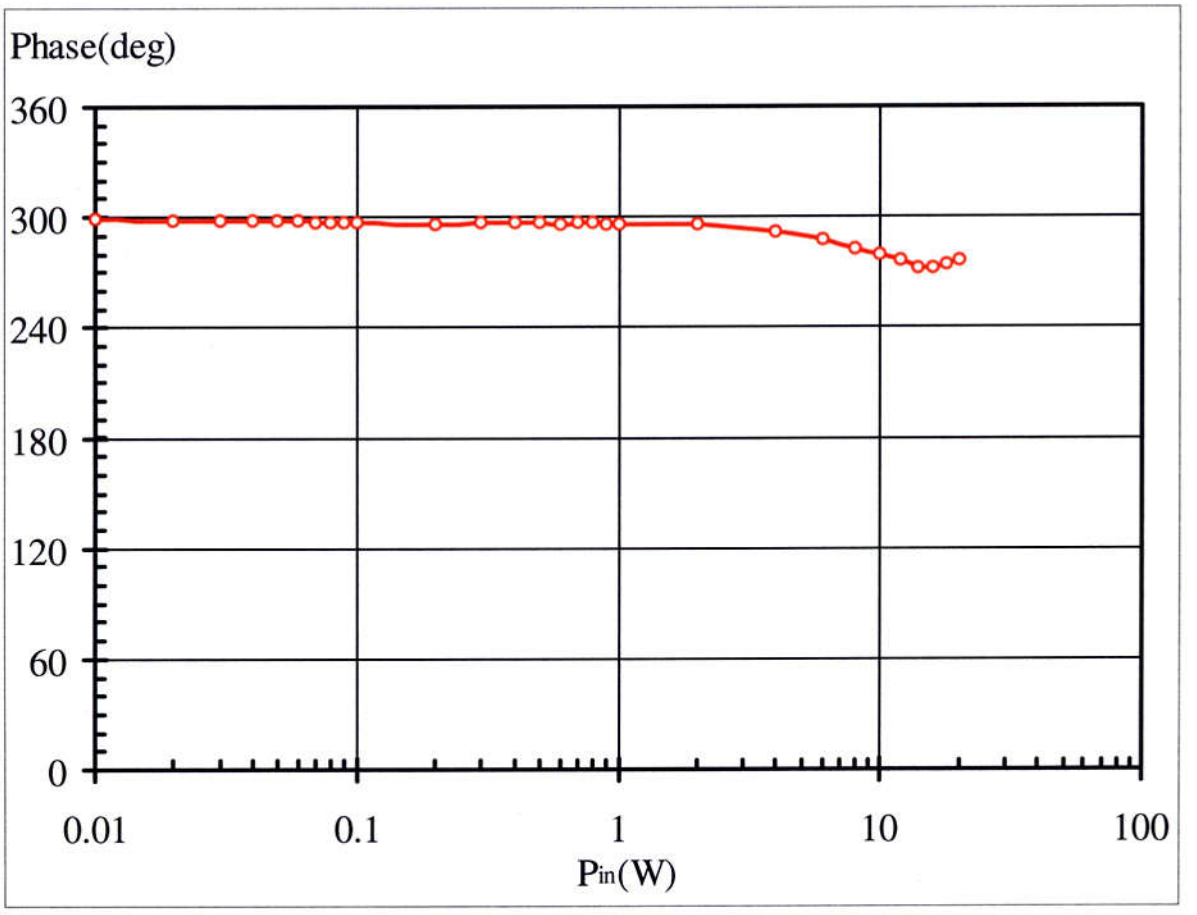

Figure 5-4: Phase of 324MHz klystron #1 at the beam voltage 110kV.

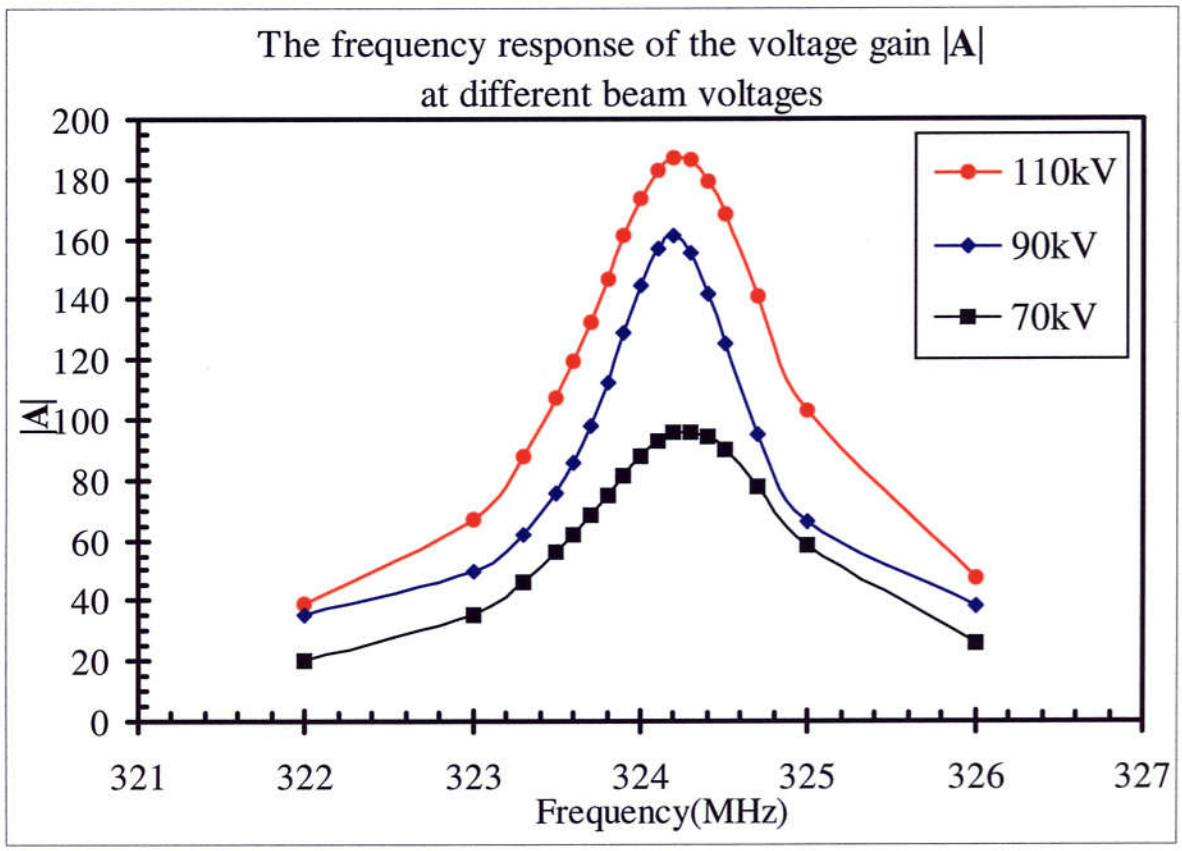

Figure 5-5: Frequency response of the voltage gain |A| of tube #1 at the beam voltages 70kV, 90kV, and 110kV.

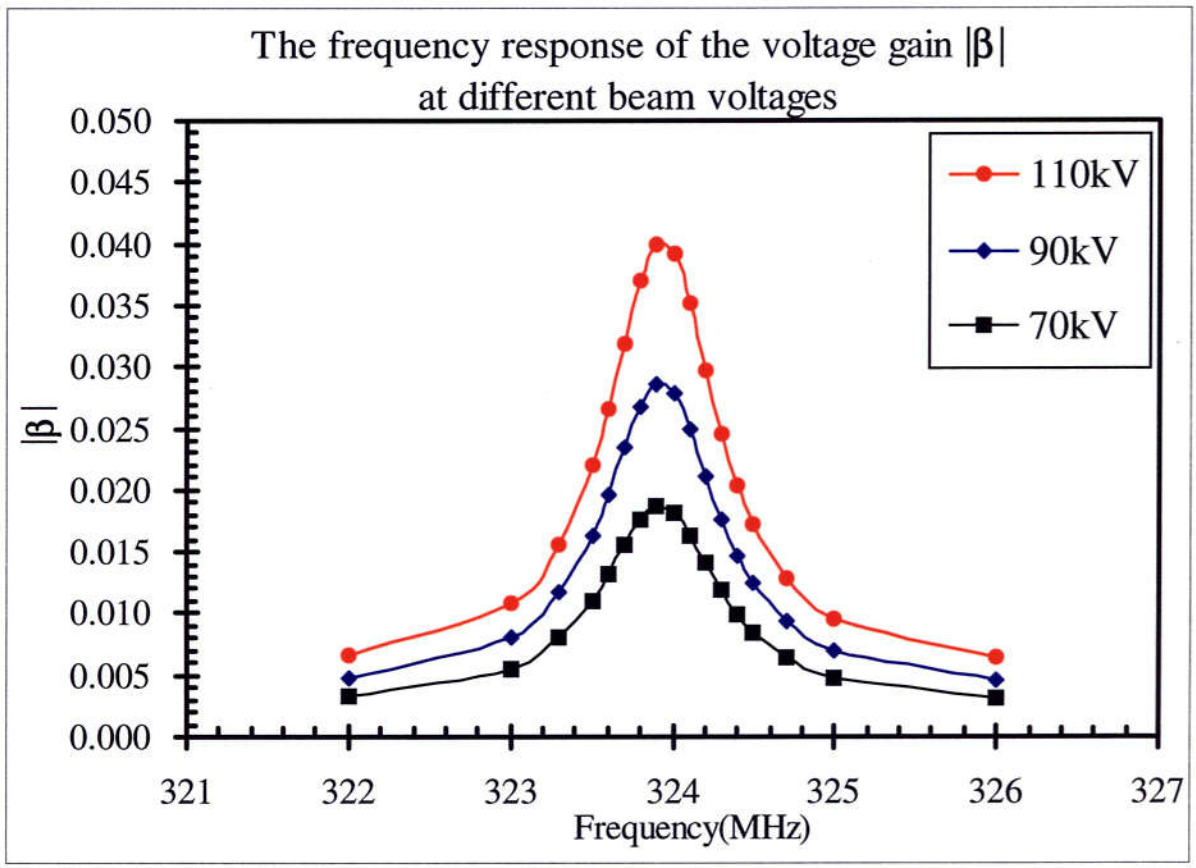

Figure 5-6: Frequency response of the feedback coefficient $|\beta|$ of tube #1 at the beam voltages 70kV, 90kV, and 110kV.

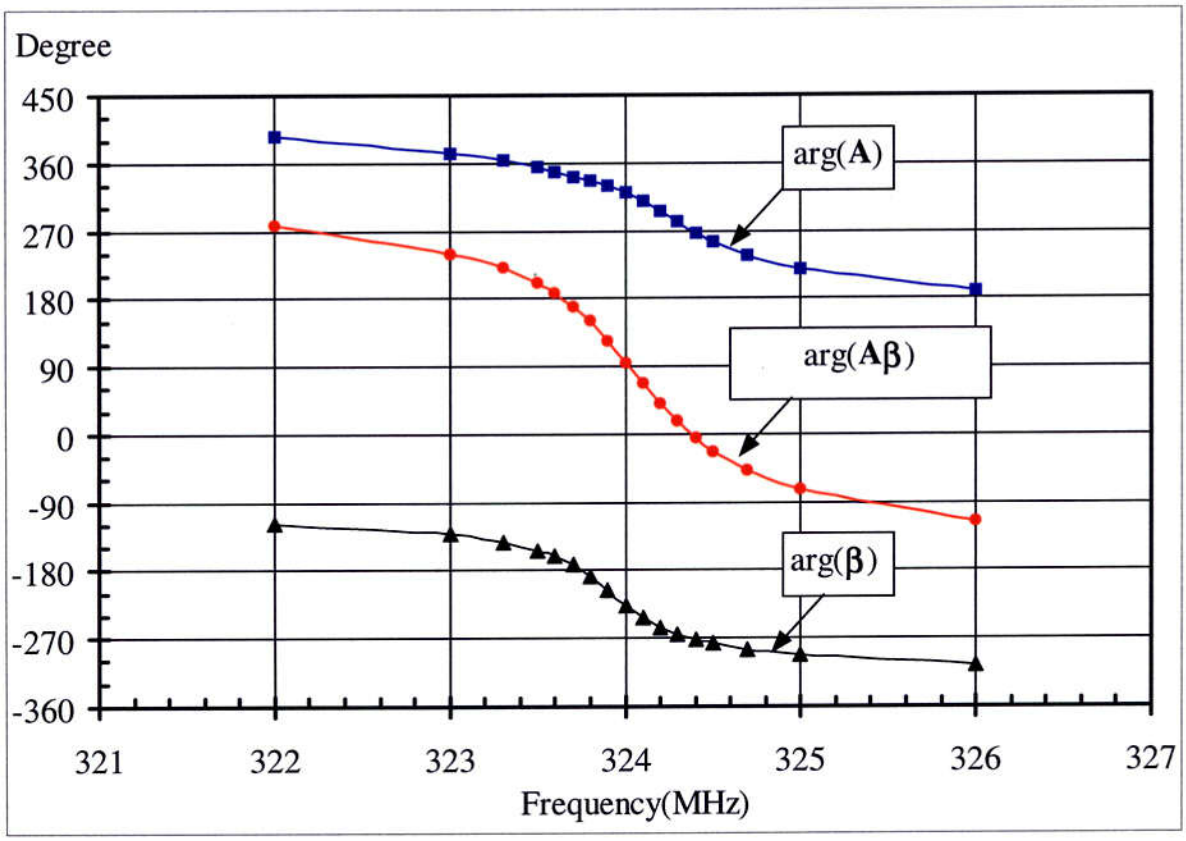

Figure 5-7: Phase of the complex values **A**, **β**, and **Aβ** as functions of the frequency for tube #1 at the beam voltage of 70kV.

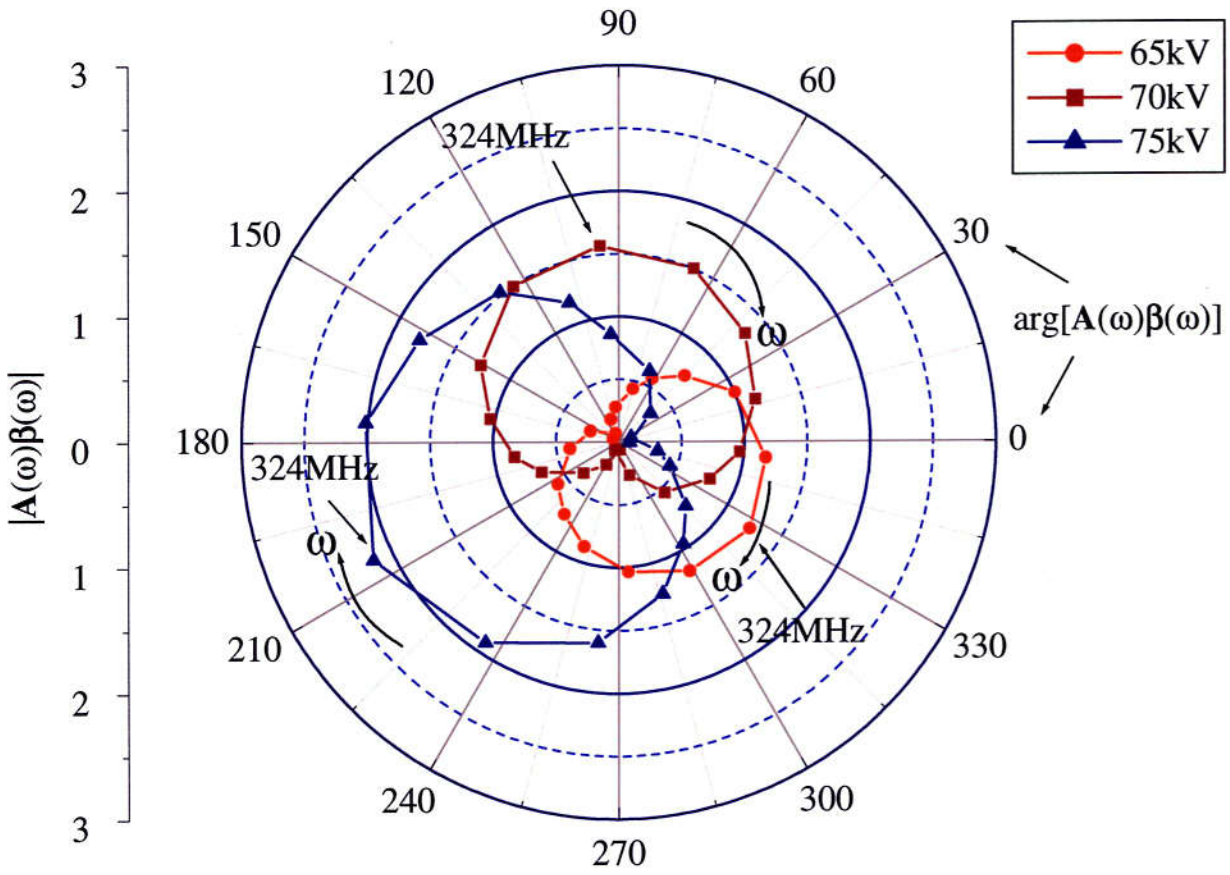

Figure 5-8: Curves of $\mathbf{A}(\omega)\beta(\omega)$ as function of frequency of 322 ~326MHz for tube #1 under beam voltages of 65kV, 70kV, and 75kV.

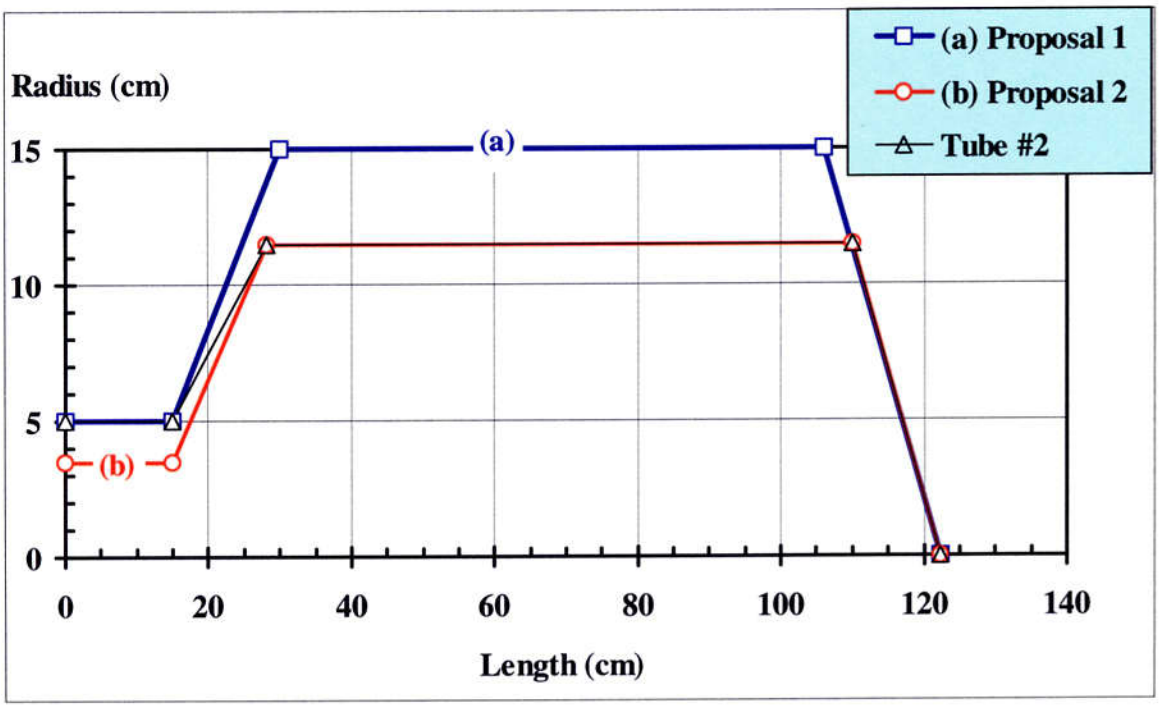

Figure 5-9: Proposals for collector of 324MHz klystron.

Chapter 6

Conclusion

A study on the spurious oscillations due to the backstreaming electrons from the collector has been successfully performed, including the production of the backscattered electrons on the collector surface, the formation of the backstreaming electrons into the drift tube, and the oscillation mechanism due to the interaction between the electrons and rf fields.

The electron backscattering process has been investigated and simulated using the EGS4 Monte Carlo method. The electron backscattering coefficients and energy distributions have been obtained under different conditions of incident energy and angle. For example, for normal incidence on copper, the backscattering coefficient is equal to 0.3, and it increases with the incident angle. The EGS4 simulation results agree well with the experimental data of the reflected electrons.

After the above confirmation of the EGS4 code validity for the fundamental process, the simulations of the backstreaming electrons from a klystron collector have been performed by using the EGS4 code. The simulation method includes three steps. (1) The trajectory calculation for the incident beam in the collector up to the collector wall. The calculation results have shown a good agreement with the EGUN95 simulation results. (2) The simulation of the electron backscattering in the collector using the EGS4 Monte Carlo method. (3) The post-process for the backscattered and backstreaming electrons. Some simulation results are also given in this thesis. The backstreaming electron coefficients and energy distributions have been obtained under different conditions of the klystron. The simulation results indicate that the backstreaming electrons are essentially independent of the beam voltage. For klystron #1, #1A, and #2, the backstreaming electron coefficients are 0.66%, 0.17%, and 0.13%, respectively. The contributions to the backstreaming coefficients from the cylindrical surface and cone-shaped surface of the collector have also been investigated. The former contribution

mainly comes from the backscattering of the beam edge, and the latter contribution increases with the collector length shortening due to the direct reflection. The backstreaming coefficients as function of collector diameter and length have been carried out. Furthermore, the backstreaming electrons as function of various materials are obtained.

Finally, the study of the oscillation mechanism and conditions due to the backstreaming electrons has been performed, and relevant calculations of the oscillation conditions have also been executed using the results of the backstreaming electrons obtained in the previous part. The oscillation conditions are expressed by the complex product of the klystron voltage-gain and feedback coefficient caused by the backstreaming electrons: (1) the amplitude of the product should be larger than unity, and (2) the phase of the product should be zero or integral times of 2π. Based on the calculations of the oscillation conditions, the beam-voltage regions of the oscillations for the 324MHz klystrons have been worked out. For klystron #1, the beam-voltage regions are 65~70kV and higher than 79kV. For the collector of #1A and #2, the regions are higher than 100kV and 105kV, respectively. These results show a good agreement with the experiments. With these analyses and calculations, the oscillation mechanism including oscillation phenomena has been understood physically and numerically. Suitable collector dimensions are proposed for 324MHz klystron in order to suppress the oscillations due to backstreaming electrons completely. Furthermore, some discussions and directions for future investigation on the oscillations are presented.

Acknowledgements

First of all, I'd like to express my special thanks to my supervisor, professor Shigeki Fukuda, who has given me a great help which will benefit all my life, and who not only gives me a guide of a bright prospects for the study, but also favors me a great of advice for studying method. Here I wish to express my thanks from my heart to my teacher, to whom I am greatly indebted. Thank you very much!

Also I wish to extend my thanks to Dr. Shinichiro Michizono, who gives me help all the time, helping me to use many simulation codes, giving me lot of good advice in discussion, encouraging me to go on with my study, and so on.

I want to say thanks to Dr. Seiya Yamaguchi, who helps me a lot in experiments of tests and measurements for klystrons and microwave devices.

Besides, I would like to thank professor Hideo Hirayama, who gives me a lot of help for using the EGS4 code.

I am grateful to Dr. Stefan Simrock, who discusses with me and helps me to understand rf feedback theory.

I wish to thank Nihon Koshuha Company members, K. Suzuki, M. Matsuo, Y. Niimura, K. Shinohara, and S. Aizawa et al., who give me a lot of convenience and helps for the development of microwave devices during my staying in the company for one month.

Also I wish to thank Toshiba members, M. Sakamoto, K. Tetsuka and K. Hayashi, for their cooperation in klystron experiments and discussion on backstreaming electrons.

I'd like to express my thanks from my heart to other professors who give me warm lectures during my studies in Japan, professor Toshio Kasuga, professor Masaaki Isawa, and professor Yongho Chin. They give me enormous indispensable and essential knowledge, which is greatly useful for me not only for the study in this thesis but also for my future study.

Finally, I'd like to thank my mother, my wife and my daughter for their encouragement, support and pressure. And I wish to thank Prof. Bo Hong, Dr. Ping Huai and Dr. Lanfa Wang for their a lot of help and cooperation during my study.

References

In Chapter 1:

[1-1] Y. Yamazaki et al., "The construction of the low-energy front 60-MeV linac for the KEK/JAERI joint project", Proceedings of the 20th International Linac Conference, Monterey, CA, USA, Aug. 2000.

[1-2] S. Fukuda et al., "The RF source of the 60-MeV linac for the KEK/JAERI joint project", Proceedings of the 20th International Linac Conference, Monterey, CA, USA, Aug. 2000.

[1-3] S. Fukuda et al., "Development of a high-power VHF klystron for JHF", Proceedings of the first Asian Particle Accelerator Conference, 112-114, Tsukuba, Japan, Mar. 1998.

[1-4] M. Kawamura et al., "High-power test of a klystron beam-test-tube and an anode modulator", Proceedings of the 24th Linear Accelerator Meeting in Japan, 200-202, Japan, Jul. 1999.

[1-5] Z. Fang et al., "Development of microwave waveguide components for UHF klystron of JHF", Proceedings of the 24th Linear Accelerator Meeting in Japan, 215-217, Japan, Jul. 1999.

[1-6] M. Kawamura et al., "Developments and high-power tests of the 324MHz pulse klystrons", Proceedings of the 25th Linear Accelerator Meeting in Japan, 198-200, Japan, Jul. 2000.

[1-7] Z. Fang et al., "Investigation of spurious oscillation in klystron due to back-going electrons from collector", Proceedings of the 25th Linear Accelerator Meeting in Japan, 216-218, Japan, Jul. 2000.

[1-8] S. Isagawa etal., "Suppression of SBO and stability improvements of TRISTAN 1MW high power klystrons", Proceedings of 9th Symposium on Accelerator Science and Technology, KEK, Tsukuba, Japan, 128-130, 1993.

[1-9] A. Staprans, E. W. McCune and J. A. Ruetz, "High-power linear-beam tubes", Proceedings of the IEEE, Vol. 61, No. 3, 299-330, March, 1973.

[1-10] M. J. Smith and G. Phillips, "Power klystrons today", Chapter 7,

Research Studies Press, Ltd., 1995.

[1-11] J. F. Gittens, "Power travelling wave tubes", The English Univ. Press, Ltd., pp. 143-152, 1964.

[1-12] A. S. Gilmour, Jr., "Principles of travelling wave tubes", Artech House Press, Ltd., 1994.

[1-13] H. G. Kosmahl, "Modern multistage depressed collectors- A review", Proceedings of the IEEE, Vol. 70, No. 11, 1325-1334, November, 1982.

[1-14] J. R. Hechtel, "A novel electrostatic-focusing depressed collector for linear beam tubes", IEEE Trans. Electron Devices, Vol. ED-24, No. 1, 45-53, 1977.

[1-15] P. Ramins and B. T. Ebihara, "Improvements in MDC and TWT overall efficiency through the application of carbon electrode surfaces", IEEE Trans. Electron Devices, Vol. ED-33, No. 11, 1915-1924, 1986.

[1-16] M. E. Reads, W. G. Lawson, A. J. Dubas and A. Singh, "Depressed collectors for high-power gyrotrons", IEEE Trans. Electron Devices, Vol. ED-37, No.6, 1579-1589, 1990.

[1-17] E. W. McCune, "A UHF-TV klystron using multistage depressed collector technology", IEEE IEDM, pp. 160-163, 1986.

[1-18] E. W. McCune, "Klystron performance using a multistage depressed collector", IEEE IEDM, pp. 157-159, 1987.

[1-19] W. R. Nelson, H. Hirayama and D. W. O. Rogers, "The EGS4 code system", SLAC-report-265, 1985.

[1-20] W. R. Nelson and Y. Namito, "The EGS4 code system: solution of gamma-ray and electron transport problems", SLAC-PUB-5193, February, 1990.

[1-21] Z. Fang et al., "Returning electron simulation for a collector of klystron using EGS4", Proceedings of the 2nd International Workshop on EGS, 272-279, Tsukuba, Japan, Aug. 2000

[1-22] Z. Fang et al., "Simulation of returning electrons from a klystron Collector", Proceedings of the 20th International Linac Conference, Monterey, CA, USA, Aug. 2000.

In Chapter 2:

[2-1] S. Fukuda et al., "The RF source of the 60-MeV linac for the KEK/JAERI joint project", Proceedings of the 20th International Linac Conference, Monterey, CA, USA, Aug. 2000.

In Chapter 3:

[3-1] J. R. M. Vaughan, "A new formula for secondary emission yield", IEEE Trans. Electron Devices, Vol. ED-36, No. 9, 1963-1967, 1989.

[3-2] A. J. Antolak and W. Williamson, Jr., "Electron backscattering from bulk materials", J. Appl. Phys., Vol. 58, No. 1, 526-534, 1985.

[3-3] E. H. Darlingtion, "Backscattering of 10-100keV electrons from thick targets", J. phys. D : Appl. Phys. Vol.8, 85-93, 1975.

[3-4] A. J. Dekker, "Solid state physics", Prentice-Hall Press, Ltd.,1957

[3-5] W. R. Nelson, H. Hirayama and D. W. O. Rogers, "The EGS4 code system", SLAC-report-265, 1985.

[3-6] W. R. Nelson and Y. Namito, "The EGS4 code system: solution of gamma-ray and electron transport problems", SLAC-PUB-5193, February, 1990.

[3-7] E. J. Sternglass, "Backscattering of kilovolt electrons from solids", physical review, Vol. 95, No. 2, 345-358, July, 1954.

[3-8] G. Neubert and S. Rogaschewski, "Backscattering coefficient measurements of 15 to 60 keV electrons for solids at various angles of incidence", Phys. Stat. Sol. (a) 59, 35-41, 1980.

[3-9] H. Hirayama and Y. Namito, "Lecture notes of EGS4 course at KEK", KEK-internal 99-5, July, 1999.

In Chapter 4:

[4-1] L. Kumar, S. Spadtke, R. G. Carter and D. Perring, "Three-dimensional simulation of multistage depressed collectors on micro-computers", IEEE Trans. Electron Devices, Vol. ED-42, No.9, 1663-1673, 1995.

[4-2] W. B. Herrmannsfeldt, "Electron trajectory program", SLAC-Report-226, Nov. 1979.

[4-3] H. Hirayama and Y. Namito, "Lecture notes of EGS4 course at KEK", KEK-internal 99-5, July, 1999.

[4-4] A. N. Curren, "Carbon and Carbon-coated electrodes for multistage depressed collectors for electron-beam devices-A technology review", IEEE Trans. Electron Devices, Vol. ED-33, No.11, 1902-1914, 1986.

[4-5] P. Ramins and B. T. Ebihara, "Improvements in MDC and TWT overall efficiency through the application of carbon electrode surfaces", IEEE Trans. Electron Devices, Vol. ED-33, No. 11, 1915-1924, 1986.

In Chapter 5:

[5-1] M. J. Smith and G. Phillips, "Power klystrons today", Chapter 7, Research Studies Press, Ltd., 1995.

[5-2] H. Yonezawa and Y. Okazaki, "A one-dimensional disk model simulation for klystron design", SLAC-TN-84-5, May 1984.

[5-3] A. N. Sandalov, V. M. Pikunov, V. E. Rodyakin, G. Fallion and Y. Thaler, "Animation of nonlinear electron-wave interaction in klystron", Proceedings of 3rd workshop on pulsed rf sources for linear collider (RF96), KEK proceedings 97-1, 1999.

[5-4] T. Shintake, "Klystron simulation and design using the field charger interaction (FCI) code", Nucl. Instr. and Method A363, 83-89, 1995.

[5-5] M. Chodorow and C. Susskind, "Fundamentals of microwave electronics", McGraw-Hill, Inc., Chapter 3, 1964.

[5-6] K. Masuda, K. Yoshikawa, M. Ohnishi and Y. Yamamoto, "Improvement of klystron efficiency by use of direct energy recovery from spent beam", Proceedings of 3rd workshop on pulsed rf sources for linear colliders (RF96), KEK proceedings 97-1, 1999.

[5-7] S. Isagawa etal., "Suppression of SBO and stability improvements of TRISTAN 1MW high power klystrons", Proceedings of 9th Symp. On Acc. Sci. and Tech., KEK, Tsukuba, Japan, 128-130, 1993.